Synthesis and Functionalization of Soft Colloidal Probes based on Poly(ethylene glycol) as Carbohydrate Biosensors

Inaugural-Dissertation
to obtain the academic degree
Doctor rerum naturalium (Dr. rer. nat.)

submitted to the Department of Biology, Chemistry and Pharmacy
of Freie Universität Berlin

by
Daniel Pussak
from Berlin, Germany

Berlin, May 2014

The work presented in this thesis was accomplished in a period between January 2011 and May 2014 in the Department of Biomolecular Systems at the Max Planck Institute of Colloids and Interfaces and Free University of Berlin, Institute of Chemistry and Biochemistry under supervision of Dr. Laura Hartmann.

1st Reviewer:	Dr. Laura Hartmann
2nd Reviewer:	Prof. Dr. Sebastian Seiffert

Date of defense: 27.08.2014

Author Contributions: Thesis and Related Publications

The work presented in this thesis has led so far to three first author publications and three co-author publications of Daniel Pussak, the author of this thesis. In the following, the contributions of Daniel Pussak, co-authors, supervisors, graduate students and technical staff on this thesis and according publications are listed chapter wise (for first author publications all contributions are listed, for co-author publications only the contributions of Daniel Pussak are specified).

Chapter 3: Synthesis and Characterization of PEG SCPs

Contributions thesis:

D. Pussak (Ph.D. student, author of this thesis):

Synthesis of PEG-dAAm macromonomers, characterization of macromonomers by NMR, measurements of the cloud point of aqueous macromonomer solutions, synthesis of PEG microgels, characterization of PEG microgels by microscopy and AFM indentation measurements to obtain the Young's modulus

S. V. Ruiz (master student):

PEG with a molecular weight of 20 kDa was prepared and characterized as part of Ms. Ruiz master thesis and was applied by D. Pussak for the synthesis of PEG microgels and the following adhesion studies.

Dr. L. Hartmann (supervisor):

Design of research and research coordination, collaborative data analysis

Dr. S. Schmidt (co-supervisor):

Design of research, collaborative data analysis, roughness measurements on the SCPs

H. Runge (technical assistant):

SEM measurements

Parts of this chapter have been published by the author as:

- D. Pussak, M. Behra, S. Schmidt, L. Hartmann, *Soft Matter* **2012**, *8*, 1664–1672. http://dx.doi.org/10.1039/c2sm06911c

Author contributions:

D. Pussak:

Synthetic and analytical work as described in the thesis, preparation of the manuscript

Dr. Muriel Behra (researcher at MPIKG):

Dendrimer synthesis, proof-reading of the manuscript

Dr. S. Schmidt (co-supervisor):

Design of research, collaborative data analysis, Roughness measurements on the SCPs and paper writing

Dr. L. Hartmann (supervisor):

Design of research, collaborative data analysis, paper writing, submission of manuscript

- The syntheses of PEG SCPs lead to a contribution as co-author in:

M. Glaubitz, N. Medvedev, D. Pussak, L. Hartmann, S. Schmidt, C. A. Helm, M. Delcea, *Soft Matter* 2014, accepted manuscript http://dx.doi.org/10.1039/c4sm00788c.

Contributions D. Pussak:

Synthesis of PEG hydrogels writing experimental part of the particle synthesis

Chapter 4: Functionalization of PEG SCPs

Contributions thesis:

D. Pussak (Ph.D. student, author of this thesis):

Functionalization of SCPs *via* benzophenone chemistry and optimization of the conditions, characterization of the SCPs by ATR FT-IR, colorimetric titration, confocal spectroscopy, and analysis of Raman spectra, HPLC measurements and analysis of the homopolymer formation of the monomers during functionalization of the SCPs and support of the development of the theoretical model, coupling strategy and post-modification of carboxylic functionalized SCPs with various ligands, except PEG-CA and SCPs with Young's modulus of 15 kPa and 4 kPa

S. V. Ruiz (master student):

Preparation of SCPs with Young's modulus of 15 kPa and 4 kPa as part of Ms. Ruiz master thesis that was co-supervised by D. Pussak.

H. Wang (master student):

Preparation and characterization of PEG-CA probes as part of Mr. Hanqing Wang master thesis that was co-supervised by D. Pussak.

Dr. Admir Masic (researcher at MPIKG)

Recording Raman images

Dr. Muriel Behra (researcher at MPIKG):

Dendrimer synthesis

Dr. S. Mosca (researcher at MPIKG):

Synthesis of aminoethyl-mannose

D. Ponader (researcher at MPIKG):

Synthesis of aminoethyl-galactose

Dr. L. Hartmann (supervisor):

Design of research and research coordination, collaborative data analysis

Dr. S. Schmidt (co-supervisor):

Design of research, collaborative data analysis and ligand density calculation

J. Steffen (technical assistant):

Measurement of the amino acid content

Parts of this chapter have been published by the author as:

- D. Pussak, M. Behra, S. Schmidt, L. Hartmann, *Soft Matter* **2012**, *8*, 1664–1672. http://dx.doi.org/10.1039/c2sm06911c

Author contributions: see above

- D. Pussak, D. Ponader, S. Mosca, S. V. Ruiz, L. Hartmann, S. Schmidt, *Angew. Chem. Int. Ed.* **2013**, *52*, 6084–6087. http://dx.doi.org/10.1002/anie.201300469

Author contributions:

D. Pussak

Synthetic and analytical work as described in the thesis, RICM measurements and analysis, preparation of the manuscript

D. Ponader (researcher at MPIKG):

SPR measurements, glycooligomer synthesis, proof-reading of the manuscript

Dr. S. Mosca (researcher at MPIKG):

Synthesis of aminoethyl-mannose

S. V. Ruiz (master student):

Preparation of SCPs with Young's modulus of 15 kPa and 4 kPa

Dr. S. Schmidt (co-supervisor):

Design of research, collaborative data analysis, paper writing

Dr. L. Hartmann (supervisor):

Design of research, collaborative data analysis, paper writing, submission of manuscript

- The synthesis of PEG SCPs and the functionalization with AA lead to a contribution as co-author:

S. Schmidt, A. Reinecke, F. Wojcik, D. Pussak, L. Hartmann, M. J. Harrington, *Biomacromolecules* **2014**, *15*, 1644–52. http://dx.doi.org/10.1021/bm500017u

Contributions D. Pussak:

Synthesis and functionalization of PEG hydrogels with AA, writing experimental part of the particle synthesis, proof-reading of the manuscript

Chapter 5: Adhesion Measurements via RICM Using SCPs as Sensors

Contributions thesis:

D. Pussak (Ph.D. student, author of this thesis):

RICM measurements and calculation of adhesion energies, glass surface functionalization, inhibition/competition studies and analysis of data, reusability of surfaces

S. V. Ruiz (master student):

Preparation of SCPs with Young's modulus of 15 kPa and 4 kPa

H. Wang (master student):

Preparation and characterization of PEG-CA probes

D. Ponader (researcher at MPIKG):

SPR measurements, glycooligomer synthesis

Dr. F. Wojcik (researcher at MPIKG):

Synthesis of thioethyl-mannose and Man(2,4,6,8,10)-10

Dr. L. Hartmann (supervisor):

Design of research and research coordination, collaborative data analysis

Dr. S. Schmidt (co-supervisor):

Design of research, collaborative data analysis, estimation of functional groups on SCPs and theoretical binding events, roughness measurements

J. Steffen (technical assistant):

Measurement of the amino acid content

Parts of this chapter have been published by the author as:

- D. Pussak, M. Behra, S. Schmidt, L. Hartmann, *Soft Matter* **2012**, *8*, 1664–1672. http://dx.doi.org/10.1039/c2sm06911c

Author contributions: see above

- D. Pussak, D. Ponader, S. Mosca, S. V. Ruiz, L. Hartmann, S. Schmidt, *Angew. Chem. Int. Ed.* **2013**, *52*, 6084–6087. http://dx.doi.org/10.1002/anie.201300469

Author contributions: see above

- The measurements of IC_{50} values of heteromultivalent glycooligomers with the developed inhibition/competition assay *via* the SCP-RICM method lead to a contribution as co-author:

D. Ponader, P. Maffre, J. Aretz, D. Pussak, N. M. Ninnemann, S. Schmidt, P. H. Seeberger, C. Rademacher, G. U. Nienhaus, L. Hartmann, J. Am. Chem. Soc. **2014**, 136, 2008–2016. http://dx.doi.org/10.1021/ja411582t

Contributions D. Pussak:

Synthesis and functionalization of PEG hydrogels, RICM measurements, writing experimental part of the particle synthesis, proof-reading of the manuscript

Chapter 6: SCP-AFM Measurements

Contributions thesis:

D. Pussak (Ph.D. student, author of this thesis):

SCP-AFM measurements and analysis, preparation of cantilevers with the probe, inhibition kinetic measurements, optimization of concentration and measurement parameters

D. Ponader (researcher at MPIKG):

Glycooligomer synthesis

Dr. L. Hartmann (supervisor):

Design of research and research coordination, collaborative data analysis

Dr. S. Schmidt (co-supervisor):

Design of research, collaborative data analysis

Parts of this chapter have been published by the author as:

- D. Pussak, D. Ponader, S. Mosca, T. Pompe, L. Hartmann, S. Schmidt, *Langmuir* **2014**, *30*, 6142–6150. http://dx.doi.org/10.1021/la5010006

Author contributions:

D. Pussak:

Synthetic and analytical work as described in the thesis, AFM measurements and analysis, preparation of the manuscript

D. Ponader (researcher at MPIKG):

Glycooligomer synthesis

Dr. S. Mosca (researcher at MPIKG):

Synthesis of aminoethyl-mannose

Prof. Dr. Tilo Pompe (Uni Leipzig):

Collaborative data analysis and proofreading of manuscript

Dr. L. Hartmann (supervisor):

Design of research, collaborative data analysis, paper writing

Dr. S. Schmidt (co-supervisor):

Design of research, collaborative data analysis, paper writing and submission

Acknowledgements

First I would like to thank my supervisor Dr. Laura Hartmann for this interesting and challenging topic, her countless ideas and her steady motivation, giving me the scientific and personal support to manage my work and helping me to successfully move my thesis forward.

I also want thank Prof. Dr. Peter H. Seeberger for giving me the opportunity to accomplish my Ph.D. thesis in his department and his support, as well as Prof. Dr. Sebastian Seiffert for spending his valuable time to review my thesis.

I am very grateful to Dr. Stephan Schmidt for the fruitful collaboration and support during the preparation of this thesis. I learned so much from our discussions, and his input has been essential for the results of this thesis. Furthermore, I would like to thank Prof. Dr. Helmut Möhwald for his support and proof-reading of my thesis.

I am grateful to the former and present members of the Polymeric Biomimetic group, namely Dr. Muriel Behra, Dr. Simone Mosca, Daniela Ponader, Dr. Felix Wojcik, Sinaida Igde, Nina Mujkić-Ninnemann and Maciej Czarnecki for their great help and many pleasant moments over the past years. Furthermore, I would like to thank the former master students Salomé Ruiz Vargas and Hanqing Wang for their great work and nice collaboration.

I would like to thank the whole Biomolecular Systems Department for their help and for sharing their analytical instruments.

I appreciate all the research facilities at the Max Planck Institute of Colloids and Interfaces in Golm. In this light I like to thank Anneliese Heilig for a pleasant time at the AFM lab, Dr. Admir Masic for his help in measuring the Raman spectra. Heike Runge and Dr. Jürgen Hartmann are acknowledged for measuring the SEM pictures. I like to thank also Jeanette Steffen for performing the amino acid analysis.

I am very grateful to my family, especially to my parents, Danuta and Roman, who always supported me and had a great impact on my life. My father, though he is not more among us, for his love.

There is the special person I need to thank. Stephanie! Your love, your support and your patience gave me the strength to bring this task to a close. Thank you for every day shared with me. I hope you still think it was worth it.

Finally, I like to thank my friends for their support and for many pleasant moments.

Table of Contents

Summary

Cells interact with their environment *via* their surface. Therefore, cell surfaces play a crucial role in cellular processes such as signaling, communication, viral infections and adhesion. Every process on the cell surface relies on molecular forces that are a complex interplay of chemical, biological and physical interactions. Those interfacial interactions are mediated by ligands and receptors and are the basis of the commonly known 'lock and key principle' that controls cellular behavior. However, the exact mechanisms of such binding interactions at interfaces are not fully understood yet. This is especially true for ligand-receptor interactions at soft surfaces that are based on sugar ligand and protein receptor recognition. Sugar ligands are abundant on every cell as part of the glycocalyx and take part in cell-cell interactions such as tissue growth or viral infections although sugar ligands have only low affinities towards receptors. Nature overcomes this problem by using multivalency – the presentation of multiple low affinity sugar ligands e.g. anchored to a cell membrane that then leads to a stronger, since multivalent binding event.

Understanding the interactions of sugar ligand modified surfaces is not only relevant in biology and medicine but can also help to use sugar ligand modification in material sciences to create e.g. novel tissue scaffolds or antiviral coatings. Therefore, it is the broad aim of this thesis to construct a robust experimental platform to precisely measure surface interactions focusing on carbohydrate mediated interactions and to elucidate the structural and physiochemical parameters that affect those interactions at interfaces. As main parameter the *adhesion* between a presenting carbohydrate ligand surface and protein receptors surface is determined.

There are several methods, like atomic force microscopy (AFM) or surface plasmon resonance (SPR) that are suitable to quantify adhesion. However, they require a high level of technical knowledge, rather expensive equipment and most importantly do not allow for the straightforward variation of the physicochemical properties of the investigated surfaces e.g. a controlled change in mechanical properties.

Therefore this work uses a novel approach *via* soft, hydrogel based probes to detect carbohydrate interactions. In the first part, the synthesis of soft colloidal probes suitable for adhesion measurements will be presented (**Figure 1**). These soft colloidal probes are based on a biocompatible PEG scaffolds in order to reduce non-specific interactions and allow for surface functionalization. A surfactant free synthesis of PEG microparticles using kosmotropic electrolytes to salt out PEG in an aqueous solution was performed. In order to use the hydrogel probes for the analysis of interfacial interactions, in the second part radical

surface chemistry was introduced by using benzophenone as the photoinitiator to graft polymerizable monomers to the SCPs. With this highly versatile method, various functionalities such as carboxy or amine groups can be directly introduced into the PEG network. The obtained SCPs were further modified with more complex structures such as sugars or peptides and then tested for their use as SCPs in adhesion measurements.

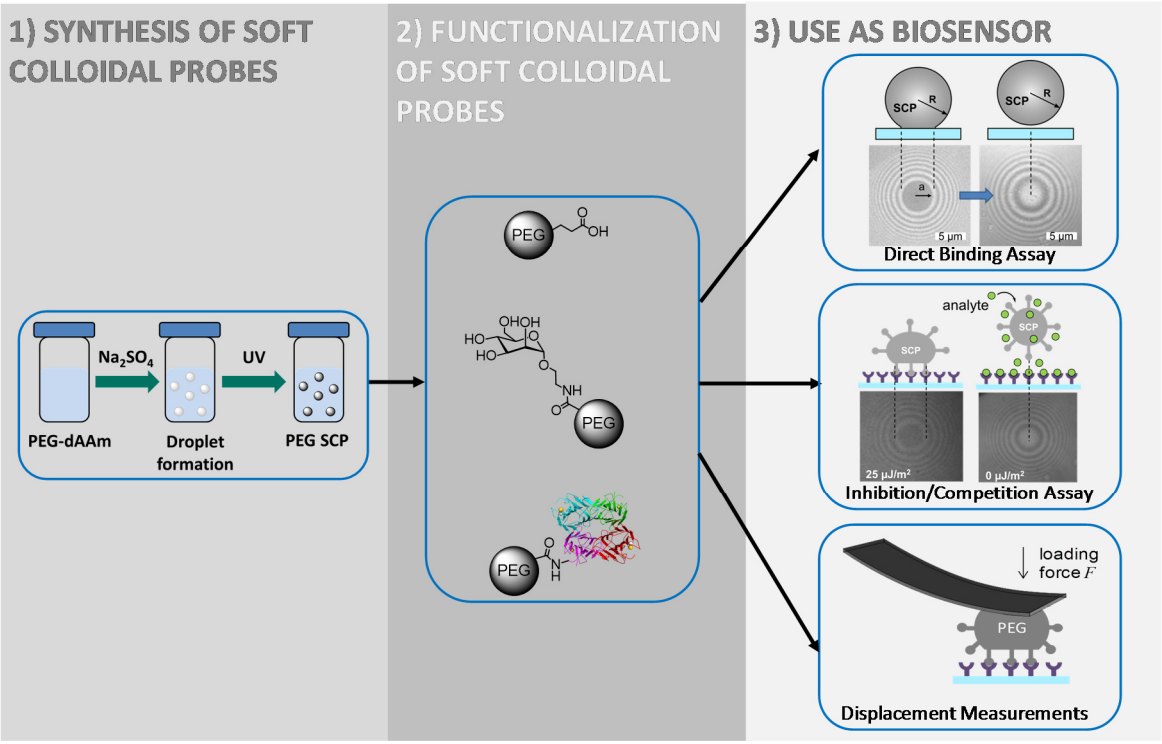

Figure 1: Schematic representation of the work. After the synthesis of PEG SCPs (1), they are functionalized with (bio)molecules (2). With these SCPs, carbohydrate mediated surface interactions can be measured (3). Here, three methods have been developed: The direct binding assay to evaluate the carbohydrate/receptor interactions at surfaces; the inhibition/competition assay that uses the direct binding assay and allows to evaluate various analytes towards their affinity to the receptor; and the combination of these methods with AFM to measure surface interactions depending on the applied force and the displacement of bound analytes from the receptors at a loading force.

In the third part, the differently functionalized SCPs were used to measure adhesion forces by Reflection Interference Contrast Microscopy (RICM). RICM is a simple method based on contact mechanics theory (JKR theory) which correlates the adhesion induced elastic deformation of the SCPs directly to their surface energy. Special focus was devoted to the measurement of sugar/lectin mediated adhesion. As a model system; the well-known interaction between mannose and ConA was evaluated. Here the influence of the elasticity of the SCP, the surface bound ligand concentration and the type of grafting chemistry, was evaluated in terms of changes in the adhesion process.

Then, the inhibition of the previously characterized direct binding of mannose/ConA with different monosaccharides was evaluated. Therefore, a new inhibition/competition assay based on the adhesion induced elastic deformation of the SCPs was developed. This method allowed for inhibition measurements and give fast and straightforward access to relative affinities of a variety of sugar ligands. In addition, more complex molecules like multivalent glycooligomers were used as inhibitors and screened for their relative affinities, thereby analyzing the role of multivalent ligands and their surface interactions.

Finally, the combination of RICM with AFM is presented as a new technique to measure first adhesion forces between receptor-modified surfaces and the SCPs under variation of loading rate, loading forces as well as the contact time. In the same time the contact area of the adhering object can be detected. The use of such ligand modified hydrogels as force probes is supposed to mimic the physiological situation, where the soft hydrogel-like glycocalyx interacts with cell receptors. Secondly it allowed studying the ability of multivalent carbohydrates to remain bound to the receptor surface upon forced contact and competition with a ligand presenting SCP. Different ligands such as mannose or multivalent glycooligomers were used as inhibitors and screened for their inhibitory potential.

In general, a new method based on PEG SCPs was developed that is suitable for the measurement of adhesion with high sensitivity allowing the detection of very weak biological interactions. On the one hand, physiochemical influences can be studied by measuring direct binding between ligands on the probes and receptors on a surface. On the other hand, stepwise inhibition of these interactions with an analyte permits the performance of an inhibition/competition assay. Thus, IC_{50} values suitable for determining relative affinities of molecules towards their binding to the corresponding receptors can be evaluated. Based on those adhesion measurement techniques, kinetics can be measured by combining them with AFM. Therefore, more sensitive measurements are achieved which additionally allow the measurement of forces between these two bodies.

Future work will focus on expanding the techniques to further ligand/receptor pairs and to develop for high throughput screenings as a new method to determine ligand affinities. Moreover, the application of the hydrogel probes as extracellular matrix model will be tested for direct cell interaction studies *via* AFM.

Zusammenfassung

Durch die spezifische Wechselwirkungen an der Zelloberflächen werden viele biologischer Funktionen gesteuert. Beispielhaft hierfür ist die Signaltransduktion, die Adhäsion zweier Zellen oder das Anhaften eines Virus an die Zelloberfläche. Diesen Prozessen liegt die Bindung von Liganden und Rezeptoren an der Zelloberfläche zugrunde. Die strukturelle Komplexität der Bindungspartner und ermöglicht eine sehr selektive Ausbildung von Bindungen und die Steuerung einer erstaunlichen Vielzahl von Prozessen nach dem sogenannten Schlüssel-Schloss-Prinzip. Die Mechanismen solcher Bindungswechselwirkungen an Oberflächen und die physikalisch-chemischen Einflüsse der Membran sind dabei nicht vollständig bekannt. Dies gilt insbesondere für die Ligand/Rezeptor-Wechselwirkungen auf weichen, flexiblen Oberflächen wie der Zellmembran oder der Glykokalyx. Die Zell-Glykokalyx ist eine Kohlenhydrat-reiche Schicht, die jede eukaryotische Zelle umschließt. Die spezifischen Wechselwirkungen zwischen den Zuckerliganden der Glykokalyx und Proteinrezeptoren sind ein wichtiger Teil der Erkennungsprozesse von Zellen. Dies ist insofern erstaunlich, da Zuckerliganden nur eine geringe Bindungsaffinität zu ihren Rezeptoren zeigen. Die Natur löst das Problem der geringen Affinität durch Multivalenz – dabei werden mehrere Zuckerliganden mit ihrer geringen Affinität präsentiert, z.B. verankert an einer Zellmembran, die dann zu einem stärkeren, da mehrwertigen, Bindungsereignis führt.

Das Verständnis von der Wechselwirkung von Zuckerligand-modifizierten Oberflächen ist nicht nur in der Biologie und Medizin relevant, sondern wird auch in den Materialwissenschaften angewendet, um z.B. Gewebegerüste oder antivirale Beschichtungen herzustellen. Deshalb ist es das Ziel dieser Arbeit eine robuste Plattform für die Quantifizierung von schwachen Wechselwirkungen zwischen weichen Oberflächen zu schaffen, um insbesondere zuckergesteuerte Wechselwirkungen zu analysieren zu können. Dabei sollen die strukturellen und physikalisch-chemischen Parameter aufgeklärt werden, die diese Wechselwirkungen beeinflussen können, z.B. die Weichheit der Oberfläche oder Dichte der Zuckerliganden. Der zentrale Messparameter bei dem entwickelten Prinzip, ist die *Adhäsion*, die zwischen einer Zucker- und Rezeptoroberfläche wirkt.

Es gibt mehrere Verfahren, wie die Rasterkraftmikroskopie (AFM) oder Oberflächenplasmonresonanz (SPR), die geeignet sind, um spezifische zwischen Biomolekülen Adhäsion zu quantifizieren. Allerdings erfordern sie ein hohes Maß an technischem Wissen, teuren Ausrüstungen. Zudem erlauben sie nicht die einfache Variation von physikalisch-chemischen Eigenschaften der zu untersuchenden Objekte z.B. eine

gezielte Änderung der mechanischen Eigenschaften der bindenden Oberflächen. In dieser Arbeit wird eine neue Methode präsentiert, welche weiche Hydrogelsonden (SCPs, soft colloidal probes) für die Adhäsionsmessungen verwendet. Im ersten Teil dieser Arbeit wird die Synthese dieser weichen Hydrogelsonden beschrieben. Dabei wird Poly(ethylenglykol) (PEG) als Hydrogelmaterial verwendet, da es unspezifische Wechselwirkungen reduziert und somit die Spezifität der Adhäsionsmessung erhöht. Die Synthese der Sonden erfolgt durch das Ausfällen von PEG aus einer kosmotropen Salzlösung. Um die Hydrogelsonden für Adhäsionsmessungen nutzen zu können, wird im zweiten Abschnitt die PEG Oberfläche mittels radikalischer Oberflächenchemie durch Verwendung von Benzophenon funktionalisiert. Dabei entstehen Radikale am PEG Gerüst, die das Graften von polymerisierbaren Molekülen ans PEG ermöglichen. Mit dieser Methode lassen sich eine Vielzahl an funktionellen Gruppen wie Carboxyl- oder Amingruppen an die PEG Sonden addieren. Diese funktionellen Gruppen können dann genutzt werden um komplexere Moleküle wie Zucker oder Peptide an die Sonden zu binden.

Im dritten Teil der Arbeit werden Adhäsionsmessungen der funktionalisierten Sonden auf Oberflächen mittels Reflektionsinterferometrie (RICM) gemessen. RICM ist eine optische Methode um Kontaktflächen der adhärierenden Hydrogensonden sichtbar zu machen. Mit Hilfe der Kontaktmechanik (JKR Theorie) kann aus der elastischen Deformation der Sonden die Adhäsionsenergie bestimmt werden. Ein besonderes Augenmerk liegt auf der Messung von Ligand/Rezeptor Wechselwirkung von Zucker/Proteinen an Oberflächen. Um die Anwendbarkeit der neuen Methode zu zeigen, wurde das bekannte Zucker/Lektin-Paar Mannose und Concanavalin A (ConA) gewählt. Die Einflüsse von der Elastizität der Sonden, der Ligandenkonzentration sowie der Art der Funktionalisierung auf die Adhäsion wurde evaluiert.

Anschließend wurde die Inhibierung der zuvor charakterisierten direkten Bindung von Mannose/ConA durch verschiedene Monozucker getestet. Daher wurde eine neue Inhibitionsmessung, basierend auf der spezifischen Adhäsion des SCPs entwickelt. Dieses Verfahren zur Inhibitionsmessung erlaubt schnellen und einfachen Zugang zur relativen Affinitäten einer Reihe von Zuckerliganden. Desweiteren wurden auch komplexere Strukturen, die sogenannten sequenzdefinierten Glykooligomere auf ihre inhibierende Wirkung getestet.

Im letzten Teil der Arbeit wird die Kombination von RICM mit AFM als neue Technik vorgestellt, um Adhäsionskräfte zwischen rezeptormodifizierten Oberflächen und den SCPs unter Variation der Beladungsrate, Krafteinwirkung als auch der Kontaktzeit zu messen. Die

Verwendung von ligandmodifizierten Hydrogelen als Kraftsensor soll die physiologische Situation der weichen Glykokalyx und ihrer Wechselwirkung mit Zellrezeptoren nachahmen. Zudem erlaubt es die Untersuchung der Fähigkeit mehrwertiger Zucker unter Kontakt und unter Konkurrenz mit einem ligandpräsentierenden SCP an den Rezeptoren zu binden und die Adhäsion der SCP zu unterbinden. Verschiedene Liganden, wie Mannose oder mehrwertige Glykooligomere wurden als Inhibitoren verwendet und auf ihre inhibitorische Wirkung getestet.

Generell wurden neue Methoden entwickelt, die mit Hilfe von funktionalisierten PEG SCPs Messungen von Adhäsion mit hoher Empfindlichkeit erlauben und schwache biologische Wechselwirkungen nachzuweisen. Einerseits konnten physikalisch-chemische Einflüsse durch direkte Bindungsstudien zwischen Liganden und Rezeptoren an einer Oberfläche getestet werden, andererseits konnte durch eine schrittweise Hemmung der Wechselwirkung durch einen Analyten die Durchführung einer Inhibitionsmessung ermöglicht werden. Dies ermöglichte die Etablierung eines *screening assays*, welcher relative Affinitäten der Analyten entsprechend ihrer Bindung an die Rezeptoren liefert. Basierend auf den SCP Adhäsionsmessung wurde die Kinetik durch die Kombination mit AFM gemessen. Dadurch konnten empfindliche Messungen erreicht werden, die zusätzlich Kraftmessungen zwischen einer weichen und harten Oberfläche erlauben.

Zukünftige Arbeiten werden sich auf die Erweiterung der Techniken konzentrieren und weitere Ligand/Rezeptor Paare testen, sowie auf die Entwicklung von High Throughput Screenings. Darüber hinaus wird die Anwendung der Hydrogel SCPs als Zellmimetik für direkte Zell-Wechselwirkungsstudien mittels AFM untersucht werden.

1. General Introduction

1.1. Hydrogel Microparticles in Biotechnology

The experimental technique developed in this work uses microscopic hydrogel particles as sensors. Therefore hydrogels and microgels in particular are discussed in the first chapter.

Hydrogel materials are studied increasingly for applications in biological sensing, drug delivery, and tissue regeneration. Hydrogels are water-swollen hydrophilic polymeric materials that maintain a distinct three-dimensional structure. The high water content of the material contributes to their biocompatibility. Furthermore their hydration results in tissue-like mechanical properties and makes them highly suitable for *in vivo* applications.[1] Hydrogel networks can be composed of either homopolymers or copolymers and are insoluble due to the presence of chemical or physical cross-links.[2] The latter are also called 'reversible', or 'physical' gels that are held together by molecular entanglements and/or secondary forces including ionic, H-bonding or hydrophobic forces. Physical hydrogels can reversibly degrade into the corresponding precursors upon external stimuli. Hydrogels that are covalently cross-linked are called ‘permanent’ or ‘chemical’ gels. Chemical hydrogels may be generated by cross-linking of water-soluble polymers in the presence of cross-linkers. In the cross-linked state, hydrogels reach an equilibrium swelling level in aqueous solution that depends mainly on the cross-link density.

Hydrogels can be obtained as macroscopic networks or in smaller dimensions as so-called microgels. Microgels are usually spherical, have sizes from 100 nm to 100 µm and thus large surface area. In the context of biomaterials and biotechnology, the microgel surface is often modified by bioconjugation in order to introduce ligands, e.g. carbohydrates or proteins that specifically bind to targeted sites.[2,3] Scheme 1 shows some examples of the most common mono- and macromonomers for the synthesis of chemical gels.

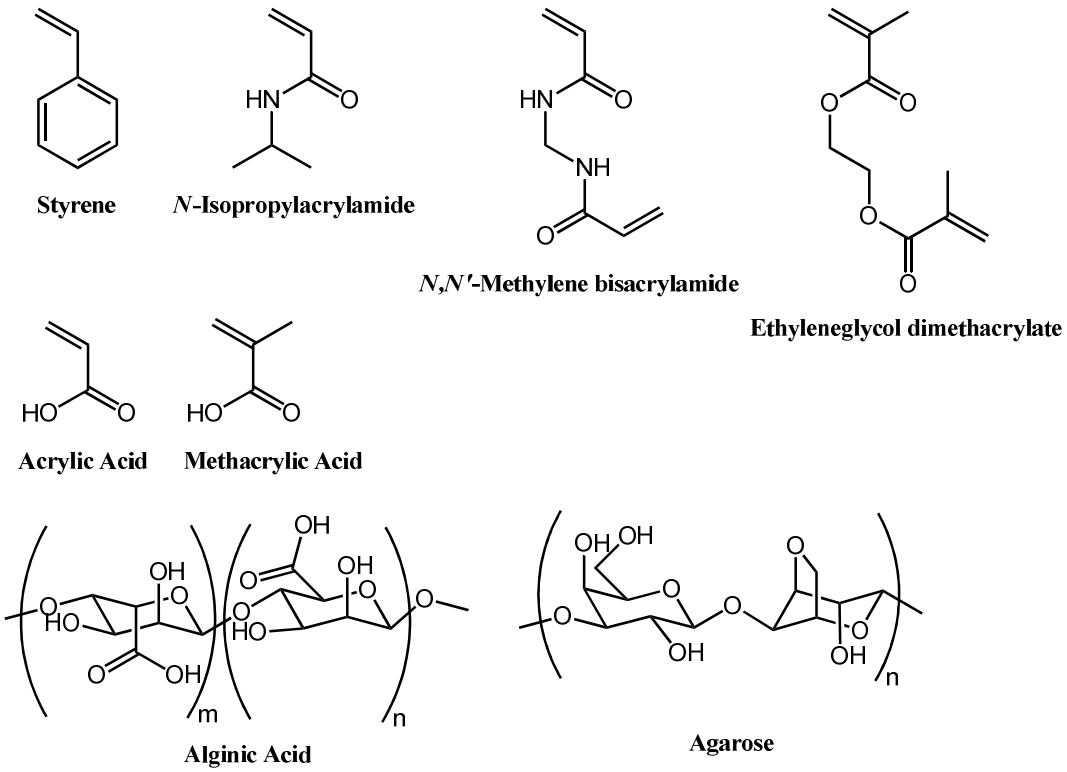

Scheme 1: Structures of common monomers and macromonomers used to prepare microgels

Some microgels are able to respond to chemical and physical stimuli, like temperature, pH changes, ionic strength or light, changing e.g. their shape, aggregation behavior, degradation or swelling/collapsing.[4] One of the most important properties of hydrogels is their swelling behavior. This, and specifically the swelling degree, depends on the polymer-polymer and polymer-water interaction. When the microgels are dispersed in a good solvent, the polymer chains extend to increase the polymer-water interaction thereby swelling the gel. Gels undergo a transition from swollen state in a good solvent to collapse in a bad solvent, when the polymer-polymer interaction becomes dominant. Microgels prepared of hydrophilic polymers will therefore swell in water and collapse in organic solvents with low dipole moment, whereas microgels composed of non-polar polymers such as polystyrene swell in non-polar solvents such as toluene. For hydrogels made of polyelectrolytes such as methacrylic acid, a pH dependent swelling can be observed. For example, methacrylic acid as well as acrylic acid microgels aggregate and collapse at neutral pH and re-swell at basic conditions.[5] Here, the deprotonated acid groups show electrostatic repulsion under basic conditions leading to a swelling of the microgel. The most widely studied so-called 'smart' microgel is made of poly(*N*-isopropylacrylamide (PNIPAm). PNIPAm is a thermoresponsive polymer with lower critical solution temperature (LCST) around 32-33°C. PNIPAm microgels exist in swollen state at temperatures below 32°C,

where PNIPAm associates water by hydrogen bonding. When the temperature is increased, water is released due to entropic effects, the polymer-polymer interactions are favored and the polymer reorganizes to a collapsed state by dehydration of the polymer.[6]

Microgels present many other attractive features such as their colloidal stability and their chemical versatility. They can be synthesized in a variety of sizes, morphologies, chemical compositions and with different functionalities. In the following chapter, the synthesis of microgels will be discussed in more detail.

1.1.1. Synthesis of Microgels

The preparation of microgels can be divided into two groups: physical cross-linking or chemical cross-linking. The physical cross-linking method involves hydrophobic or electrostatic interactions to cross-link polymer chains into particles. This is a common procedure for the preparation of microgels from polyelectrolytes such as alginate or chitosan.[7,8] Chemical cross-links can be achieved for example *via* free radical polymerization in the presence of multifunctional cross-linkers, e.g. acrylic monomers can be cross-linked by bisacrylamide. Precipitation, suspension or emulsion polymerization are the most commonly applied routes towards microgel preparation. In a precipitation polymerization, the monomer and the initiator are soluble in a solvent and upon cross-linking of the monomer, the polymer collapses and precipitates forming a separate phase (dispersion) in the solvent. As the reaction proceeds, flocculation and aggregation of the initially formed nuclei take place. In case of continuous formation of new nuclei, a polydisperse precipitate with a broad spectrum of irregularly shaped particles is formed.[9] Monodisperse microgels can result, if all nuclei are formed in a time frame that is much shorter than the time frame of the nuclei growth process. This technique has been used for the synthesis of PNIPAm and other thermoresponsive microgels.[10] In suspension polymerization the initiator and the monomer are stabilized by stirring and a suitable droplet stabilizer suspended in the medium in the form of microdroplets. The polymerization is then initiated and the monomer microdroplets are converted directly to the corresponding polymer microgels usually with the same size as the microdroplets.[11] In emulsion polymerization, the polymerization takes place in monomer microdroplets that form spontaneously in the continuous phase where the initiator and free surfactant is placed to

stabilize the monomer emulsion. Emulsion polymerization usually leads to submicron sized particles and narrow particle size distributions.

The size of the microgel particles in the aforementioned techniques is either limited by the nucleation and growth kinetics (e.g. precipitation) or thermodynamics (emulsion polymerization of the polymer phase. Microfluidic techniques can be used for the synthesis of monodisperse microparticles of virtually arbitrary sizes. To this end, microfluidic devices are used to prepare emulsions of the monomer solution in the size range of 1-50 µm followed by physical or chemical cross-linking.[12]

1.1.2. Post-modification of Microgels

For a variety of applications of microgels, it is of interest to include additional functional groups within the hydrogel, e.g. for the bioconjugation with ligands or labels. Functional groups increase the stability of the suspension due to repulsive forces and enhance the immobilization of biomolecules such as proteins, carbohydrates, antibodies or nucleic acids.[13] To incorporate chemically reactive groups, different strategies can be used. They can be introduced during polymerization by a functionalized radical initiator, an emulsifier or by a functional monomer. Mostly co-monomers like acrylic acid with carboxylates or aminoethyl methacrylate introducing amines are used to introduce functional groups in the microgel. Besides their use for functionalization, such co-monomeric hydrogels can show two stimuli responsive properties like pH and temperature dependent swelling e.g. when co-polymerizing NIPAm and methacrylic acid.[14]

Functional groups can be also incorporated on readily prepared microgels. There are three methods that are used: physiosorption, e.g. *via* layer-by-layer (LbL) technique, post-functionalization of present functional groups and by polymerization techniques. In the first case, the molecules are bound due to electrostatic interactions whereas the last two are linked *via* covalent bonding. In the LbL process, the stepwise adsorption of oppositely charged polymers on the particle surface is performed, and core/shell particles can be obtained.[15]

The attachment of (bio)molecules can be also achieved *via* condensation reactions e.g. the reaction of an amine with a carboxylic group. Here, the already present functional groups can be used and further functionalized. This method is standardly used in the solid phase synthesis were the functional groups on a resin are reacted with amino acids *via* standard

peptide coupling chemistry. Also sensitive molecules such as proteins can be attached. Usually, bioconjugation is done by pre-activating the carboxyl groups on the particles with carbodiimides and subsequent binding of amine groups e.g. from the lysine groups of peptides and proteins. Alternatively, conjugation *via* maleimide chemistry is widely used as it specifically binds to free thiol groups e.g. of cysteine residues. The binding of functional groups on the particles is also called grafting-on approach. A further possibility is the attachment of monomers to the microgels *via* the 'grafting from' polymerization. Here, a growing polymer chain is formed *via* radical polymerization onto the particle surface. In the first step, an initiator species on the substrate surface is used to initiate polymerization. Upon exposure to a monomer solution high grafting densities can be achieved. The graft polymerization of polymer materials is well known for its potential in modifying the surface properties of polymer materials without changing their inherent properties.

1.1.3. PEG Microgels

When microgels are introduced into a living tissue, the tissue is able to recognize the hydrogels as potentially harmful as foreign by specialized cells such as macrophages that adhere on the hydrogel. As a result potentially harmful immunological responses take place. One approach to suppress such a response is minimizing the initial process of protein adhesion to the hydrogel *via* surface modification.[15] Poly(ethylene glycol) (PEG) is known to avoid immunological recognition because of its high resistance to protein adsorption.[16,17]

PEG is a neutral, hydrophilic, and highly biocompatible polymer. PEG is a polyether and synthetically derived from ethylene oxide *via* anionic polymerization. The initiation of the reaction with hydroxide ions leads to PEG chains with hydroxyl groups on both ends. Different terminal groups can be obtained when the type of initiator is changed. The PEG geometry is not limited to linear chains. Other geometries have been prepared such as branched or star PEG. It is believed that PEG's inertness comes from the hydrophilicity, the inability to donate hydrogen bonds, and conformational flexibility of the backbone that makes it difficult for proteins to adhere on e.g. PEGylated surfaces.[15] The term PEG is used for polyethers of molecular weights below 20000 g/mol while poly(ethylene oxide) (PEO) refers to larger polymers.[18] PEG is commercially available and with molecular weights below 1000 g/mol it is a colorless viscous liquid while larger PEG's are white solids at room temperature. The melting point of PEG increases with molecular weight and reaches a

plateau at 67°C.[18] PEG is also a thermoresponsive polymer that phase separates in an aqueous solution at temperatures higher than 100°C.[19] Addition of salts can lower the LCST of PEG which will be discussed in chapter 3.1 for the synthesis of PEG microparticles.

In most applications PEG is conjugated to drugs or surfaces (PEGylation) to protect against degradation or coagulation.[20] Additionally, PEG is used in hydrogels by cross-linking PEG-macromonomers. A variety of PEG-macromonomers is available either by choosing the appropriate initiator during polymerization or by post-functionalization of the terminal end-groups of PEG, most often the functionalization of terminal hydroxyl groups.[21] In this way functional groups such as carboxylates, amines, thiols or azides can be introduced. All these groups can be used to prepare PEG chains with cross-linkable end-groups. By introducing acrylates or acrylamides as end-groups no additional cross-linker is needed for the preparation of hydrogels, thus resulting in 100% PEG materials. The synthesis of PEG-diacrylamides (PEG-dAAm) is shown in chapter 3.1.

As PEG does not have any further functional groups on the backbone, different strategies are available to achieve functional PEG microparticles. A second monomer bearing vinyl groups can be co-polymerized with PEG-dAAm to obtain additional functionalities. However, this method does not give pure PEG hydrogels anymore but always leads to changes of the particle properties such as the cross-linking density and the mechanical stability. Alternatively, ready-made PEG microgels can be functionalized in a polymer analogue fashion. The post-functionalization of PEG particles *via* radical surface chemistry will be described in chapter 4.1.

1.1.4. Microgels in Biotechnological Applications

The versatile properties of microgels make them very valuable for a large variety of applications. They are already industrially employed as additives to control the properties of the final composite materials. In particular, they have found extensive use in the coatings industry in order to improve the rheological properties and increase the viscosity of paints.[3,22] Microgels have also been employed in enhanced oil recovery to absorb water and avoid water mixing with oil.[22] In addition microgels are widely used in biotechnology for biosensing or bioseparation. Their high surface areas and surface functionalization makes microgels also very useful in sensing and separation e.g. *via* chromatography.[3] Their high biocompatibility and low protein adhesion as well as their functionalization promote specific

interactions between molecules which can be used for active drug targeting. They are stable under physiological conditions, and therefore hydrophilic microgels can mimic biological cells as they can be adjusted to the right mechanical properties, sizes and colloidal stability.[23] Furthermore, microgels can show stimuli-responsive properties like swelling/collapsing in response to specific environmental conditions allowing for the entrapment and release of molecules as well as biosensing applications. In the following, the applications of microgels in bioseparation and biosensing will be presented in more detail.

Bioseparation and Biosensing:

A major application of microgels is the separation of biomolecules like bacteria, proteins or DNA in aqueous solution.[3,24] Here, microgels are usually called beads. Such beads are firstly functionalized with specific ligands that can bind only to the target molecule. The principle bead-based separation consists of first: the binding of the target molecule to the bead, second: washing of the beads to remove all unbound molecules and finally: the recovering of the target molecule from the bead. One example is the purification of DNA using hydrogel beads as presented by Kadonaga et al. Therefore DNA was immobilized onto latex particles *via* an amine-epoxide reaction.[25,26] Furthermore Kadonaga et al. covalently coupled complementary DNA to Sepharose CL-2B gel beads with cyanogen bromide to yield the affinity resin.[27] With these beads transcription factors were successfully purified not only from pre-purified samples but also from crude cell extracts. Another example makes use of boronic acid-carrying particles that can be used to separate *cis*-diol-bearing saccharides, as boronic acid has a high specificity for *cis*-diols.[28] To improve the separation properties of microgels, porosity can be introduced into the particles which increase the surface area of the particles. Another example is the use of porous PEG microparticles to separate bacteria that can specifically bind to monosaccharides that were covalently attached to the particles.[29] The application of microgels with specific ligands attached to the surface is not only limited for separation, but the geometry and the softness of the constructs offer also an advantage as it closely mimics the cell surface. This way the microgels can also be used as biosensors. As this thesis will describe a new biosensor, a short definition of biosensors will be given and some examples in literature that use microgels as biosensors.

Biosensors are used to convert molecular binding events into a measureable and quantifiable signal. In most microgel applications, this transduction is observable in the change in the cross-linking network, electrochemical or optical properties. One example are

colored polystyrene microgels (15 µm) which were used to measure the regional blood flow, which is the major factor to decide oxygen transport and tissue oxygenation. The injected microgels were withdrawn from the blood and the concentration of extracted dyes was determined by spectrophotometry.[30] Another example makes use of the swelling ability of microgels that can be used for the detection of glucose in the blood to assist in the management of diabetes mellitus. Therefore, core/shell microparticles of PNIPAm with 3-aminophenylboronic acid (APBA) were synthesized and showed glucose-induced swelling.[31] The characterization of carbohydrate interactions is of great interest, as carbohydrates cover the cell surfaces (glycocalyx) and are therefore responsible for many processes like cell communication or viral infections. A sensitive biosensing method to detect weak interactions is surface plasmon resonance (SPR) or quartz crystal microbalance (QCM). For the quantification of specific carbohydrate/lectin interactions, alginate microparticles (60-80 µm) were functionalized with wheat germ agglutinin (WGA) and the interaction to the glycoprotein pig mucin, which was coupled to the gold surface was characterized by SPR.[32] Dissociation constants (k_d), association constants (k_a) as well as affinity constants (K_A) can be determined by using SPR. The developments in this field are directed towards enhanced sensitivity. Here, direct force-based detection by atomic force microscopy (AFM) offers increased sensitivity. As an example, Castro et al. used hybrid colloidal particles consisting of poly(methyl methacrylate) and carboxymethylcellulose attached to an AFM cantilever and probed them against a Concanavalin A (ConA) surface. Adhesion forces could be measured between these two surfaces and also in the presence of mannose as carbohydrate inhibitor.[33] The change in the force can be e.g. used for the characterization of the inhibitor itself. The principle of force-based detection can be used to construct new biosensors for the screening of biomolecular interactions of various carbohydrate compounds.

In general, microgels are useful materials for biosensing techniques as they can be easily tailored in size, material, mechanical properties and functionalization. These characteristics allow for the fabrication of flexible materials with known properties. In addition, many different ligands can be easily attached to them allowing for different studies e.g. on the interaction of ligands and receptors. They can be also used in combination with known biosensing techniques like SPR or AFM allowing the mimicry of cells in such experiments. Applying those microgels to AFM raises the sensitivity of force-based measurements. Due to the flexibility of the microgels the contact between the microgel and the surface is

increased which results in more precise measurements. To eliminate unspecific interactions in these measurements, the use of e.g. PEG microgels consisting of a neutral scaffold is favorable. The creation of such a biosensor for adhesion measurements and screening of carbohydrates will be described in this thesis.

1.2. Atomic Force Microscopy (AFM) and Colloidal Probe AFM

AFM is a scanning probe technique and was invented by Binnig, Quate and Gerber in 1986.[34] It has become an important tool for imaging the topography of surfaces with high resolution. Besides surface topography mapping, AFM has been used to measure force-versus-distance curves. Such force-distance curves are useful as they can provide information about all kinds of surface forces or local material properties like elasticity, adhesion or surface charge densities.[35] As AFM can also be applied in liquid, it has become essential in a variety of research fields like material science or cell biology and molecular biology where specimen down to the size of single proteins can be studied in their native aqueous environment.

A typical drawback of the AFM technique is the poorly defined geometry of the cantilever tip that makes it difficult to interpret force-distance data. A step forward was the invention of the so called 'colloidal probe technique' by Butt[36] and Ducker.[37] Here, the tip is replaced by a colloidal particle of well-defined spherical shape. The accessible range of the particle size is between 1-50 µm. The well-defined spherical geometry improves the sensitivity of the measurements as the total force increases due to a larger contact area.[35,38] The measured forces still depend on the actual contact geometry but it remains a difficult task to precisely determine the contact of colloidal objects.[35,39] Therefore there is ongoing effort to develop models for the mechanical contact for AFM force-distance data. In first approximation, the colloidal probe AFM force data is given as a reduced force e.g. the force divided by the particle radius. The measuring principle of the colloidal probe technique is identical to that of a standard AFM (**Figure 2**).

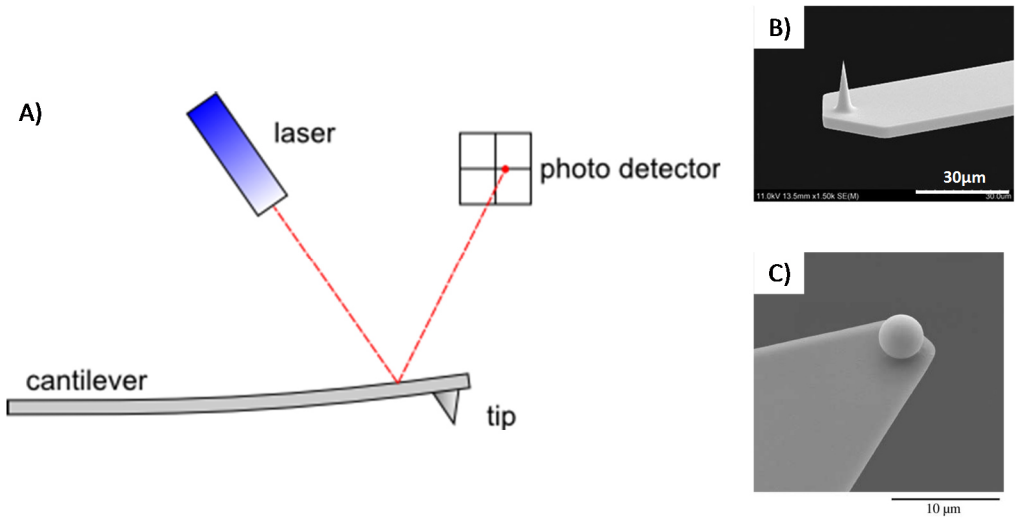

Figure 2: A) Principle of an AFM. The deflection of the cantilever is detected with an optical lever technique. Therefore, a laser-beam is reflected from the cantilever onto the photo detector and the change in position of the laser spot is recorded. B) SEM of a sharp tip on a cantilever with a tip apex of a few nanometers.[40] C) SEM of a silica particle glued on the end of a tipless cantilever.[38]

In a typical force measurement the tip is moved up and down by applying a voltage to the piezoelectric translator and the deflection of the cantilever is measured. The deflection is normally measured by the optical lever technique[41], where light from a laser source is focused on the end of a cantilever and the reflected light is monitored by a position sensitive detector. When a force is applied on the cantilever, the cantilever bends and the reflected light-beam moves on the detector.

The result of such force measurement is the detector signal in volts ΔV, versus the position of the piezo Δz_p, normal to the surface. To obtain a force-distance curve, ΔV and Δz_p, have to be converted into force and distance (**Figure 3**). To calculate the cantilever deflection z_c from the detector signal, a conversion factor is needed which can be obtained from the slope of the deflection signal versus piezo position curve. The tip-sample separation (distance) D is then calculated by adding the deflection to the piezo position: $D = z_p + z_c$. The force F is obtained by multiplying the deflection of the cantilever with its spring constant k_c: $F = k_c z_c$.

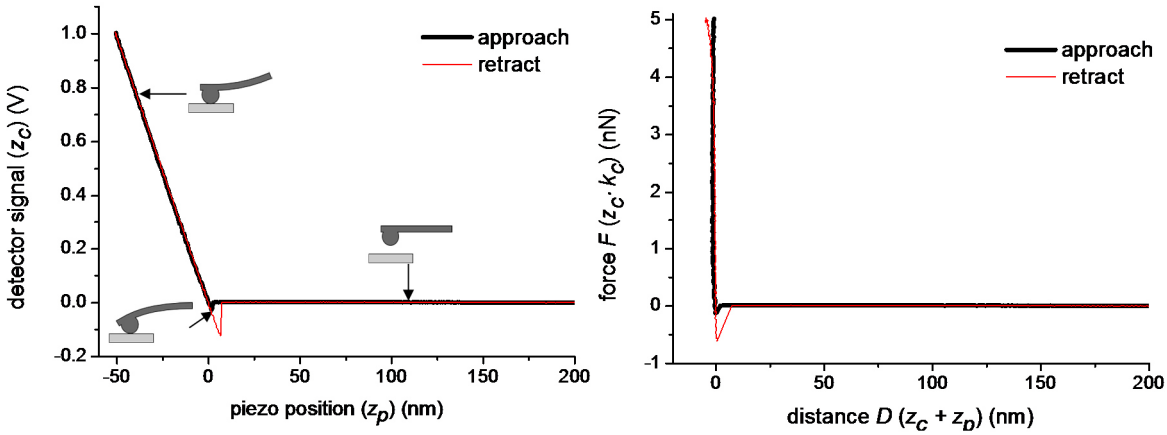

Figure 3: A typical cantilever deflection vs. piezo height (z_c vs z_p) (left) and corresponding z_c vs. D plot.

To obtain the spring constant of the cantilever, it has to be calibrated. In principle, the spring constant can be calculated from the material properties and the geometry of the cantilever. But the thickness and the modulus of the cantilever are difficult to determine. Therefore, it is desirable to determine the spring constant experimentally. Often a reference cantilever with a known spring constant is used. When pressing the cantilever against the reference one, the spring constant can be calibrated from the deflection.[42] Hutter and Bechhoefer introduced an elegant and widely used method based on the fluctuation of the cantilever due to the thermal noise.[43]

Before the measurements can be done, the colloidal probe has to be attached to the end of a cantilever. Theoretically every material that can be glued can be used. It is preferable to use spherical particles with a smooth surface as this minimizes the influence of surface roughness. Commercially available particles are usually coated with a layer of adsorbed molecules which helps to keep them in dispersion.[35] Most widely used are silica particles as they have a low surface roughness and are commercially available in different sizes. In our case functionalized PEG particles are used that have a neutral backbone and can be easily made by precipitation polymerization. The attachment of the particle can be done with an optical microscope attached to the AFM. First a small amount of epoxy glue is placed on the end of the cantilever and then the cantilever is moved to a particle. It should be ensured that no glue is on the bottom of the particle which leads to contamination and false results. Before the adhesion measurements with the glued probe one has to wait until the glue is hardened.

1.2.1. Adhesion Force Measurements

A main parameter in this thesis that is measured by the developed techniques is *adhesion.* Generally adhesion is a phenomenon that takes place between two similar or dissimilar interfaces. In the context of this work it is important to note that the overall adhesion between two interfaces is not only governed by the surface forces, like electrostatic or dispersion forces, etc. For deformable materials like hydrogels also the deformation of the bodies in contact affects their mutual adhesion (see eq. 11). In the biosciences and material science the adhesion interactions between two interfaces are evaluated by measuring the force required to separate the adhering bodies. On the microscopic level this type of measurement is conducted *via* the Surface Force Apparatus (SFA), Atomic Force Microscope (AFM), optical tweezers and micropipette aspiration. The theoretical concept behind these adhesion measurements will be discussed in the following with special focus on deformable probes which is the general case for natural adhesion phenomena.

Derjaguin approximated that the interaction force F between a flat surface and a sphere with radius R is related to the interaction energy $W(d)$ per unit area:[44]

$$F(d) = W(d)2\pi R \tag{1}$$

where d is the distance between the two surfaces. From this relationship it can be seen that a larger radius results in a higher force. To compare force curves it is useful to normalize the forces by the radius

$$\frac{F(d)}{R} = W(d)2\pi \tag{2}$$

thus the interaction energies can be obtained independently of the interaction geometry. Several theories describe the elastic deformation of the sample. Differences in the relations between the applied load F and the contact radius a or the deformation δ is due to the role played by the adhesion in the considered system. The three most commonly used theories have been developed by Hertz[45], Johnson, Kendall and Roberts (JKR)[46] and Derjaguin, Müller and Toporov (DMT).[47] In 1882, Hertz solved the contact problem of two elastic bodies with curved surfaces. The relationship between the load F and the contact radius a is

$$a = \sqrt[3]{\frac{RF}{K}} \tag{3}$$

where R is the radius of the particle, K is the reduced elastic modulus

$$\frac{1}{K} = \frac{3}{4}\left[\left(\frac{1-v_{tip}^2}{E_{tip}}\right) + \left(\frac{1-v_{sample}^2}{E_{sample}}\right)\right] \tag{4}$$

and v the Poisson ratio. Considering a hard sample or a hard tip, one of the moduli E will be infinite and the term approaches 0. With increasing load F the contact area increases. When no load is applied there is no contact area and the contact radius a equals 0. The relationship between the indentation δ and the contact radius a is

$$\delta = \frac{a^2}{R} = \left(\frac{F^2}{RK^2}\right)^{1/3} \tag{5}$$

In the Hertz model the surface forces between the contacting interfaces are neglected, whereas the two other theories take account of them. Therefore, the Hertz theory can only be applied when the adhesion forces are much smaller than the mechanical forces. In the DMT model, surface interactions outside the contact zone are included, predicting a somewhat larger contact radius and adhesion force. They apply to rigid systems, low adhesion and small radii of curvature.[48] They account for long-range attraction around the periphery of the contact area, but constrain the tip-sample geometry to remain Hertzian. The relationship between the load F and the contact radius a is

$$a = \sqrt[3]{\frac{R}{K}(F + 2\pi RW)} \tag{6}$$

where W is the adhesion work per unit area. The relationship between the indentation δ and the contact radius a is

$$\delta = \frac{a^2}{R} = \frac{(F + 2\pi RW)^{2/3}}{\sqrt[3]{RK^2}} \tag{7}$$

In short, the DMT model is the Hertz model with an offset due to surface forces. The deformation and the contact radius increase due to adhesion. In the case that adhesion is

absent, the contact radius remains Hertzian again. When no load is applied the contact radius has a finite value

$$a_0 = \sqrt[3]{\frac{2\pi W R^2}{K}} \tag{8}$$

When the sphere is unloaded (negative load) from the surface, the contact radius and the deformation decrease till they equal 0 ($a = \delta = 0$) (no hysteresis) and the adhesion force is

$$F_{adh} = -2\pi RW \tag{9}$$

The DMT theory can be applied in the case of small tips and stiff samples with small surface forces. In the DMT model the contact area can be underestimated due to the restricted geometry.

The JKR model predicts the adhesion between particles and a substrate, assuming that all materials deform elastically and all interactions occur within the contact zone. When the surfaces are not in contact, there are no forces between them, upon contact short-ranged attractive forces appear within the contact area, and the tip-sample geometry is not constrained to remain Hertzian. This set of assumptions applies well to highly adhesive systems that have large radii of curvature and low stiffness. During unloading, a connective neck is formed between the tip and sample, and the contact is ruptured at negative loads (**Figure 4**). This causes adhesion hysteresis. The relationship between the load F and the contact radius a is

$$\mathrm{a} = \sqrt[3]{\frac{R}{\mathrm{K}}\left(F + 3\pi RW + \sqrt{6\pi RWF + (3\pi RW)^2}\right)} \tag{10}$$

and the indentation δ and the contact radius a is

$$\delta = \frac{a^2}{R} - \frac{2}{3}\sqrt{\frac{6\pi Wa}{K}} \tag{11}$$

Here again, the JKR model is the Hertz model with an offset due to surface forces. The deformation is reduced due to the adhesion but the contact radius increases. When no

adhesion is present, the contact radius remains Hertzian. When no load is applied, the contact radius has a finite value

$$a_0 = \sqrt[3]{\frac{6\pi W R^2}{K}} \tag{12}$$

and a deformation of

$$\delta_0 = \frac{a_0^2}{3R} \tag{13}$$

Using eq. 11 it can be show that when an increasingly negative load is applied on the two surfaces, at a critical point the surfaces detach and the resulting adhesion force F_{adh} or 'pull-off-force' is[49]

$$F_{adh} = -\frac{3}{2}\pi R W \tag{14}$$

The JKR theory can be applied in the case of large tips and soft samples with large adhesion interactions. This model will be also used in this work as it describes highly elastic soft colloidal probes with large contact radius better than the DMT model.

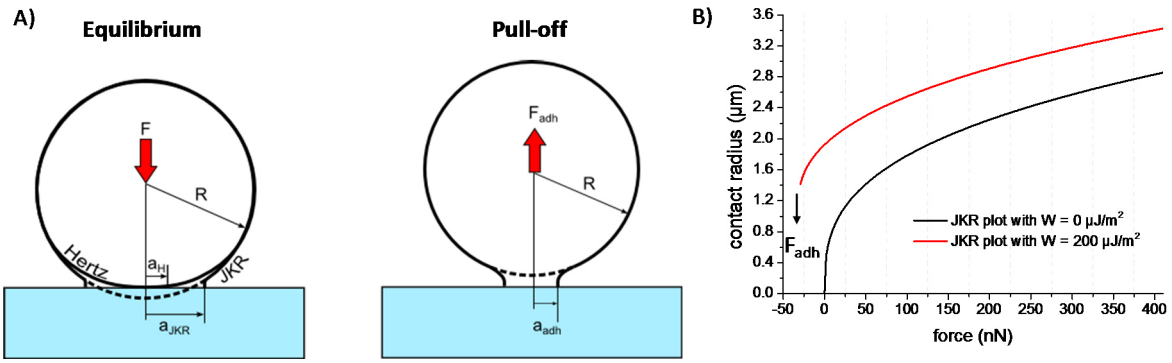

Figure 4: A) Schematic illustration of the different geometries of deformable elastic spheres of a typical JKR-type loading and unloading. B) Contact radius vs force curves for the JKR model with and without adhesion with E=330 kPa, R=33 µm and ν=0.5. The red plot shows that at a certain force F_{adh} the probe has to detach with a certain contact radius a_{adh}.

1.3. Reflection Interference Contrast Microscopy (RICM)

By means of optical methods, adhesion can be quantified by measuring the mechanical deformation of the adhering bodies *via* Reflection Interference Contrast Microscopy (RICM). RICM is an interferometric technique that allows the determination of the vertical distance and of the contact area between the interfaces.[50] RICM was initially devised from Adam Curtis in 1960 in order to study the interaction of cells with a glass substrate under water by using an optical microscope.[51] He named this technique 'interference reflection microscopy' (IRM). Later the technique has been improved by Ploem *et. al.* by introducing the antiflex method to enhance the optical contrast.[52] Sackmann *et. al.* showed in the 1980s that the related technique of RICM has improved contrast by studying the inter-surface distance between planar transparent substrates and objects with better optical properties like colloidal beads[53,54] and lipid vesicles.[55] The image recorded is a two-dimensional matrix of intensities known as Newton rings. Its main advantage is the simplicity of the setup as it can be implemented with relative ease and very little investment on a standard inverted microscope and it does not require any labeling of the sample. A standard version of a RICM set-up consists of a light source, an inverted microscope equipped with an antiflex objective and a CCD camera. The optical configuration of the microscope for obtaining the RICM images is illustrated in **Figure 5**.

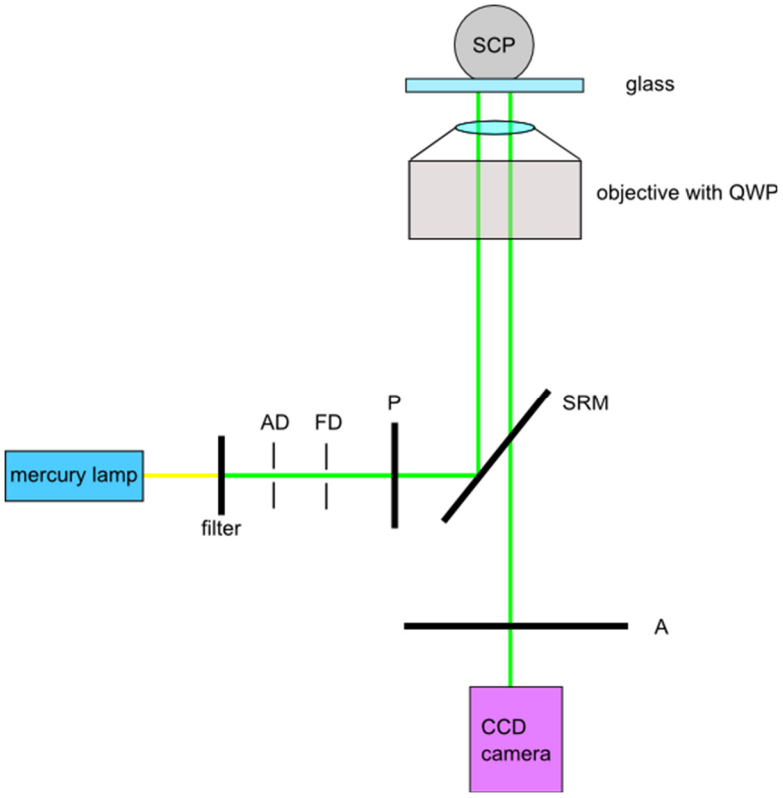

Figure 5: Typical experimental set-up and optical path for RICM. AD: aperture diaphragm; FD: field diaphragm; P: liner polarizer; QWP: quarter-wave plate; SRM: semi-reflecting mirror; A: analyzer

Here, the incident light from a high-pressure mercury lamp passes first trough a filter to separate the monochromatic light with a wavelength of 546 nm. The light beam passes two adjustable diaphragms, namely the aperture diaphragm (AD) and the field diaphragm (FD), which are positioned with respect to the sample and objective to realize a Köhler illumination that generate an extremely even illumination.[50] Then, the light passes a linear polarizer to a semi-reflecting mirror (SRM) and follows its trajectory through a quarter wave plate (QWP) located in front of the objective. This optical system converts the light from linearly polarized into circularly polarized light, which is subsequently transmitted and reflected by the glass substrate and the object. The reflected light beam passes the quarter wave plate a second time and becomes linearly polarized, with a switch on its direction of 90° with respect to the incident light. The change on the light direction allows to separate the reflected light by the samples from the stray light reflected on the components of the microscope, by means of crossed analyzer located in front of the detector. Finally, the CCD camera captures the image that represents the periodic variation of the intensity, which yields the vertical distance between the SCP and glass substrate.

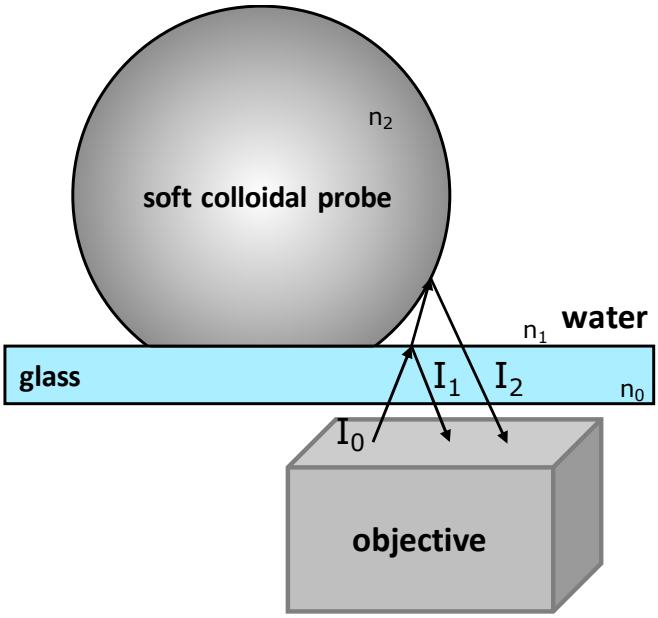

Figure 6: Schematic representation of the RICM principle and the resulting interference pattern of a SCP on a surface

The basic principle of interferometry is shown in **Figure 6**. Polarized light waves reflected from the upper glass surface (I_1) and the surface of the bead (I_2) interact to create an interference image. The intensity at a given position in the image depends on the separation h(x) between the two surfaces:

$$I(x) = I_1 + I_2 + 2\sqrt{I_1 I_2}\cos(2kh(x) + \pi) \qquad (15)$$

where $k = 2\pi n/\lambda$, and n and λ are the index of refraction of water and the wavelength of the monochromatic light, respectively. In order to detect the interference pattern, stray light was reduced by the antiflex technique.

The reflected beam I_2 travels an optical distance of $2dn_1\cos(\theta)$ more than the beam I_1, by going through the thin film of the medium with thickness d, where n_1 represents the refraction index of the medium and θ its refraction angle. In addition, as the probe has a refraction index higher than water, the light beams reflected at this interface undergoes a phase reversal. Thus, the optical path difference between the beams I_1 and I_2 increases by $2dn_1\cos(\theta + \lambda/2)$. When it is a multiple of the wavelength of the incident beam ($m\lambda$), the reflected beams are aligned peak to peak, giving a maximum of intensity in the obtained image. In the above example, a maximal intensity is obtained when the distances between the interfaces is $d = \lambda/4n_1$. By increasing or decreasing the interfacial distance beyond this value, the reflected beams come out of phase, producing an image with less intensity. A

minimum in the intensity or darkest area are present in the image, when the reflected beams are aligning peaks to trough. The superposition of the beams in this configuration is given if their optical phase difference is (m + ½) λ. In this sense, the first minimum is generated when the soft colloidal probe and the glass substrate are in contact. These innovations make RICM a very powerful technique to study inter-surface interactions, in particular adhesion, and it can be also combined with several other microscopy techniques like AFM.[56]

2. Aims and Outline

Many processes in cell biology are governed by molecular interactions at interfaces. For example, cell surfaces play a crucial role in cellular processes such as signaling, communication, sensing, adhesion, and viral or bacterial infections.[57] Every process of the cell surface relies on molecular forces that are a complex interplay of chemical, biological and physical interactions. Typical interactions occurring at biological surfaces include hydrophobic, hydrophilic, electrostatic, Van der Waals and hydrogen bonding interactions.[58]

Specific interfacial interactions are typically mediated by ligands and receptors, which control the adhesion process of cells. In particular, carbohydrate ligands are highly relevant in many cellular interactions as they control a myriad of cellular processes [59] It has been long thought that the large amount of carbohydrates in the cells surrounding, the glycocalyx, merely presents a physical barrier. However, there is growing evidence that the glycocalyx is associated with many controlled processes such as signaling, adhesion or inflammation.

The most relevant binding partner for cell carbohydrate ligands are lectins which are protein receptors specifically interacting with carbohydrates. In general, single carbohydrate ligands bind only very weakly to their corresponding protein receptor, with low affinity usually in the millimolar range (see chapter 5.2.4). To achieve biologically relevant binding, multivalency is often involved in natural carbohydrate recognition events where several carbohydrate ligands are presented in close proximity allowing for strong binding to the according protein receptor.[59] This principle not only applies for natural surfaces, but non-natural interfaces functionalized with monovalent ligands or receptors can act as multivalent systems purely based on the immobilization of the monovalent agents at the interface. However, the exact binding mechanisms involved in such multivalent interfacial adhesion processes are so far only poorly understood.[60,61] For example, carbohydrate/protein interactions do not only depend on the affinity and concentration of the interacting molecules, but they are also influenced by the physical and chemical properties of the biointerface, e.g. ligand density and mechanical properties. Thereby, nature uses a complex interconnection between these three factors: affinity, ligand density and elasticity, as the perfect mechanism to regulate biomolecular interactions at interfaces. It has been proposed that these factors are associated cooperatively to enhance the biomolecular interactions.[62]

One limiting factor towards a fundamental understanding of ligand-mediated adhesion is the applicable methods. So far interaction forces at interfaces have been measured by surface

force apparatus (SFA), atomic force microscopy (AFM)[35] or reflection interference contrast microscopy (RICM).[50,63] These methods allow to directly measure the strength of weakly adherent surfaces as it is necessary for determining cell surface related adhesion processes. However, usually the contact area is ill-defined and cannot be independently determined thus hampering precise determination of adhesion energies.[64] To overcome this problem, micrometer sized colloidal particles have been used and attached for example to an AFM cantilever (colloidal probe AFM). Typically silica particles or plastic beads with a diameter of 1-50 µm are used. However, these are hard, non-elastic materials and thus have only little biological context and do not allow to study the proposed interconnection of all three factors - affinity, ligand density and elasticity. Furthermore, the contact area of hard colloidal particles is small and the contact geometry is still unknown so that the determination of adhesion forces is inaccurate.

Therefore, in order to overcome the limitations of current methods and to gain new insights into ligand-mediated adhesion, soft colloidal probes should be used and combined with different techniques such as RICM and AFM in order to allow high sensitivity measurements of adhesion forces in soft material and living tissue.

Thus, in a first part of this work, PEG based hydrogel particles are synthesized as novel soft colloidal probes (SCPs) as they are biocompatible, highly water swollen and have non-adhesive properties towards proteins and cells (see chapter 3). The mechanical properties of PEG-based hydrogels can be easily controlled by varying the molecular weight of PEG or the initiator concentration and will allow for the investigation of the influence of the mechanical properties on the adhesion process.

In a next step, SCPs will be modified in order to introduce different functionalities to induce both, specific and unspecific, surface interactions. For the modification of PEG SCPs; a synthetic route based on radical chemistry will be adopted to introduce different functionalities on PEG SCPs such as carboxylic or amine moieties. These functionalities can then be applied for further functionalization with a large variety of molecules such as sugar ligands and protein receptors.

The major part of this work will then focus on the use of differently functionalized SCPs in combination with RICM and AFM to perform adhesion studies. Due to their elastic properties, SCPs will deform upon adhesion on a glass surface, e.g. mediated by specific ligand/receptor interactions. This deformation can be optically detected and directly correlated to the adhesion energy. This basic principle will allow for the direct measurement of adhesion between a large variety of modified SCP and glass surfaces. Special focus is

devoted to the carbohydrate ligand/lectin interactions, specifically the interactions of Mannose and ConA as well-established model system. As the physical properties of the SCPs are tunable, probes with different Young's moduli and functionalization degrees can be prepared and the influence of these parameters can be then directly analyzed in adhesion measurements giving new insights into the correlation of these factors.

Furthermore, this method allows for inhibition measurements by addition of specific inhibitors interfering with the adhesion of the SCP. Concentration dependent inhibition experiments will determine relative affinities of various ligands and study potential multivalent effects of the analyzed molecules in competition with the polyvalent ligand presentation on the SCP or glass surface. In comparison to current inhibition assays e.g. performed *via* Surface Plasmon Resonance (SPR), this method can be expected to present a number of benefits such as high sensitivity, robustness, cost efficiency and direct insights into specific binding of soft biointerfaces, e.g. ligand presenting hydrogels.

To further advance the method, the optical detection of SCP adhesions will be combined with AFM force spectroscopy. Attaching the SCP to a tipless cantilever allows for the direct measurement of adhesion forces between ligand-modified SCPs and receptor-modified surfaces, studying the displacement kinetics of initially bound ligands as well as analyzing the effect of external forces on ligand/receptor interactions. By employing soft interfaces in the AFM force assays, new insights into bio-adhesion can be obtained.

Overall, this thesis aims at developing a platform of sensors based on soft colloidal probes and to show their potential in a variety of assays such as direct adhesion measurements, inhibition assays and force spectroscopy. Through the control of the SCP properties and functionalization, new insights into the interplay of affinity, ligand density and elasticity as a mechanism to regulate biomolecular interactions at interfaces can be expected. Special focus is devoted to the sugar ligand/lectin receptor interactions, as they are known to play an important role in many cell-adhesion mediated phenomena, but their multivalent interactions at interfaces are not yet well understood.

3. Synthesis and Characterization of PEG SCPs

A major objective of this work is to measure ligand/receptor interactions that take place at surfaces. There are three factors controlling the strength of adhesion: affinity, flexibility and the ligand density. The existing methods usually measure those interactions in solution or at hard surfaces. This lacks the biological context of flexible or soft interfaces and does not allow measuring the influence of the flexibility of soft interfaces on adhesion. To To obtain well defined sensitive probes, soft hydrogel microparticles with optimized material properties have been synthesized in this work for RICM and soft colloidal AFM measurements. These allow for the direct measurement of adhesion at soft interfaces by electrostatic interactions, hydrophobic interactions or interactions between a ligand and a receptor. Therefore, the envisioned soft colloidal probes have to fulfill certain requirements. First, they have to be in the size range of 10-50 µm and to be observable *via* optical microscopy and of well-defined spherical shape. Second, the probes should be highly elastic to form a large contact area between the probe and the sample as well as to mimic the elastic properties of biological tissue and cells. Moreover, a high compliance of the probe increases the sensitivity of the AFM and RICM measurements. Third, the probe should have no unspecific interactions towards proteins and cells so that the probes have no influence on measuring specific adhesion. Fourth, the surface of these probes should be modifiable to obtain functionalized particles for the measurements of electrostatic or hydrophobic interactions or for the attachment of biological ligands for the measurements of specific interactions.

In this thesis, PEG hydrogels were chosen as suitable material for SCP synthesis (see chapter 1.1.3). The lack of hydrogen bond donating groups, a feature that has been shown to be critical in reducing non-specific interactions, sets PEG apart from many other hydrogel materials. The high water content of the material contributes to its biocompatibility. PEG has non adhesive properties towards cells or proteins and thus should avoid any kind of non-specific interactions during adhesion measurements. Furthermore, PEG can be easily end-group functionalized to obtain chemically cross-linked microgels.

In order to form a PEG hydrogel, PEG chains have to be end-group functionalized allowing for a cross-linking. Commonly used are acrylate or acrylamide end-group functionalities that can be polymerized *via* radical reactions and lead to covalently cross-linked hydrogels. Here, a PEG-diacrylamide macromonomer was chosen as precursor.

In the next step, hydrogel particles of the right size have to be prepared. Generally, there are different possibilities for particle preparation such as emulsion or dispersion polymerization. Here, the so called 'salting-out' approach was used. The PEG-macromonomers are dissolved in a kosmotropic sodium sulfate solution and form micrometer sized droplets of higher PEG concentrations due to the limited solubility of the polymer. This ability is related to the lower critical solution temperature (LCST) of a polymer in solution and can be measured by turbidimetric measurements. Through addition of a photoinitiator the droplets can be polymerized by UV irradiation. The particles were then characterized by optical light microscopy measuring their size distribution as well as by AFM for the Young's modulus measuring the particle elasticity.

3.1. Synthesis of PEG SCPs *via* Precipitation Polymerization

PEG microgels were synthesized from the telechelic macromonomer PEG-diacrylamide (PEG-dAAm). The synthesis of PEG-dAAm was described previously by Hartmann *et. al*[65] as adapted from Elbert and Hubbell.[66] Here, an acrylamide instead of the more common acrylate (PEG-dAc) was chosen in order to obtain a stable amide linkage in the resulting hydrogel avoiding the risk of ester hydrolysis as a possible degradation reaction during functionalization and storage.[67] PEG-dAAm can be readily polymerized by radical initiation leading to highly cross-linked hydrogels. To produce the PEG-dAAm, first PEG-diamine was synthesized (**Scheme 2**). Therefore, commercially available poly(ethylene glycol) of four different molecular weights (M_n of 1450, 4600, 8000 and 20000) presenting terminal hydroxyl groups were transformed into the dimesylate precursor. By varying the molecular weight and thereby the chain length of the macromonomer as well as the cross-linking density the resulting mechanical properties were controlled. The conversion of the alcohol to a mesylate group is straightforward, and 100% conversion can be routinely achieved. The presence of a mesylate group on the PEG terminus was detected by NMR, based on the presence of a singlet at 3.1 ppm, corresponding to the protons on the methyl group (chapter 8.1).

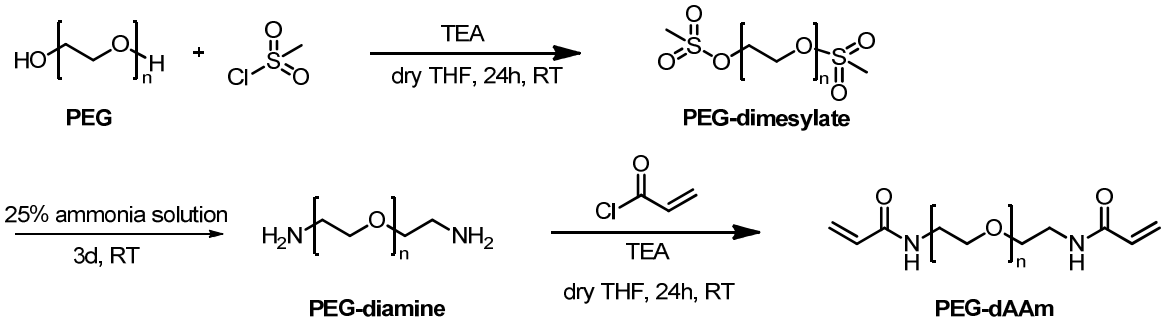

Scheme 2: Synthesis route of end-group functionalized PEG for SCP preparation

The PEG-dimesylate was dissolved in 25% ammonia solution and the reaction flask was tightly sealed. The reaction was stirred for three days. During this time, the color of the solution changed from orange to yellow. The yields of PEG-diamines increased with molecular weight. This can be explained with the less amphiphilic character of PEG with higher molecular weights. During the extraction, the mixture forms an emulsion due to the interaction of the polymer with both, the aqueous and the organic phase. Addition of NaCl and the use of smaller portions of dichloromethane helped to minimize the loss of product due to emulsion formation. The presence of an amine group on the PEG terminus was detected by NMR, based on the presence of a triplet at 2.9 ppm, corresponding to the protons on the carbon in the alpha position relative to the amine (chapter 8.1). The diamine was then reacted with acryloyl chloride to obtain the final PEG-dAAm. THF is an ideal solvent for this reaction because the resulting TEA hydrochloride precipitates in this solvent and can be easily separated by filtration. The presence of the double bonds on the PEG terminus was detected by NMR, based on the presence of peaks in the range of 5.6 - 6.3 ppm (chapter 8.1). For the PEG-dAAm with M_n = 1450 Da, different equivalents were used and as a result the product was not pure enough after precipitation, and an additional purification step was performed. The PEG-dAAm with the molecular weight of 20000 Da showed also some ester formation as byproducts that can be seen in the NMR (chapter 8.1). This might result from an incomplete amine formation during synthesis as traces of water are also able to react with the mesylate groups.

The conversion of all reaction steps was followed by NMR as well as IR (**Figure 7**). The IR indicated that the characteristic S-O band at 1174 cm^{-1} decreased during the amine formation. The final conversion of the amine results in the amide band formation at 1664 cm^{-1} (Amide I) and 1546 cm^{-1} (Amide II).

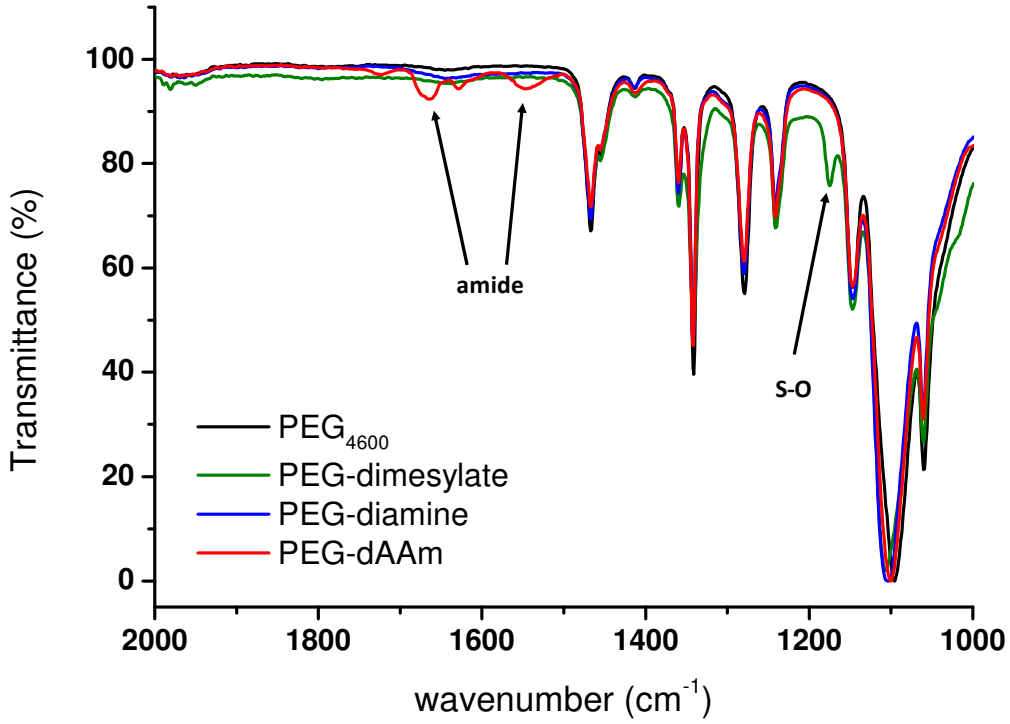

Figure 7: Zoomed ATR-FTIR spectrum for the end-group modification of PEG (Mn = 4600 Da) with its characteristic bands

The conversion of the end-groups to the final acrylamide was obtained with a 100% yield as confirmed by NMR. These macromonomers can be now used for the preparation of microparticles.

Bisacrylamide macromonomers can be easily radically polymerized to obtain a highly cross-linked hydrogel network. For the use as SCPs, hydrogels need to be obtained as hydrogel particles in the size range of 10-50 µm. To obtain such microparticles, a method was developed allowing for suitable-sized droplets that can be further polymerized. Solution-phase methods such as precipitation/dispersion or emulsion polymerization are highly scalable but often require the use of organic solvents, surfactants or other additives that may negatively impact purity and biocompatibility.[68] Due to the ability of PEG to resist unspecific protein adsorption, it would be desirable to produce PEG microparticles by a method that does not rely on organic solvents or surfactants, as they may be difficult to remove later. PEG-dAAm has the ability to precipitate in aqueous solution at elevated temperature when water becomes a poor solvent for PEG.[69] The temperature of the phase transition is called lower critical solution temperature (LCST) or cloud point. In the presence of kosmotropic salts like sodium sulfate, the temperature of the cloud point can be lowered to less than room temperature. The lowering of the LCST or the 'salting out potential' of salts can be estimated from the Hofmeister series.

The Hofmeister series is a classification of ions based on their relative influence of ions on the physical behavior of a wide variety of aqueous processes ranging from phase behavior of macromolecules[70,71] to protein folding.[72] This behavior is more pronounced for anions than cations.[70] The typical order for the anions is as follow:

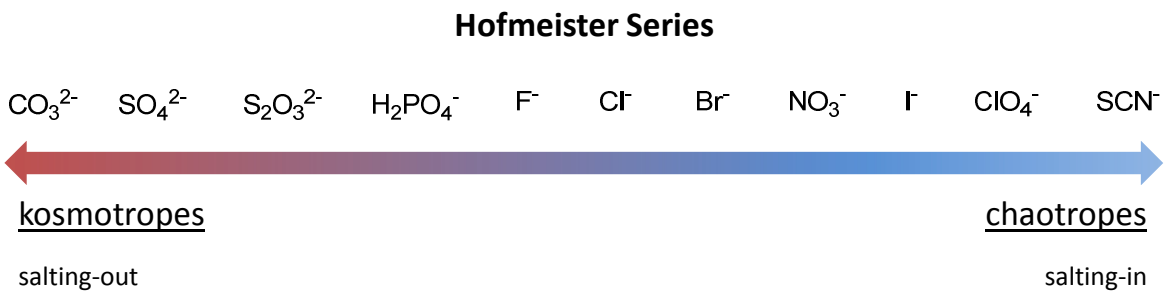

Figure 8: The Hofmeister series show the classification of anions based on their influence on the precipitation of proteins and polymers

The species to the left of Cl^- are referred to as kosmotropes, which tend to precipitate proteins from solution (salting-out) and prevent protein unfolding. Those to its right are called chaotropes, which increase solubility (salting-in) and promote the denaturation of proteins.

Poly(ethylene glycol) (PEG) is a thermoresponsive polymer that separates in a PEG-rich phase and a salt-rich phase in an aqueous solution containing salts. An aqueous solution of PEG macromolecules with an average molecular weight of 20 kDa has a LCST of 112°C.[73] The effectiveness of salts inducing the formation of two phases in PEG solutions also correlates with lowering their LCST in dilute solutions of PEG. The mechanism of the phase separation in PEG solutions is attributed to the competition between the formation of water-PEG and water-water hydrogen bonds.[74] The oxygen in the polymer chain interacts with water molecules to form a hydration layer around the polymer. If a well hydrated anion approaches this hydrophilic surface, the interaction of water molecules with the oxygen in the polymer chain will be reduced. Therefore, the polymer will be less soluble in the presence of well hydrated anions.[75]

This ability can be used to form droplets in aqueous solutions at room temperature. In order to find the optimal conditions and evaluate the influence of salt concentration on the droplet formation, the cloud point at different concentrations and temperatures has to be measured. To determine the cloud point, turbidimetric measurements were performed.[76] Turbidimetry is a chemical analysis based on the phenomenon whereby light, passing

through a medium with dispersed particles of a different refractive index from that of the medium, is lowered in intensity by scattering. In turbidimetry, the intensity of light transmitted through the medium is measured. The results of these measurements give the conditions where droplets are formed. Using the information obtained from these measurements, optimized conditions for particle synthesis by dissolving PEG-dAAm and a water-soluble photoinitiator in salt solution were determined.

The cloud point of PEG-dAAm in sodium sulfate solutions was determined at different concentrations of polymer and salt. **Figure 9** shows the results for the turbidimetric measurements of the PEG M_n = 4600 Da macromonomer.[76] As expected, the cloud point can be lowered by increasing the sodium sulfate concentration or the concentration of the PEG-dAAm. This can be attributed to the direct interactions of the sulfate anions with the polymer and its adjacent hydration shell. Raising the temperature increases the hydrophobicity of the polymer chains and leads to their aggregation and precipitation as water becomes a poorer solvent for PEG-dAAm.

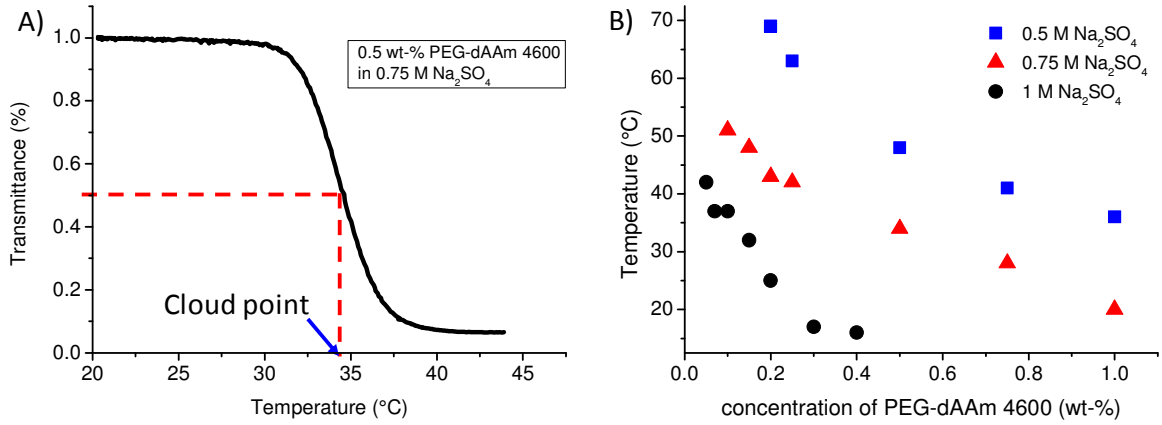

Figure 9: A) Typical curve for the determination of the cloud point. The cloud point was defined at 50% transmittance. B) Turbidimetric measurements of PEG-dAAm (M_n = 4600 Da) in sodium sulfate solutions at different concentrations.

For example, the cloud point of PEG-dAAm is decreased from 42°C to 15°C at a 1 M sodium sulfate solution by increasing the polymer concentration from 0.02 wt-% to 0.3 wt-%. This allows for the formation of stable droplets even at RT as a turbid dispersion is immediately formed after mixing the components (**Figure 10**). Taking the information from the turbidimetric measurements, the following standard particle synthesis protocol was established: At a polymer concentration of 0.5 wt-% PEG-dAAm and a 1 M sodium sulfate solution the cloud point was lower than RT, and just by shaking a turbid dispersion of PEG-

dAAm droplets was formed. In order to covalently cross-link the macromonomers, a water-soluble photoinitiator (Irgacure 2959) was added to the macromonomer solution at a concentration of 0.01 wt-% and polymer droplets were photopolymerized with UV light for 90 s.

It is noteworthy that the PEG-dAAm droplet dispersion is stable for several hours until complete phase separation was observed. The phase-separated domains grow in size by coalescence. Ultimately, this leads to an aqueous two-phase system with two layers, a PEG rich phase (top) and a water-rich phase (bottom).

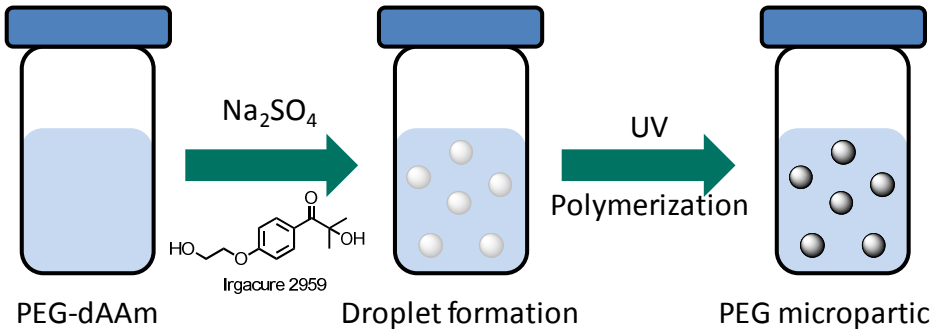

Figure 10: Schematic presentation of the PEG microparticles preparation *via* precipitation polymerization in a sodium sulfate solution

The resulting cross-linked particles are stable and do not dissolve in water anymore. Optical light microscopy (chapter 3.2) showed size distributions in the range of 10-50 µm in dependence of the molecular weight of the macromonomers. The influence of the reaction parameters on the resulting particle sizes was studied by variation of the salt concentration (0.5 M to 1 M) as well as the molecular weight of the macromonomers.

Table 1 summarizes the results: smaller particles with mean diameters around 6 µm can be obtained at a salt concentration of 0.5 M and 60°C. An increase of the salt concentration to 0.75 M leads to a drop of the cloud point to 35°C and results in particles with a larger mean diameter of around 27 µm. Here again an increase in salt concentration leads to a decrease in solubility of the PEG macromonomers and thus to the formation of larger droplets and accordingly larger hydrogel particles. A further increase in particle size up to 60 µm can be obtained by increasing the molecular weight of the PEG-dAAm from 4600 to 20000 Da.

Table 1: Particle size of PEG hydrogel particles synthesized at different salt concentrations and with different PEG-dAAm molecular weights

M_n PEG-dAAm [Da]	PEG-dAAm conc. [wt-%]	Sodium sulfate conc. [M]	Mean diameter [µm]
1450	0.5	1	15 ± 5
4600	0.5	0.5	6 ± 1
4600	0.5	0.75	27 ± 6
4600	0.5	1	29 ± 6
8000	0.5	1	52 ± 16
20000	0.5	1	60 ± 20

One has to keep in mind that the obtained particles are highly polydisperse and the mean diameters are a calculation based on around 100 particles. But in general it can be seen that at higher molecular weights of PEG-dAAm the particles get bigger and at lower salt concentrations and higher temperatures the particles sizes are lowered.

An efficient cross-linking strategy of PEG-dAAm droplets is required in order to impart mechanical stability to the final SCPs and to avoid the dissolution of the hydrophilic polymer chains.[77] Furthermore, the degree of cross-linking in the microparticles dictates their elastic properties. For example, a high degree of cross-linking results in a hard microparticle with a brittle structure. In contrast, low degree of cross-linking is associated with softer and highly elastic microparticles. Generally the Young's modulus of polymer hydrogels can be adjusted by changing the cross-linking density as well as the molecular weight of the polymer chains between the cross-links (**Figure 11**). Increasing the molecular weight of PEG-dAAm from 4600 to 20000 Da results in a decrease of the Young´s modulus from 80 to 15 kPa as expected, because it results in decreased cross-link density. For the adhesion measurements, PEG SCPs with lower Young´s modulus are desired as larger deformation of the SCPs during RICM measurements results in enlarged contact areas, thus strongly increasing the sensitivity of the measurements.

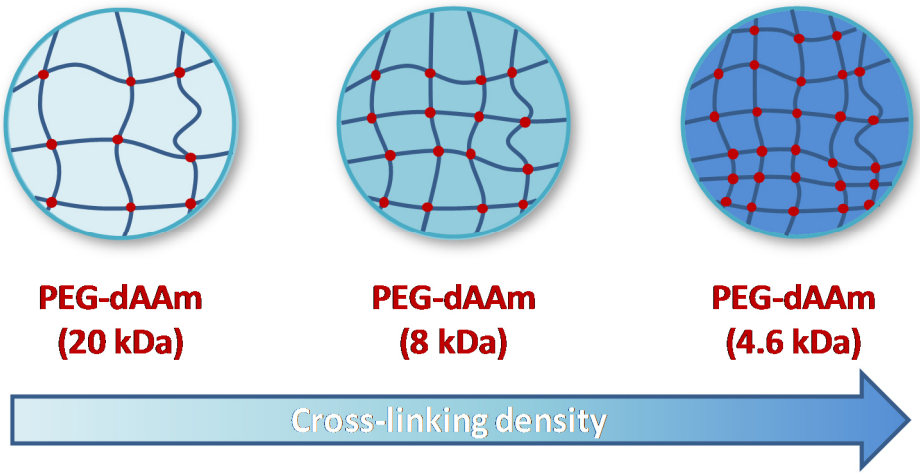

Figure 11: Variation of the cross-linking density by polymerization of PEG-dAAm with different molecular weights.

Instead of changing the molecular weight of the macromonomers to obtain softer SCPs, the ratio of macromonomer to initiator can also be varied, thus changing the resulting cross-linking density and the resulting mechanical properties. PEG-dAAm with a molecular weight of 20000 Da gave SCPs with the lowest Young's modulus. Also the influence of the initiator concentration on the mechanical properties of PEG-dAAm 20000 Da SCPs was investigated. Here, the concentration of Irgacure 2959 was varied (0.005 wt-% and 0.0025 wt-%) compared to the initial concentration (0.01 wt-%). As expected, the Young´s modules of the SCPs decreased with decreasing initiator concentration. In general, reducing the initiator concentration to a quarter of the initial concentration causes a strong decrease of the Young´s modulus by two orders of magnitude. In contrast to this finding, increasing the initial concentration threefold, the Young´s modulus increases only slightly from 15 ± 3 kPa to 22 ± 6 kPa, but remains in the same order of magnitude (**Table 2**). The sharp decrease in Young´s modulus with the reduction of initiator concentration might be explained by incomplete polymerization of the end groups of the PEG-dAAm macromolecules, resulting in SCPs with lower degree of cross-linking. In contrast, the increase of the initiator concentration does not have a major influence on the elastic properties of the sample, suggesting that the initial initiator concentration is optimal for ensuring a complete polymerization of the PEG-dAAm functional groups.

When the Young's modulus of the SCPs was decreased by decreasing the cross-linking density, more transparent particles were obtained. This is expected, as softer microparticles can contain a larger volume of water due to their lower cross-linking density, thus lowering their refractive index. Those very soft SCPs impede the adhesion measurements as their

contrast for optical imaging is very low. However, the variation on the concentration of initiator is a potent approach for the preparation of SCPs with a wide range of elastic properties. The obtained Young's moduli are in the range of the elastic properties found in mammalian cells which range from 0.5 kPa (Neurons) to 25 kPa (skeletal muscle cells).[78–80]

The optimal PEG SCPs for adhesion measurements were obtained from PEG-dAAm macromonomers with a molecular weight of 8000 Da polymerized from a 0.5 wt-% solution in 1 M sodium sulfate solution with 0.01 wt-% initiator, as they show the desired Young's modulus of around 30 kPa, a mean size of 50 µm and have good contrast in microscopy. These systems are therefore used as standard SCPs for the following functionalization experiments as well as for RICM and AFM measurements.

3.2. Characterization of PEG SCP Morphology and Young's Modulus

3.2.1. PEG SCP Morphology

The size distribution of PEG SCPs was determined from the diameter of about one hundred particles measured by optical microscopy (Keyence VHX-100, Germany). The areas of individual microparticles were measured by manually identifying the outer edge. The radius was then calculated from the projected area of the microparticle using ImageJ.

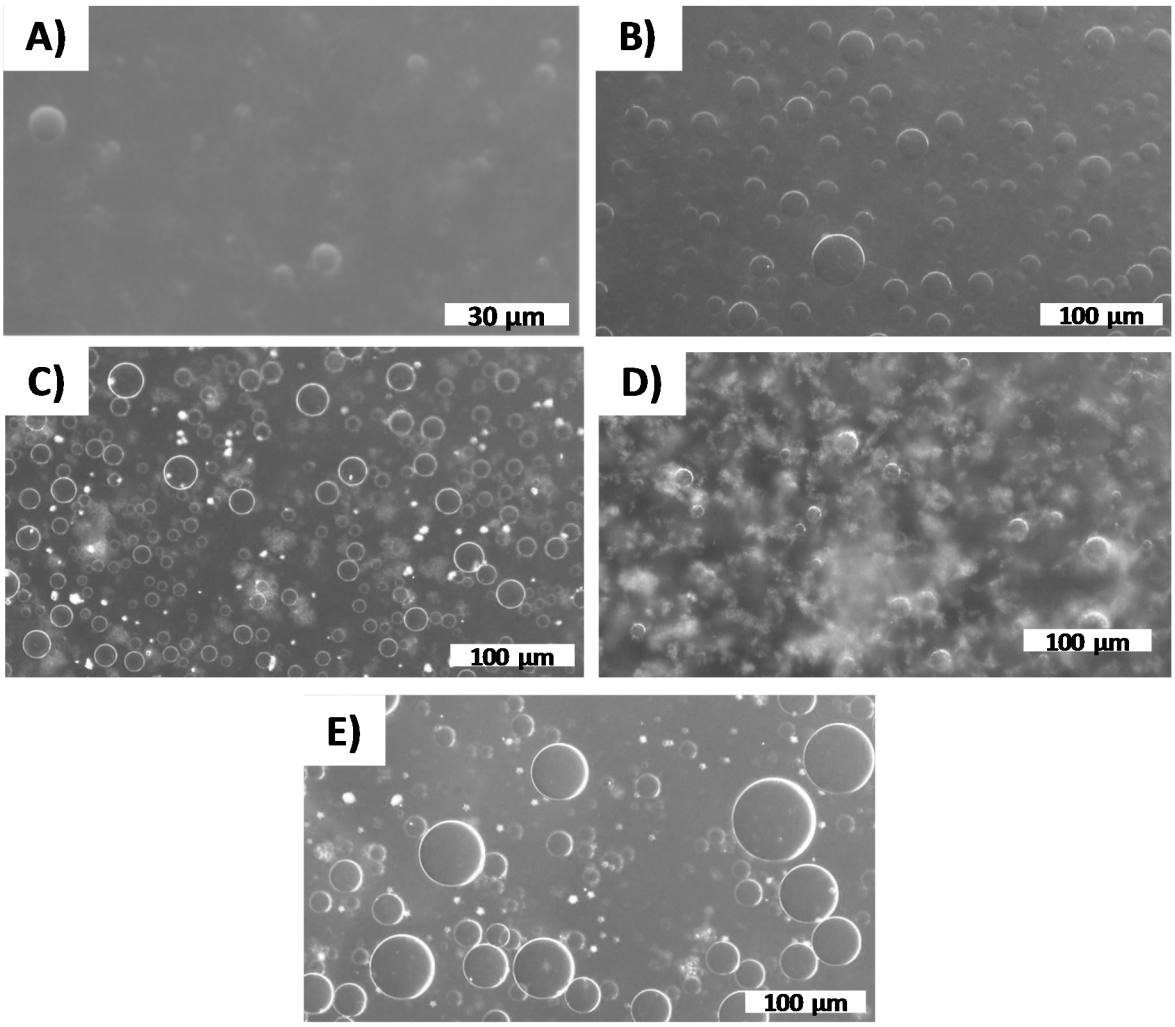

Figure 12: Microscope pictures of PEG-dAAm microparticles and their size distributions formed in different sodium sulfate concentrations. A) 0.5 wt-% PEG-dAAm (M_n = 4600 Da) in 0.5 M sodium sulfate solution. B) 0.5 wt-% PEG-dAAm (M_n = 4600 Da) in 0.75 M sodium sulfate solution. C) 0.5 wt-% PEG-dAAm (M_n = 4600 Da) in 1 M sodium sulfate solution. D) 0.5 wt-% PEG-dAAm (M_n = 1450 Da) in 1 M sodium sulfate solution. E) 0.5 wt-% PEG-dAAm (M_n = 8000 Da) in 1 M sodium sulfate solution.

Figure 12 shows the influence of the salt concentration and the molecular weight on the particles sizes. In all cases a broad size distribution is present. This is expected since the used precipitation polymerization method gives a mixture of larger and smaller particles, as a result of the absence of a stabilizer. At a salt concentration of 0.5 M and a heating of the PEG-dAAm (M_n = 4600 Da) solution to 60°C the size distribution is between 3-9 µm with a mean diameter of 6 ± 1 µm (**Figure 12**A). By increasing the salt concentration to 0.75 M, the particles became larger. Most of the particles have sizes between 25-30 µm and thus a mean diameter of 27 ± 6 µm (**Figure 12**B). A further increase in the salt concentration to 1 M led to a slight increase in the particle sizes of up to 29 ± 6 µm (**Figure 12**C). At a lower

Na_2SO_4 concentration (0.5 M) the polymer showed higher solubility leading to a more amphiphilic character of these polymers. Therefore, many small aggregates were formed in solution and also the average particle size was smaller compared to the dispersion with higher Na_2SO_4 concentration (1 M).

When lower molecular weights are used, e.g. PEG-dAAm of 1450 Da, the particles were getting smaller in size and a mean diameter of 15 ± 5 µm was obtained (**Figure 12**D). By increasing the molecular weight of the PEG-dAAm to 8000 Da, the particles increased in size. In this case most of the particles were in the range of 35-70 µm with a mean diameter of 52 ± 16 µm (**Figure 12**E). Sizes of 60 ± 20 µm were obtained when PEG-dAAm of the molecular weight of 20000 Da was used (**Figure 13**A). Overall, larger PEG chains lead to increased particle sizes, which could be explained as follows: By increasing the chain length of the polymer, the polymer is getting less amphiphilic in solution, possibly due to the lower amount of end-groups compared to smaller PEG chains. This leads to a lower surface stabilization and bigger aggregates are formed, leading to larger particles.

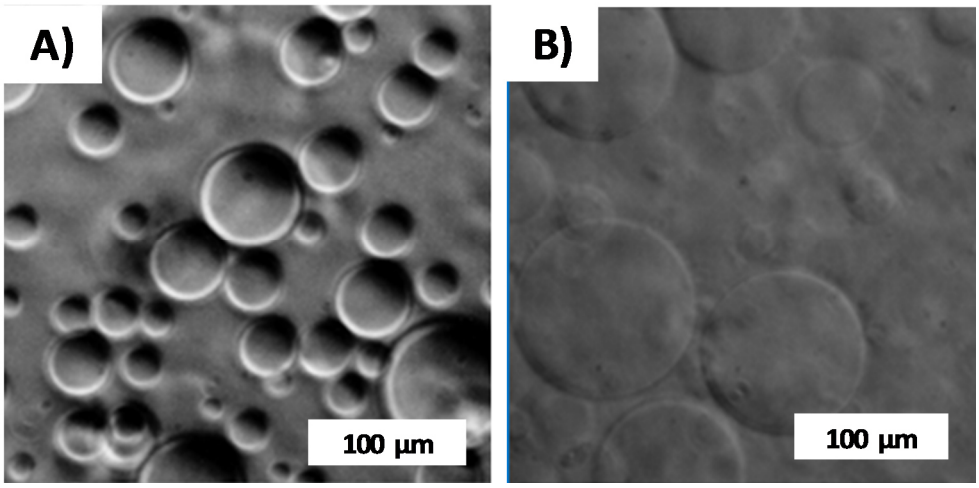

Figure 13: Micrographs of PEG-dAAm (M_n = 20000 Da) microparticles prepared at: A) 0.5 wt-% PEG-dAAm in 1 M sodium sulfate solution and an initiator concentration of 0.015 wt-%. B) 0.75 wt-% PEG-dAAm in 0.75 M sodium sulfate solution and an initiator concentration of 0.00375 wt-%.

Figure 13B shows the SCPs prepared of PEG-dAAm (M_n = 20000 Da) with a low initiator concentration (0.00375 wt-%.). It can be seen that they are more transparent compared to particles with a four-fold higher initiator concentration **Figure 13**A). The increased transparency results from a less dense PEG network and thus lowers the refractive index whereby the contrast is lowered.

Overall, the results show that by using a 1 M sodium sulfate solution and PEG-dAAm with a molecular weight of 8000 or 20000 Da and an initiator concentration of 0.01 wt-% gives particles in the desired size-range for RICM adhesion measurements (see chapter 5.2.3).

In addition to optical microscopy, the surfaces of the SCPs were characterized with scanning electron microscopy (SEM) (**Figure 14**A). All SCPs show a smooth surface, and this should result in a homogenous contact area which is required for the RICM measurements.

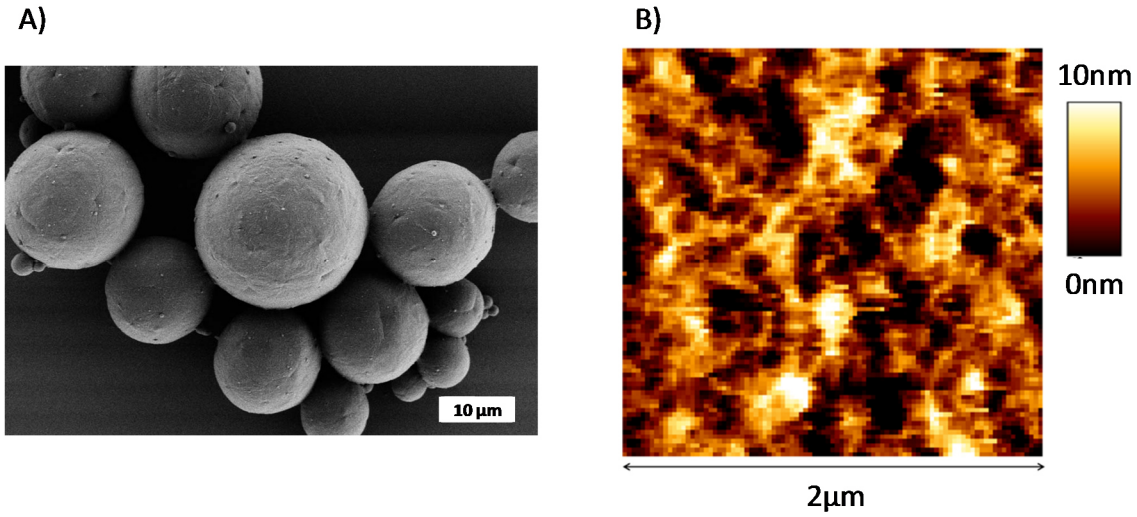

Figure 14: A) SEM picture of SCPs prepared from PEG-dAAm with the molecular weight M_n = 8000 Da. The image shows the particles in a dry collapsed state. The particles swell in water by a factor of 125 in volume (swelling ratio). B) Surface topography image of a PEG SCP measured *via* AFM showing a smooth surface with a root mean square surface roughness of 2.5 nm.

To confirm the smoothness of the SCPs analyzed by SEM the surface roughness was measured by contact mode AFM imaging in the swollen state (**Figure 14**B). The AFM image was obtained using a very soft cantilever (0.03 N/m nominal spring constant) in contact mode at a force set point of 0.75 nN. The PEG SCPs show a root mean square surface roughness of 2.5 nm. This value is comparable with other hydrogel microparticles like Ca-alginate microspheres that showed an average surface roughness in the range of 1-2 nm.[81] This low roughness makes the SCPs suitable for adhesion measurements

3.2.2. PEG SCP Young's Modulus

Another important feature is particle stiffness as measured by the Young's modulus *E* of the probes. The Young's modulus of the probes is central to the adhesion measurements (see JKR eq.10). The elasticity and stiffness of the SCPs properties also affect the sensitivity of the SCP adhesion measurements: In case of softer particles the probe deformation is increased, the contact area is enlarged and the measurements are thus more sensitive.

The elastic properties of PEG SCPs were evaluated by colloidal probe AFM indentation measurements. In this method, the AFM colloidal probe is approached to the apex of the SCP. Once the colloidal probe reaches the SCP apex, the force applied by the cantilever induces a mechanical deformation on the SCP. **Figure 15** depicts the mechanical deformation carried out on the PEG SCP by a spherical glass bead (5 µm) attached to the AFM cantilever.

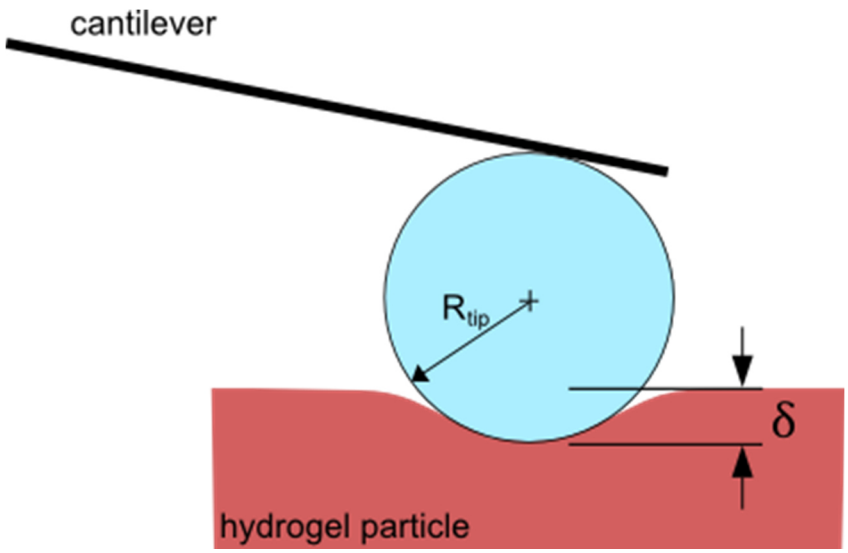

Figure 15: Principle of the measurements of the Young's modulus of PEG SCPs *via* colloidal probe AFM indentation measurements with the Hertz model.

During the force deformation process, the AFM records the tip deflection versus the z displacement. The tip deflection and z-displacement data are then transformed into force vs. sample deformation curves, which can then be used to calculate the Young´s modulus of the PEG SCPs by means of the Hertz model.[35,45] Assuming a spherical AFM tip shape, the Hertz equation describes the relation between the loading force *F* and the indentation δ as follows:

$$F = \frac{4E}{3(1-v^2)}\sqrt{R}\delta^{\frac{3}{2}} \tag{16}$$

where E is the Young´s modulus, v is the Poisson ratio and R is the effective radius of the PEG SCP and the glass bead. A Poisson ratio of 0.5 was selected based on the assumption that all hydrogel particles consist of an isotropic gel material.[81]

The Young's modulus is manly influenced by the cross-linking density. A higher cross-linking density in the hydrogels increases the Young's modulus. For example, by varying the initiator concentration the cross-linking density can be tuned. The cross-linking density and Young's modulus is also tunable by the chain length of the PEG macromonomer. Larger chains show reduced Young's moduli due to lower density of cross-linkable end-groups. This was shown by preparing SCPs with three different molecular weights of PEG 4600, 8000 and 20000 Da ($PEG_{4.6k}$, PEG_{8k} and PEG_{20k}, respectively) at 1 M sodium sulfate concentration and 0.01 wt-% initiator concentration.

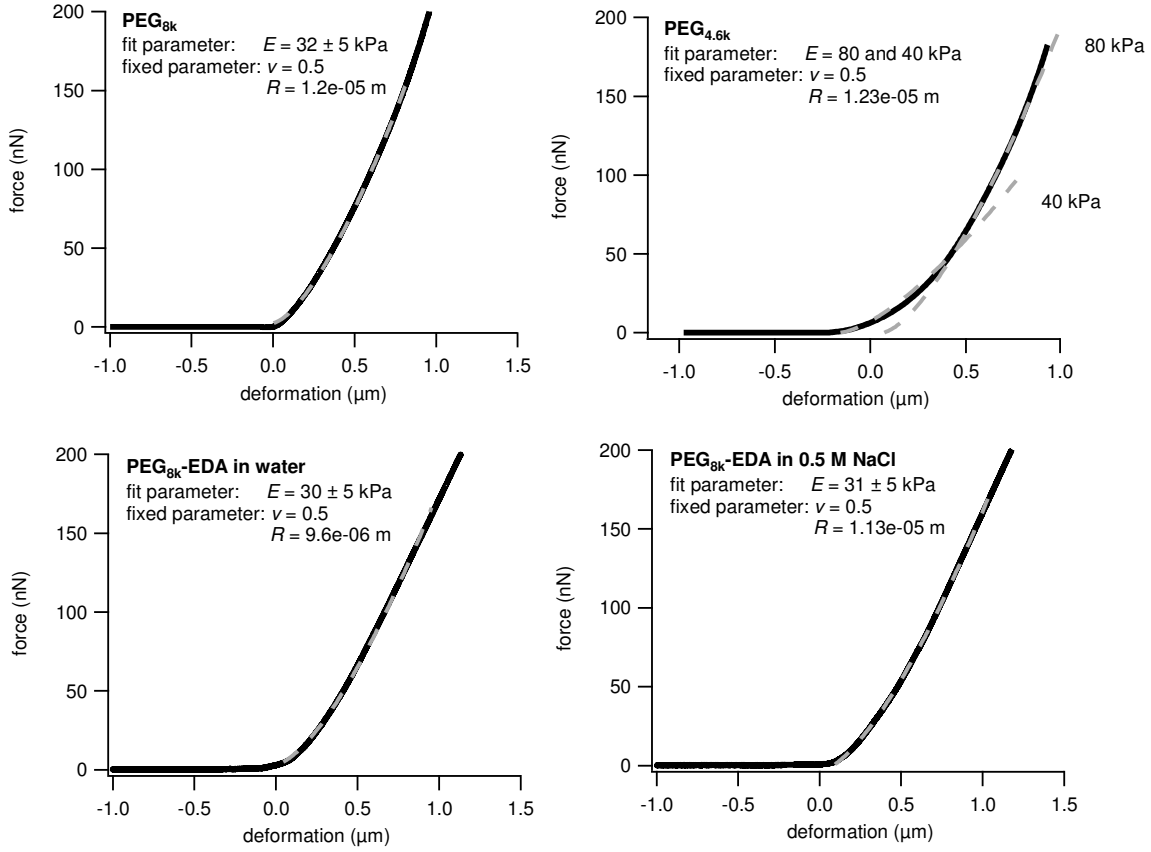

Figure 16: Typical force-deformation curves for unmodified PEG_{8k} and $PEG_{4.6k}$ (top panels) and amine-functionalized PEG_{8k} probes in different media (bottom panels). The dashed lines represent the resulting Hertz fits.

From the force-deformation curves it can be seen that the Young's modulus decreases with PEG chain length. The longer the chain of the PEG-dAAm macromonomer, the more flexible is the formed hydrogel network. The resulting Hertz fits with *E* as free parameter are represented as dashed lines. As expected the elastic moduli for $PEG_{4.6k}$ show the highest Young's modulus. Depending on the force applied on $PEG_{4.6k}$ the elastic modulus appears to range between 40 and 80 kPa as indicated by the two Hertz plots which means that the $PEG_{4.6k}$ do not show Hertzian deformation behavior. For the determination of the Young's modulus, the whole force range was used as this was described in an application note from JPK.[82] This suggests that $PEG_{4.6k}$ does not behave like a linear elastic material which could be due to material inhomogeneities. Therefore this material was not used to study surface interactions. PEG_{8k} probes are very well presented by the Hertz theory and the average elastic modulus for these probes is 32 ± 5 kPa. The reduction of the elastic modulus from 32 ± 5 kPa to 15 ± 3 kPa for the PEG_{20k} probe is due to the enhanced flexibility of the longer PEG chains.

Table 2: Young's moduli of the SCPs measured *via* colloidal probe AFM indentation measurements

Sample name	M_n of PEG-dAAm [Da]	Initiator concentration [wt-%]	Young's modulus [kPa]
$PEG_{4.6k}$	4600	0.01	80 ± 5
PEG_{8k}	8000	0.01	32 ± 5
PEG_{20k}	20000	0.01	15 ±3
PEG_{20k} (t)	20000	0.03	22 ± 6
PEG_{20k} (h)	20000	0.005	4 ± 1
PEG_{20k} (q)	20000	0.0025	0.3 ± 0.1

t: threefold; h: half; q: quarter

Furthermore, the elastic modulus does not change significantly after functionalization with charged groups (see PEG_{8k}-EDA curve). This can be explained by a relatively low degree of functionalization of the PEG backbone. The TNBS test which is a colorimetric titration test for free amines (see chapter 8.1), shows that only one functional (charged) group was introduced to a single polymer chain. Therefore, the elastic properties of the network were not altered. Consequently, addition of NaCl and screening of the charges do not affect the elastic properties either (**Figure 16**).

The use of the simple Hertz model for the analysis of the indentation measurements *via* AFM force-distance curves measured on soft probes may lead to significant

underestimations of the objects Young's modulus *E*. The Hertz Model assumes that just the upper part of the probe deforms and the bottom part stays undeformed. In a recent study the group of M. Delcea Universität Greifswald showed that also the bottom part of our PEG SCPs is deformed.[39] To correct this error, a *double contact model* (based on the simple Hertz model) was derived. The model considers two independent specimen deformation sites: 1) The upper part of the SCP is deformed by the AFM indenter, 2) the bottom part of the SCP is deformed by the substrate, which is usually overlooked. It could be shown, that for instance a compression on the cells bottom side due to gravity forces can have significant effect on the measurements and this suggests also other specimen-substrate interactions e.g. adhesive interactions to influence the resulting force-distance curves. For similar PEG_{8k} SCP used throughout this work, a Young's modulus of around 200 kPa was measured. As of yet, there is no consensus on which model applies best to analyze such force-deformation curves. For further measurements, the much more widely applied simple Hertz model was applied.

Moreover, the influence of the initiator concentration on the Young's modulus was studied. Therefore the softest probes (PEG_{20k}) were used, and the initial initiator concentration of 0.01 wt-% was halved to 0.005 wt-% (PEG_{20k} (h)) and quartered to 0.0025 wt-% (PEG_{20k} (q)).

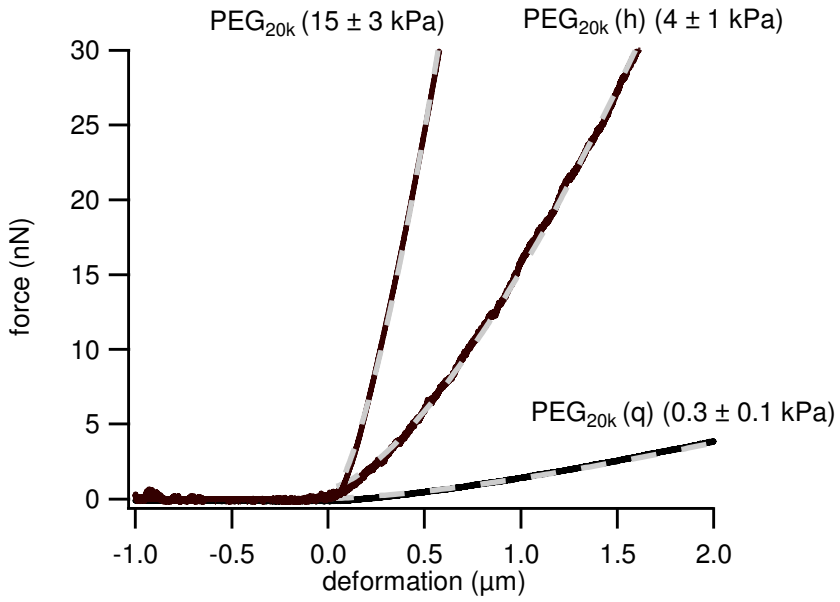

Figure 17: Force-deformation curves shown for PEG_{20k}, PEG_{20k} (h) and PEG_{20k} (q) measured by AFM indentation measurements (black curves). The dashed lines represent the resulting Hertz fits.

As shown in **Figure 17** all SCPs systems are very well represented by the Hertz theory. It can be seen that the Young's modulus is reduced to 4 and 0.3 kPa when the concentration of the initiator is halved (0.005 wt-%) for PEG_{20k} (h) and quartered (0.0025 wt-%) for PEG_{20k} (q). According to these results, it is clear that the initiator concentration has a noticeable influence on the mechanical properties of PEG SCPs. In general, reducing the initiator concentration to a half and a quarter of the initial concentration causes a strong decrease of the Young´s modulus by one and two orders of magnitude, respectively. In contrast to this finding, a threefold increase does not have a marked effect on the Young´s modulus. The sharp decrease in Young´s modulus with the reduction of initiator concentration could be associated to incomplete polymerization of the end groups of the PEG-dAAm macromolecules, resulting in SCPs with a lower degree of cross-linking. In contrast, the increment of the initiator concentration over the standard concentration does not have a major influence on the elastic properties of the sample, suggesting that the standard initiator concentration is the optimal for ensuring a complete polymerization of the PEG-dAAm functional groups.

In general, the modulus of the probes can be adjusted to match the mechanical properties of cells in physiological conditions. Thus the interaction measurements between ligands and receptors shown in the following (see chapter 5) can be considered close to the biological context. The optimal material properties for adhesion measurement *via* SCPs were found for PEG_{8k} probes, as they are in the optimal size range (52 ± 16 µm) and show a low Young's modulus of 32 ± 5 kPa that ensures a large contact area due to adhesion induced deformation. Furthermore, the probes show a sufficiently high contrast in optical microscopy which is advantageous for the adhesion measurements.

4. Functionalization of PEG SCPs

In order to measure adhesion based on different interactions such as electrostatic interactions, hydrophobic interactions or interactions between ligands and receptors, the surface of the PEG SCPs has to be chemically modified.

One possibility to insert functional coupling groups into PEG SCPs is to copolymerize PEG-dAAm with different monomers.[83,84] However, low degrees of functionalization are often observed due to the low solubility of comonomers in the PEG-rich phase. Furthermore, for every new mixture of comonomers the conditions for the precipitation polymerization have to be adjusted again in order to control the size and elasticity of the resulting SCPs. Hence, a more versatile post modification method was chosen which allows for the functionalization of readily prepared SCPs. Here, radical surface chemistry using benzophenone was applied to attach functional monomers to the PEG network.[85]

By irradiating benzophenone with UV light, its triplet state can abstract hydrogen from polymers with low surface free energies containing many abstractable hydrogen atoms, generating a radical on the polymer backbone where a grafting polymerization can take place.[86,87] Therefore benzophenone acts as a photoinitiator and allows for the addition of acryl based monomers e.g. acrylic acid (AA), 2-aminoethyl methacrylate hydrochloride (AMEA) or styrene onto the PEG network. In this way functional groups such as carboxyl or amine groups can be introduced to the SCPs without changing their mechanical properties. These functional groups allow now the coupling of different amines or carboxylates *via* standard peptide coupling chemistry.

In previous studies[76] special focus was devoted to the use of acrylic acid as monomer for the functionalization of SCPs. The thereby introduced carboxylic groups were then activated e.g. as active esters with PyBOP and used to couple a variety of amine groups containing molecules such as dendrimers. In this thesis, this approach was extended to a large number of different ligand modified SCPs. In order to investigate the influence of the degree of functionalization on adhesion between ligands and receptors, together with Hanqing Wang, a series of SCPs modified with different carboxylic acid monomers were synthesized in the first part of this section and characterized for their degree of functionalization. The effect of the grafting type and the reactivity of the carboxylic acid monomers will be discussed. Next, the post-modification with further ligands like carbohydrates and lectins will be discussed. This system is of particular interest as it mimics the cell surface that is the natural substrate for lectins or viral bacteria and was used for

determining specific adhesion between lectins and sugars as well as for affinity assays of various carbohydrate compounds (see chapter 4.3).

All modified SCP systems were characterized by IR measurements for their functionalization and by colorimetric titrations (TBO see chapter 8.1) to determine the functionalization degree. The distribution of the functional groups was tested *via* Raman spectroscopy as well as confocal microscopy.

The following chapter will first present the functionalization of the prepared PEG SCPs with carboxylic acids *via* the benzophenone chemistry. Here, a special focus will be on the grafting efficiency on the SCPs of three different carboxylic acid monomers, as this might influence the adhesion measurements. Then the post-modification of these functional groups will be presented. First, the attachment of molecules containing amine groups will be discussed in order to show the accessibility of the functional groups. Finally, the functionalization with ligands and receptors (specifically mannose and ConA) will be discussed.

4.1. Carboxylic Acid Functionalization of PEG SCPs

The use of neutral and inert PEG scaffolds reduces unspecific interactions but also complicates the bioconjugation, i.e. the post modification of PEG hydrogels with protein receptors or ligands. To tackle this problem a surface chemistry route involving radical generation at the PEG backbone by UV irradiation was adapted[88,89] for the use on PEG-SCPs. This allows for the attachment of carboxylic or amine moieties to the PEG scaffold *via* a radical benzophenone photochemistry.

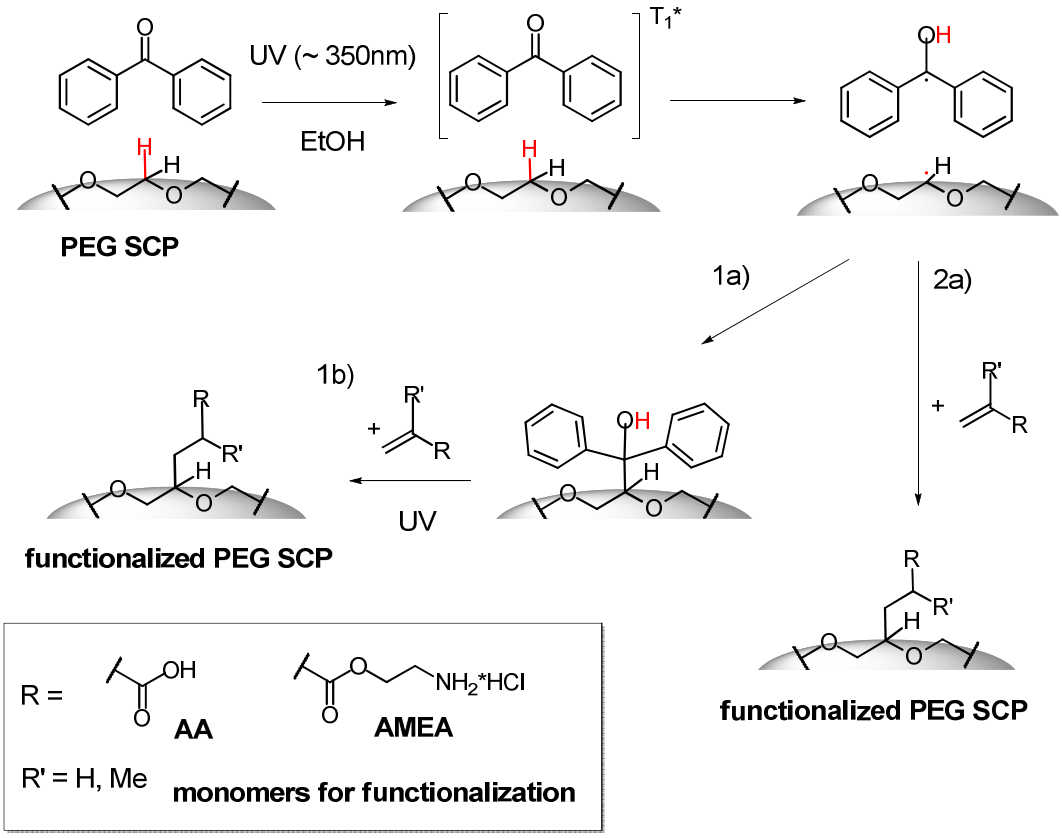

Scheme 3: PEG functionalization is based on radical benzophenone photochemistry and subsequent addition of polymerizable monomers. In the first step, benzophenone abstracts a hydrogen from the polymer surface to generate surface radicals and semipinacol radicals. The subsequent functionalization can occur either in a two-step process, where the semipinacol radicals first couple to the polymer surface in the absence of monomers (1a) and secondly add a monomer (1b) to trigger the graft polymerization by UV irradiation or in a one-step process, where the monomer is added at once to the generated surface radicals (2a).

It is known that benzophenone can absorb UV light to excite an electron in its carbonyl group from ground state (S_0) to excited state (S_1) or (S_2). Subsequently, the excited electron can attain the triplet state (T_1) through intersystem crossing (ISC). At the T_1 state, the benzophenone molecule is highly reactive and can abstract a hydrogen atom from any polymer backbone. Here the hydrogen atom is abstracted from the PEG chains to generate a radical on the PEG-backbone and a semipinacol radical on the benzophenone carbonyl group.[86] If benzophenone at the excited state does react with a H-donor, it can relax back to its ground state and the initiator is readily available again allowing for multiple re-initiation.[86] With the presence of a polymerizable monomer in the mixture, the PEG-backbone radical can attack the unsaturated carbon bond of the vinyl group resulting in the grafting of the molecule on the SCPs.

The functionalization can take place *via* a two-step or a one-step mechanism (**Scheme 3**). In the two step process, benzophenone is first bound covalently to the PEG, then the grafting of monomers is initiated from the PEG chain by UV irradiation.[88] In the one step process, the monomer and benzophenone are directly added to the particle dispersion. Here, the formed radical directly initiates grafting of the monomers on the surface, whereas in the two step process the generated radicals react first with the benzophenone radicals and then the newly formed bond has to be cleaved for further reaction. In order to increase the degree of functionalization, the irradiation step for the one-step benzophenone modification can be repeated several times using the same excess of benzophenone and monomer as before. The IR spectra of such multiply functionalized SCPs using acrylic acid as monomer (PEG-AA) showed a higher intensity of the carbonyl band at 1730 cm^{-1} in comparison to the two-step process indicating a higher degree of functionalization. Thus in the following the focus is on the one-step process for further particle functionalization.

4.1.1. Comparing the Grafting Efficiency of Different Carboxylic Acid Monomers

To obtain carboxyl functionalized SCPs, the PEG SCPs are functionalized with acrylic acid (AA), methacrylic acid (MAA) or crotonic acid (CA) (**Scheme 4**). It is known that these acrylic monomers have different reactivity; therefore it is important to study the grafting efficiency of AA, MAA and CA onto the SCPs. The comparative study of the photografting was carried out under the same reaction conditions so that all reactants are present at the same concentration. Therefore, the PEG SCPs were first dispersed in ethanol, as all reactants including benzophenone and carboxylic acids are soluble in EtOH. The suspension was irradiated for 10 times 90 s at a wavelength of 365 nm (see chapter 8.1). The presence of carboxylic acid groups on the SCPs was evaluated by ATR FT-IR (**Figure 18**). An increase of the peak around 1720 cm^{-1} can be observed that corresponds to the signal of the carbonyl group of the carboxylic acid molecule, which shows the successful grafting of the carboxylic acids to the SCPs.

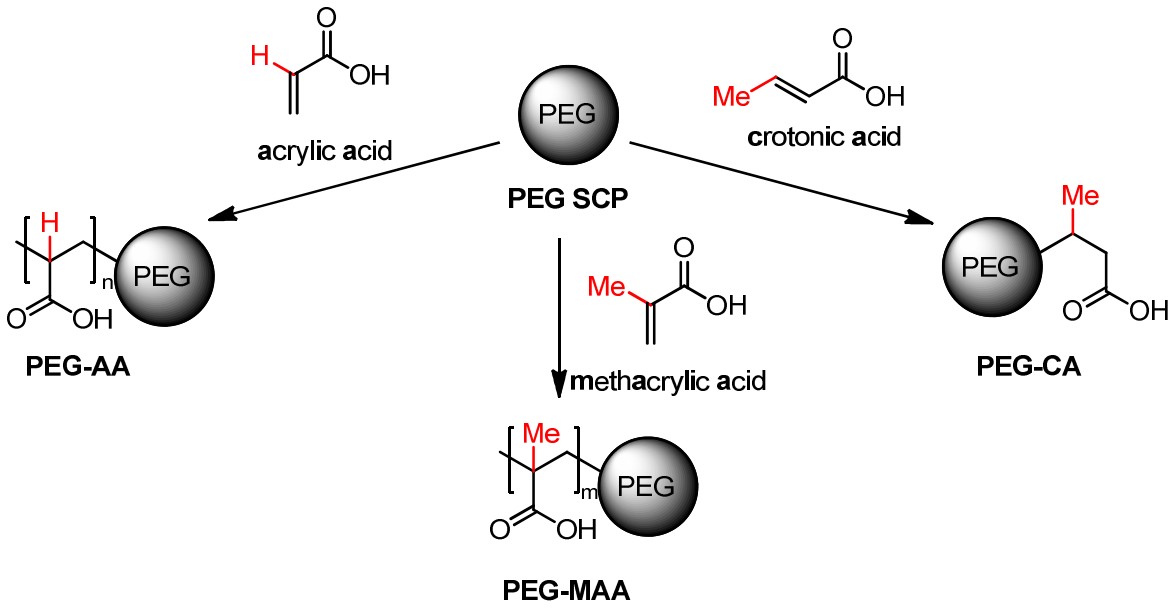

Scheme 4: Functionalization of PEG SCPs with three different carboxylic acids (AA, MAA and CA).

Moreover, the carbonyl signal intensity in the ATR FT-IR spectrum (**Figure 18**) descends in the sequence of methacrylic acid, acrylic acid, and crotonic acid. According to the data obtained by IR it can be concluded that more MAA is grafted onto the probe than AA. The CA showed the lowest reactivity compared to the other carboxylic acids.

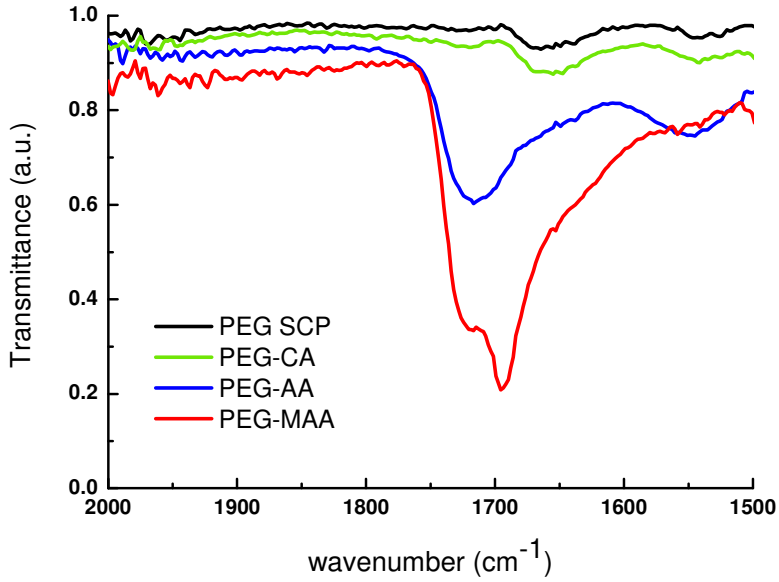

Figure 18: ATR FT-IR of the functionalized acid SCPs that confirm the grafting of the acrylate molecules. Differences in the functionalization degree can be seen in the intensity of the carboxyl band at around 1720 cm^{-1}.

This ATR FT-IR observation was further quantified by determining the carboxylic acid concentration *via* colorimetric titration using toluidine blue O (TBO). It is well known that TBO, a positively charged blue colored dye, forms a stable complex with COO^- groups in basic solutions through electrostatic interactions with a complex ratio of 1:1 (**Scheme 5**).[90,91] Therefore TBO titration was conducted by first adding an aqueous solution of $5x10^{-4}$ mol/L TBO (pH 10) (see chapter 8.1). After the completion of the reaction, the unreacted TBO was washed out under basic conditions, and 50% acetic acid was added to cleave the TBO from the SCPs. The resulting samples were analyzed *via* UV/VIS for the maximal absorption at 633 nm.

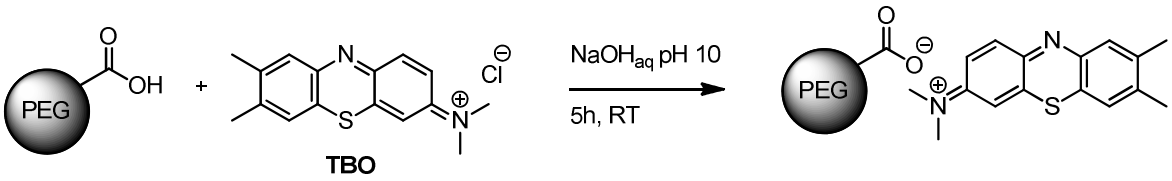

Scheme 5: Schematic picture of the reaction of carboxylic acid functionalized SCPs with TBO

As measured *via* TBO titration, the functionalization degree of methacrylic acid functionalized SCPs (PEG-MAA) was the highest with 259 ± 24 µmol/g. The functionalization degree of acrylic acid and crotonic acid functionalized SCPs (PEG-AA and PEG-CA, respectively) was 117 ± 9 µmol/g and 48 ± 10 µmol/g, respectively (**Figure 19**). These results are in a good agreement with the qualitative results from ATR FT-IR spectra (**Figure 18**).

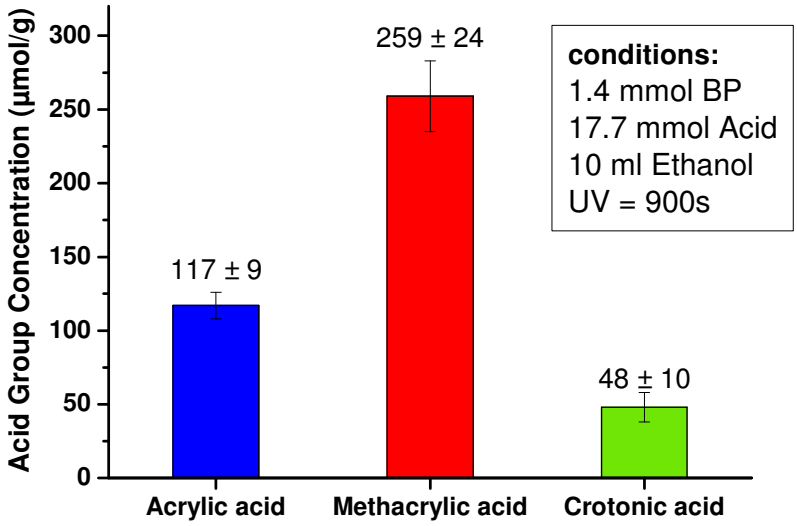

Figure 19: Results of the TBO titration of the grafting of carboxylic acid onto PEG SCPs

In order to determine the distribution of functionalities throughout the particles, Raman spectroscopy was used (**Figure 20**). These measurements were performed by Dr. Admir Masic, MPI KGF, Golm. The Raman spectra and the IR spectra look similar as most Raman and IR bands are observed at the same position. However, both spectroscopic techniques are based on different physical processes. In IR the absorption is measured, whereas in Raman the scattering is measured. In Raman spectroscopy a laser beam is interacting with molecular vibrations shifting the resulting energy of the laser up or down. The advantage of Raman is that one can measure samples in water as it does not interfere with the resulting spectra. This gives the possibility to measure the SCPs in the swollen state compared to IR where only functional groups at the surface can be observed. Raman spectra confirm a homogeneous distribution of the functional groups throughout the PEG network (**Figure 20**).

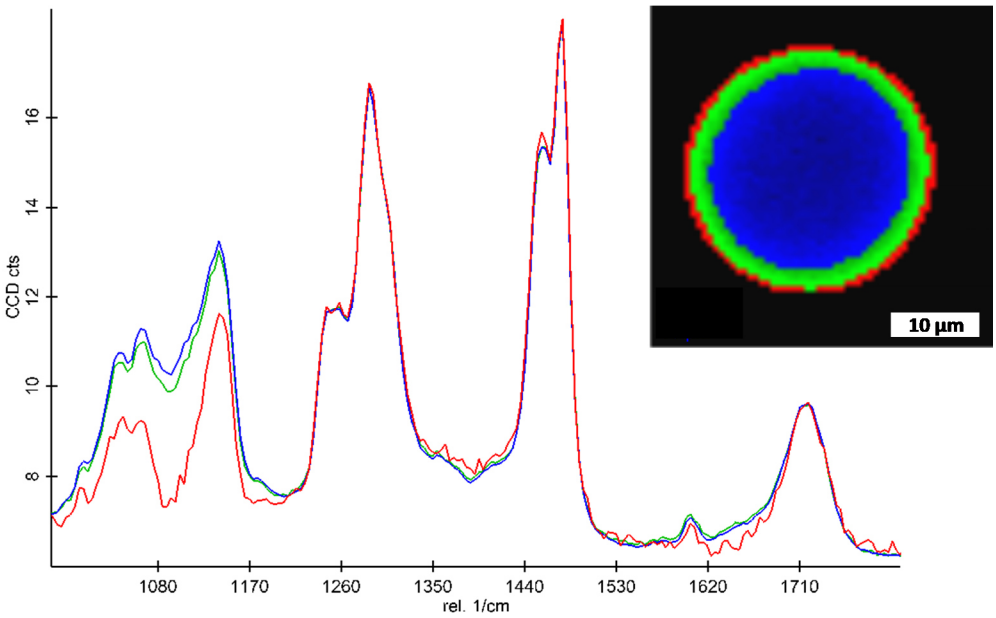

Figure 20: Raman spectrum of PEG-AA. The SCP is divided in three parts: core (blue), middle (green) and surface (red). The spectra were normalized to the CH band at 1480 cm^{-1}. The carboxylate functionalities are homogeneously distributed over the whole SCP as the carboxyl peak at 1710 cm^{-1} showed the same intensity throughout the particle. The red curve shows a difference in the range of 1170-1000 cm^{-1} which can be attributed to the C-O-C vibrations from the PEG chains which are less present on the particle surface.

The observed higher grafting reactivity of MAA than that of AA has previously been described in literature.[92,93] W. Yang et al.[89] compared the reactivity of MAA and AA grafting on low density polyethylene (LDPE) films through measuring the weight increase of the film. With the same reaction condition and reaction time, the weight increase of the MAA grafted film was 2 to 5-folds heavier than AA grafted films indicating the larger

reactivity of MAA compared to AA and is comparable to the findings in this thesis. The reactivity of the monomers can be rationalized by the influence of the substituent on the double bond. The methyl group of MAA may activate the double bond due to hyperconjugation. It is also known that the activation energies for polymerization of MAA are lower than for AA,[94] and it is likely that MAA groups lead to longer grafting units compared to AA, as their initiation reaction is slower than their propagation reaction unlike AA were the reaction kinetics are vice versa.

For CA, it is generally believed that it cannot be homopolymerized *via* free radical polymerization.[95] The CA contains a 1,2-disubstituted ethylene which has a high steric hindrance and this might explain the low reactivity. Therefore, the monomer radical may not be able to further react with other monomers and thus lead to termination instead. As a result, only one CA molecule is attached to one radical of the PEG backbone. Since the concentration of benzophenone and thus the number of grafting sites was constant and CA cannot polymerize to form multimers on the grafting sites while MAA and AA can, the absolute carboxylic acid functionalization was lowest for CA. Therefore, the low number of acid groups on PEG-CA could be expected due to grafting of monomers only. Thus it can be assumed that for all monomers used (MAA, AA and CA) a 'grafting from' mechanism is present, where polymer chains on the SCPs are formed except in case of CA which just attaches as monomer.

However, AA may also show an alternative grafting route: AA homopolymers in solution were observed as side reaction and have the possibility to attach *via* a 'grafting onto' mechanism to the SCPs. The presence of homopolymers in the reaction solution could be proved *via* HPLC (**Figure 21**). Due to the conformation of polymer chains in solution and the steric hindrance, the grafting density should be lower for the 'grafting onto' in comparison to the 'grafting from' reaction. In case of MAA and CA, no homopolymers were observed in solution. This excludes the possibility of a 'grafting onto' mechanism for these two molecules. In case of CA the 1,2-disubstituted ethylene might hamper the abstraction of a proton at the 2 position of the ethylene which would lead to the homopolymerization. The absence of a homopolymer in solution for MAA can be explained by the methyl group at the 2 position of the ethylene. This methyl group prevents the abstraction of the proton, like for AA, which would lead to the polymerization in solution. Due to the absence of the side reaction for MAA, the 'grafting from' is more pronounced which additionally explains the higher grafting efficiency of MAA compared to AA.

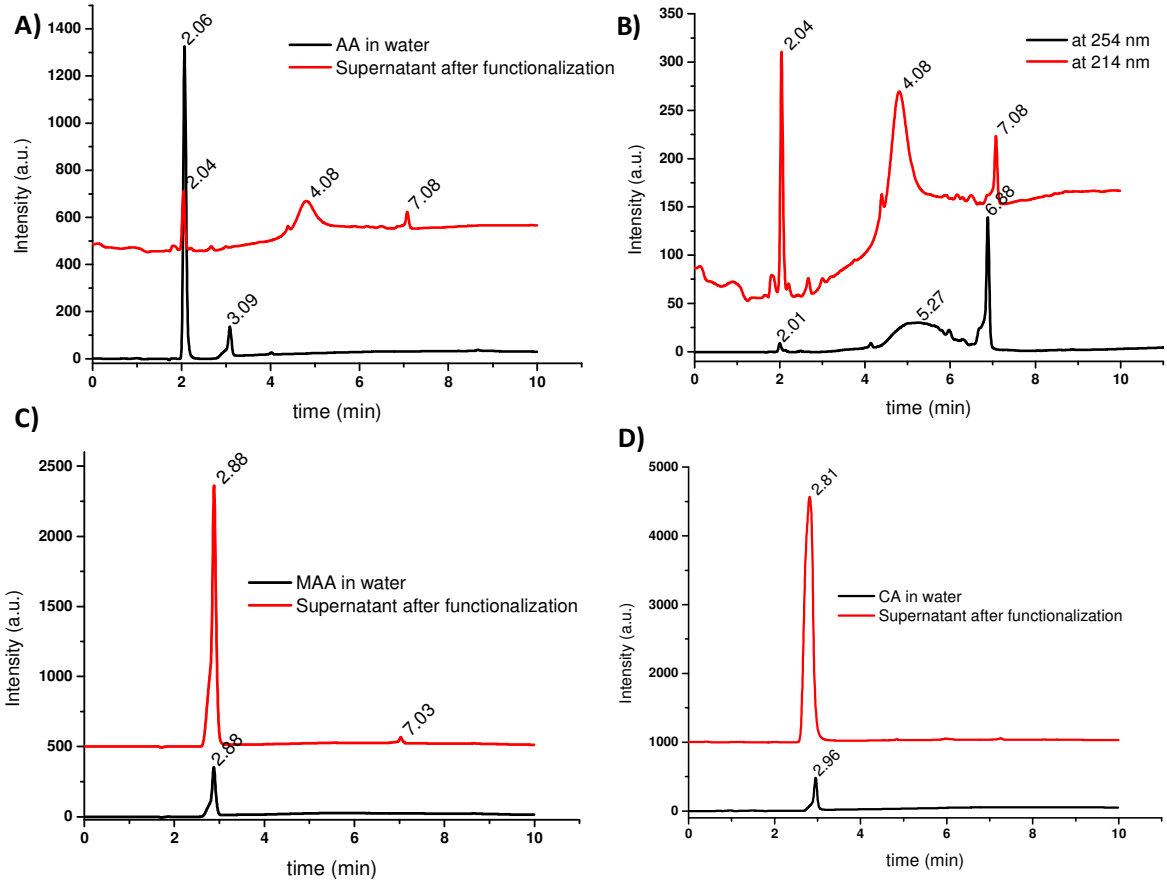

Figure 21: HPLC spectra (at 214 nm) of A) the supernatant after the functionalization of PEG with AA and pure AA in water as comparison. B) The supernatant after the functionalization of PEG with AA at two different wavelengths. The peak at 7 min corresponds to the formed benzopinacol byproduct as the peak intensity increases with increasing wavelength. C) The supernatant after the functionalization of PEG with MAA and pure MAA in water as comparison. D) The supernatant after the functionalization of PEG with CA and pure CA in water as comparison.

4.2. Post-functionalization of Carboxylic Acid Functionalized PEG SCPs

The post-modification of PEG SCPs is important for the attachment of various molecules to be investigated *via* SCP adhesion measurement, e.g. ligands. There are many possible functional groups that can be attached to the SCPs with the previously described benzophenone chemistry. Particularly important in the context of (bio)ligand functionalization is the formation of amide bonds. Therefore either amine or carboxyl groups have to be introduced within the SCP.

Scheme 7 gives an overview over the different possible routes to obtain functionalized SCPs. In the first step, SCPs can either be functionalized with amine or carboxy groups, as described in the previous chapter. Both functional groups allow for further functionalization following standard peptide or amide coupling protocols and formation of amide bonds.

For example, PEG-AMEA particles were functionalized with succinic anhydride (SUC) (**Scheme 7**). The conversion was analyzed with the TNBS method for unreacted amines (**Scheme 6**). The formation of a carboxylate was observed *via* IR spectroscopy, where the band at 1720 cm^{-1} increased. No free amines could be detected proving that all amine groups were accessible and full conversion was achieved. ζ-potential measurements showed the successful functionalization of the amine groups resulting in carboxylate functionalized particles giving a negative ζ potential of -28.9 ± 8.9 mV.

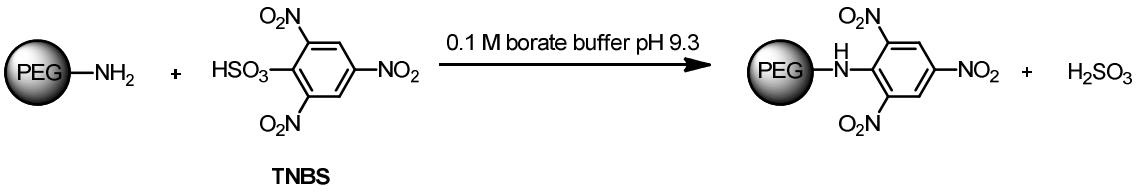

Scheme 6: Reaction of TNBS with amino compounds

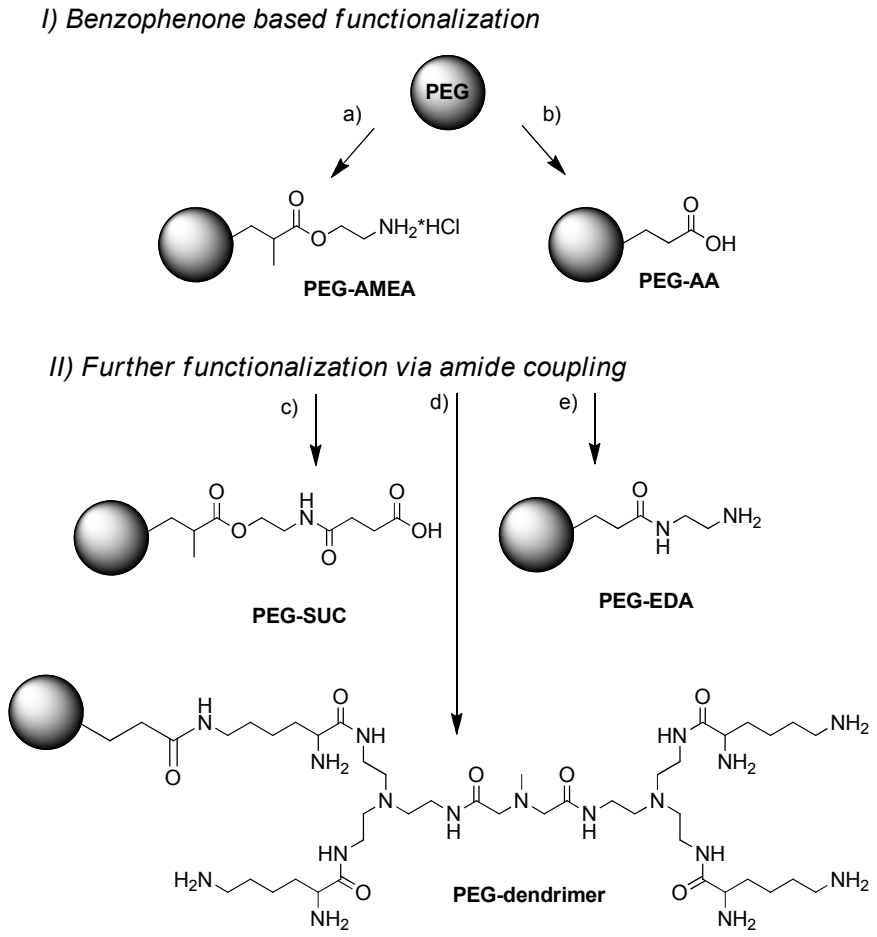

Scheme 7: Modification of PEG microparticles with benzophenone chemistry to obtain charged particles; (a) benzophenone, AMEA, ethanol, UV; (b) benzophenone, AA, ethanol, UV; (c) SUC, TEA, DMF; (d) PyBOP, HOBt, TEA, dendrimer, DMF; (e) PyBOP, HOBt, TEA, EDA, DMF

Alternatively, functionalization of the carboxylic groups of PEG-AA particles with ethylenediamine (EDA) to obtain amine groups was performed. Coupling was performed applying standard peptide coupling chemistry using PyBOP and HOBt (see chapter 8.1). The reaction mechanism is shown in **Scheme 8**. The carboxylic acid is activated by PyBOP and an activated ester is then formed with HOBt. This activated ester is more reactive than the carboxylate and reacts with the amine moiety of the EDA. An excess of coupling reagents was used to ensure complete conversion. Here again, the number of amine functionalities was determined *via* TNBS titration giving a degree of functionalization of 42 µmol/g. This functionalization degree was obtained after a 90 s irradiation time. The ζ-potential changed from -16.6 ± 7.9 mV for the negatively functionalized carboxylate particles to a value of +16.2 ± 6.1 mV for the positively charged amine particles, thus also proving conversion of the carboxylic groups. In order to determine the distribution of functionalities throughout the particles, the PEG-EDA was fluorescently labeled with FITC. Confocal microscopy shows

homogeneous fluorescence indicating a homogeneous distribution of functionalities for the overall PEG network as was previously confirmed by Raman imaging (**Figure 20**).

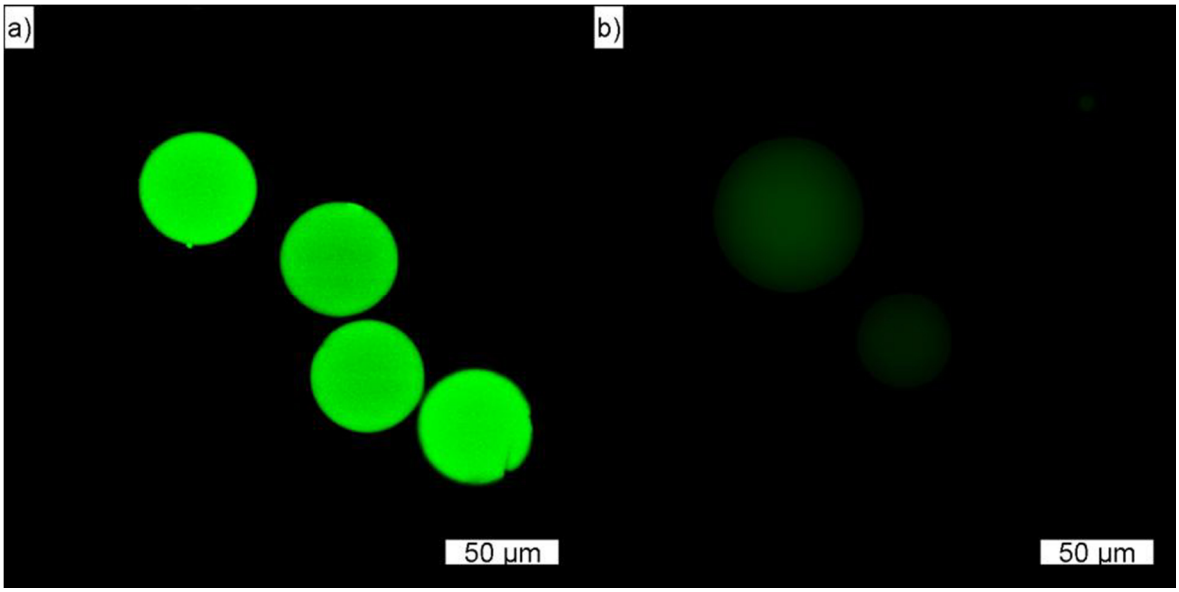

Figure 22: Confocal microscope pictures of a) FITC labeled PEG-EDA particles and b) unfunctionalized PEG SCPs.

In order to increase the degree of functionalization, the irradiation step for the benzophenone modification can be repeated several times using the same amount of benzophenone and monomer. Indeed, stepwise increase of the irradiation time leads to higher degrees of functionalization. After 20 irradiation steps of 90 s a maximum value of functionalization of 117 µmol/g was reached. A different option to increase the overall number of functional groups per probe is the attachment of dendritic structures. For this, an oligo(amidoamine) dendrimer containing eight primary amines was used and covalently linked to the carboxylated PEG-AA (**Scheme 7**). The dendrimer was synthesized by Dr. Muriel Behra according to literature.[96] A two-fold excess of the dendrimer was used to guarantee high conversion of the coupling. Again, the degree of functionalization was measured *via* TNBS titration giving a value of 27 µmol/g. This value is comparable to the previously obtained PEG-AMEA probes with a value of 26 µmol/g.

A higher increase should be expected, as an 8-fold increase in functional groups is present. However, due to the bulky structure, the oligo(amidoamine) dendrimer might not be able to diffuse into the PEG-AA probes and thus not all carboxylate groups might have reacted with the dendrimer. This potentially explains the low degree of functionalization compared to functionalization with EDA leading to PEG-EDA.

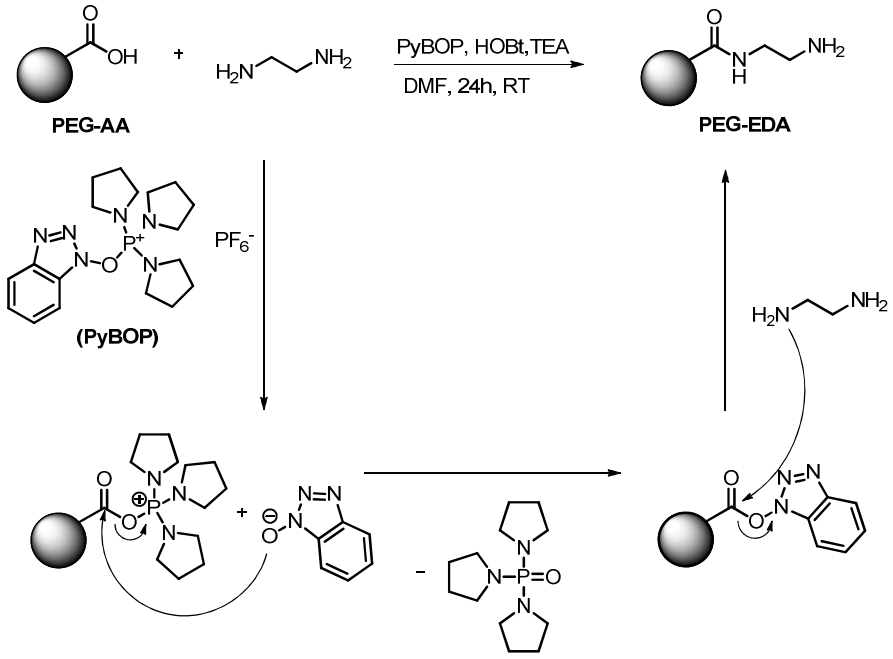

Scheme 8: Reaction mechanism of the PyBOP/HOBt coupling of EDA to PEG-AA probes.

4.3. Bio-functionalization of SCPs

The functionalized SPCs are envisioned as novel sensors in adhesion measurements testing both, non-specific interactions e.g. based on ionic interactions but also specific interactions based on ligand/receptor pairs. Special focus is devoted to the class of sugar ligand lectin receptor interactions, and the well-known ligand/receptor pair mannose/ConA was chosen as model system. Therefore SCPs modified with both, sugar ligands (mannose as binding ligand as well as galactose as non-binding ligand) and receptor (Con A) were synthesized. The following chapter will describe functionalization protocols and characterization of the obtained bio-functionalized SCPs. In the first part, carboxylic acid functionalized SCPs will be coupled with aminoethyl-linked mannose to obtain mannose functionalized SCPs (**Scheme 9**). An aminoethyl linker was used at the anomeric position of the mannose to obtain an amine group on the ligand, which can be then coupled to the carboxyl group on the SCP giving a stable amide bond. Furthermore, a protected sugar was chosen to prevent side reactions of the hydroxyl groups with the carboxyl groups. In the second part, ConA will be attached to the SCPs to obtain receptor modified SCPs. Here,

lysine residues on the ConA provide the free primary amine groups that can be coupled to the carboxyl groups giving again stable amide bonds.

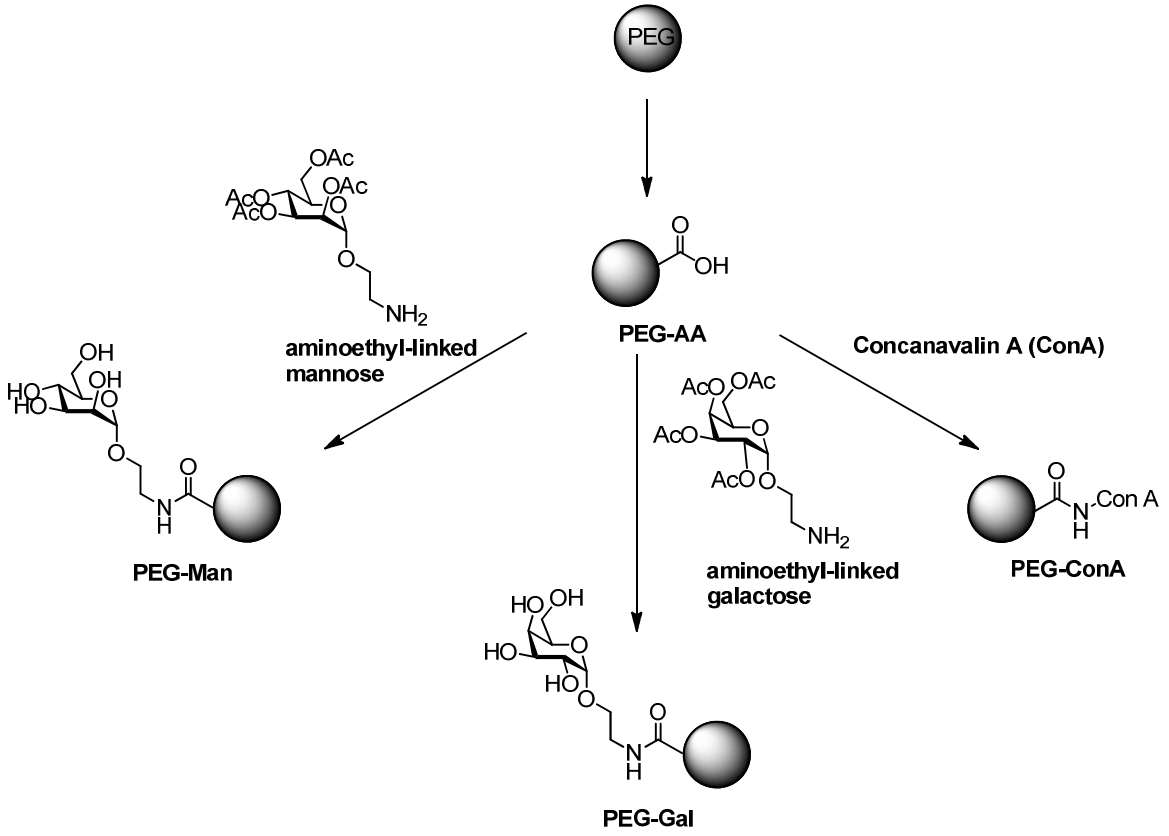

Scheme 9: Overview of the bioconjugation of SCPs

4.3.1. Functionalization with Sugar Ligands

Since mannose/ConA was chosen as ligand/receptor pair for the surface interaction measurements, the mannose residue was attached to the SCPs *via* the aminoethyl-linked mannose (synthesized according to literature protocols by Dr. Simone Mosca, MPI KGF, Golm). The coupling was performed *via* standard coupling chemistry on the PEG SCPs (**Scheme 10**).[97] The SCPs were washed with methanol to remove the unreacted mannose. The subsequent treatment with sodium methoxide in methanol removes the acetate protecting groups. Once deprotected, the SCPs were dispersed in MilliQ water. To study the influence of the degree of functionalization and the grafting type on SCP adhesion, the PEG-MAA (259 ± 24 µmol/g) and PEG-AA (117 ± 9 µmol/g) probes with high density of carboxylic acid coupling groups and PEG-CA with varying density of carboxylic groups

(synthesized by Hanqing Wang, MPI KGF, Golm) were functionalized with the aminoethyl-linked mannose. PEG-CA particles with a functionalization degree of 36 ± 2 µmol/g (PEG-CA_{low}), 57 ± 5 µmol/g (PEG-CA_{middle}) and 97 ± 7 µmol/g (PEG-CA_{high}) were functionalized.

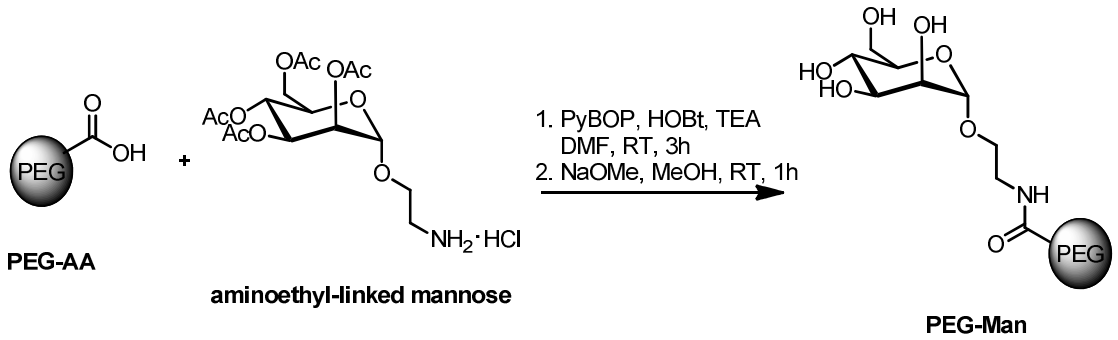

Scheme 10: Coupling of aminoethyl-linked mannose to carboxylate functionalized PEG SCPs (here PEG-AA) *via* standard peptide coupling chemistry.

To study the influence of the probe elasticity on adhesion, PEG-AA SCPs made from macromonomers of different molecular weight were functionalized according to standard protocols. This yielded two SCPs: PEG-AA-15 kPa with a degree of functionalization of 110 ± 20 µmol/g carboxylic groups and PEG-AA-4 kPa with a degree of functionalization of 54 ± 14 µmol/g carboxylic groups. The number of mannose functionalities after coupling of Mannose ligands to the carboxy-functionalized SCPs and therefore the degree of functionalization can be directly measured *via* UV titration with toluidine blue O (TBO) of the unreacted carboxyl groups and compared to the pure carboxylate functionalized probes before ligand coupling. The results are summarized in **Table 3**.

Table 3: Results of the functionalization of the carboxylate functionalized particles with mannose.

Sample	Concentration of carboxyl groups [µmol/g]	Concentration of unreacted carboxyl groups [µmol/g]	Concentration of mannose groups [µmol/g]	Yield [%]
PEG-CA_{low}	36 ± 2	14 ± 4	22 ± 6	61
PEG-CA_{middle}	57 ± 5	13 ± 3	44 ± 8	77
PEG-CA_{high}	97 ± 7	8 ± 2	89 ± 9	92
PEG-AA	117 ± 9	61 ± 5	56 ± 14	48
PEG-AA (15 kPa)	110 ± 20	54 ± 5	56 ± 25	51
PEG-AA (4 kPa)	54 ± 14	0	54 ± 14	100
PEG-MAA	259 ± 24	66 ± 5	193 ± 29	75

It can be seen that mannose did not link to every group as the yield of the conversion is less than 100% e.g. 48% for PEG-AA. Overall a set of mannose functionalized SCPs with different degrees of functionalization, different elastic properties as well as different grafting types was obtained. This set of SCPs will be then used to study the effect of the varied parameters on ligand/receptor mediated adhesion (see chapter 5.2.3.2)

Besides the degree of functionalization it is important to show that functionalization is obtained homogeneously and that the final SCPs still retain the smooth surfaces in order to guarantee high sensitivity in the following adhesion measurements. Therefore, the homogeneity and degree of SCP bioconjugation were investigated by confocal microscopy (**Figure 23**). Therefore, PEG-Man SCPs were incubated with FITC labelled ConA for 1 h and washed with lectin binding buffer to remove unbound ConA. The binding of FITC-ConA to the mannose residues on the SCPs as detected by fluorescence microscopy can be seen in **Figure 23**A.

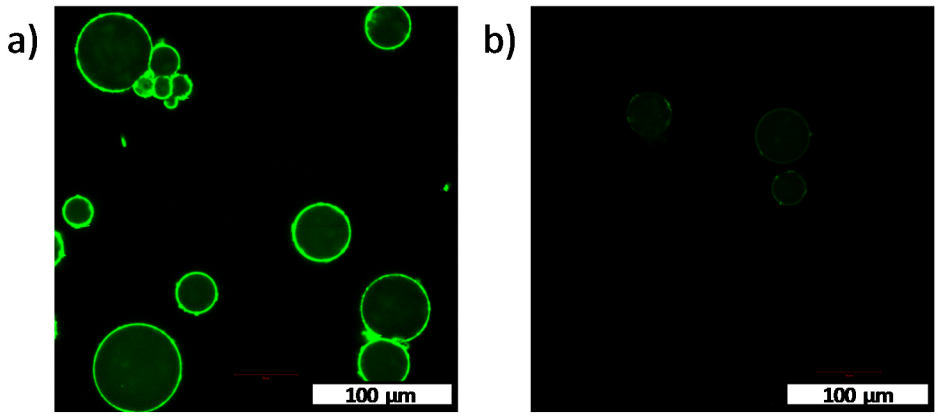

Figure 23: Confocal microscope pictures of functionalized particles a) PEG-Man with FITC labeled ConA and b) after inhibition with *α*-methyl-D-mannose.

As can be seen from the confocal images (**Figure 23**A), the FITC labeled ConA is bound to the surface of the SCPs. Due to the large structure of ConA, the diffusion into the SCP core and thus through the pores of the hydrogel network is hampered and ConA adhesion is only detected on the SCP surface. In order to test for the specificity of ConA adhesion, the labeled SCPs were washed with a 1 mM *α*-methyl-D-mannose solution. Methyl-mannose should act as a low molecular weight inhibitor and this leads to competition and detachment of the ConA from the SCPs. Indeed, no fluorescence signal was observable as the ConA was inhibited and washed out from the SCPs (**Figure 23**B). This showed that the mannose molecule was bound to the SCPs *via* specific ligand/receptor interactions.

To directly measure the capability of the SCPs to bind to ConA receptors, the density of bound ConA was determined after incubating the mannose SCPs with ConA by amino acid analysis (**Figure 24**). Amino acid analysis applies for the determination of amino acids in a protein sample by chromatography. With the known amount of protein in the sample the surface can be calculated that the protein captures. The surface area of the SCPs can be calculated from microscopy pictures. The ratio of these two values yields the coverage of the SCPs with proteins. Therefore, this method allows evaluating the amount of Con A that can be bound by the SCP and is another measure for the degree of functionalization. More specifically, this allows an estimate of the number of sugar ligands attached to the particle surface that will later take part in the surface adhesion studies. The mannose SCPs bound $4.5 \cdot 10^{16}$ ConA per m^2 as measured suggesting complete coverage of the PEG-Man SCPs with the receptors. The SCPs surface area was determined by measuring the SCP radius of all particles in a given suspension with an optical microscope before the amino acid analysis measurement.

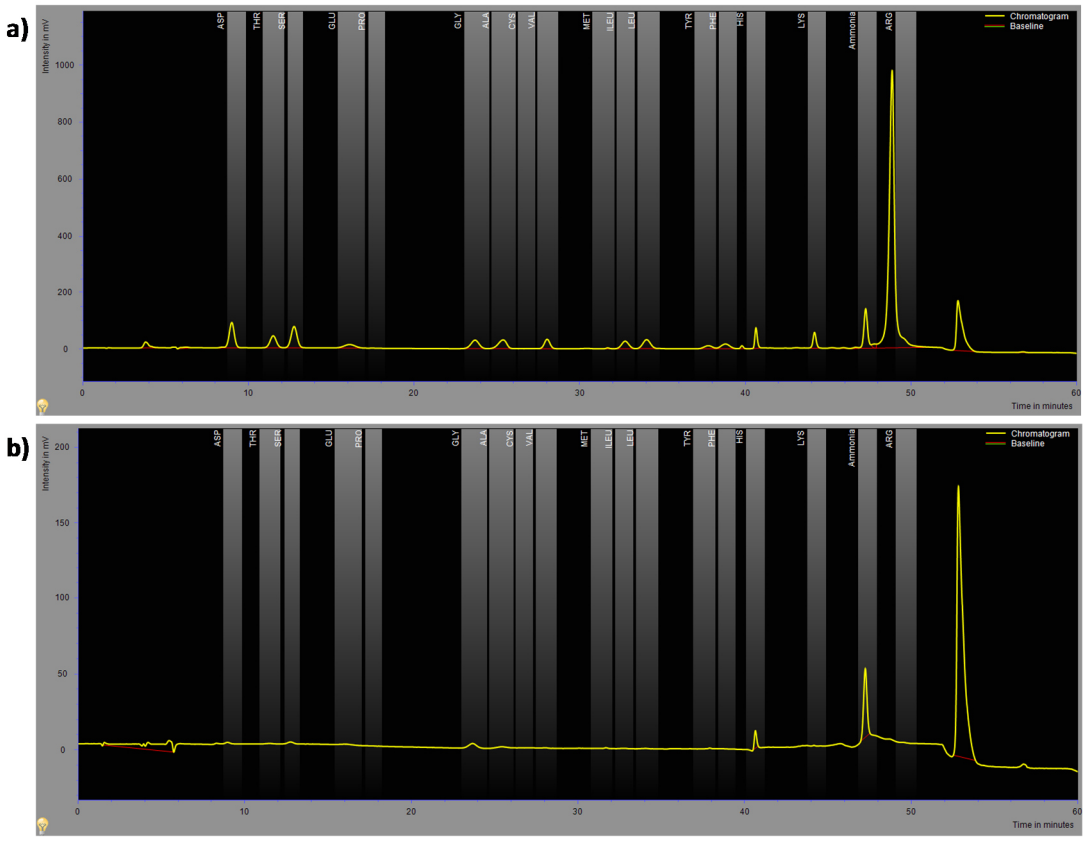

Figure 24: Amino acid analysis spectra of a) ConA bound to the PEG-Man SCPs and b) the supernatant of these SCPs.

To control that the ConA was attached to the PEG-Man SCPs, the supernatant of the suspension was analyzed by amino acid analysis and no ConA could be found in the solution. This suggests that all ConA was directly bound to the SCPs. **Figure 25** presents the AFM images of PEG-Man SCP. It shows that after the functionalization the surface is still homogenous with an average roughness of 3 nm.

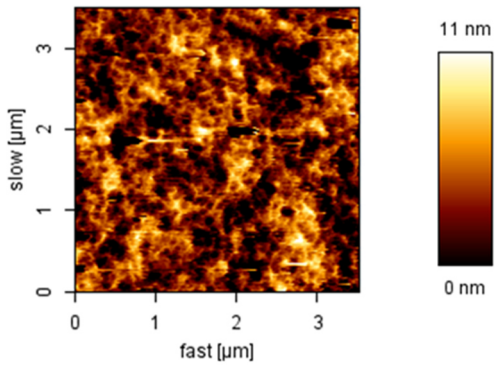

Figure 25: Topography of the PEG-Man SCP surface as measured by Dr. Stephan Schmidt, MPI KGF, Golm. Height profile of a 3x3 µm area of the SCP with a roughness (RMS) of 3 nm.

4.3.2. Functionalization of the SCPs with Proteins

In the previous chapter, the synthesis of mannose SCPs was established. Since the targeted ligand/receptor model system is mannose/ConA, SCPs functionalized with ConA have to be synthesized as well. Thus the independence of the system can be tested as it should not make any difference where the ligands and receptors are located. The advantage is that both surfaces with ligands as well as receptors can be examined. This makes one independent from the substrate to be analyzed.

The PEG-ConA SCPs were prepared by coupling to carboxylic acid functionalized SCPs in phosphate buffer pH 6.5 with free amine groups of the protein. Therefore, the PEG-AA SCPs were first activated with EDC and NHS to give reactive NHS ester on the surface which allows for reaction with the ε-amino group of lysine residues on ConA to give PEG-ConA SCPs.[98] After the activation of the carboxylic acid, the unreacted activating agents EDC and NHS have to be washed out carefully to avoid cross-linking of the protein itself which might influence the activity of the protein. IR studies confirmed the attachment of ConA to the PEG-AA SCPs, because the band for the carboxyl moiety at 1720 cm^{-1} disappeared. Two amide bands (I and II) at 1637 cm^{-1} and 1560 cm^{-1} appeared after the functionalization with ConA, which are characteristics of amides mainly in proteins **Figure 26**.

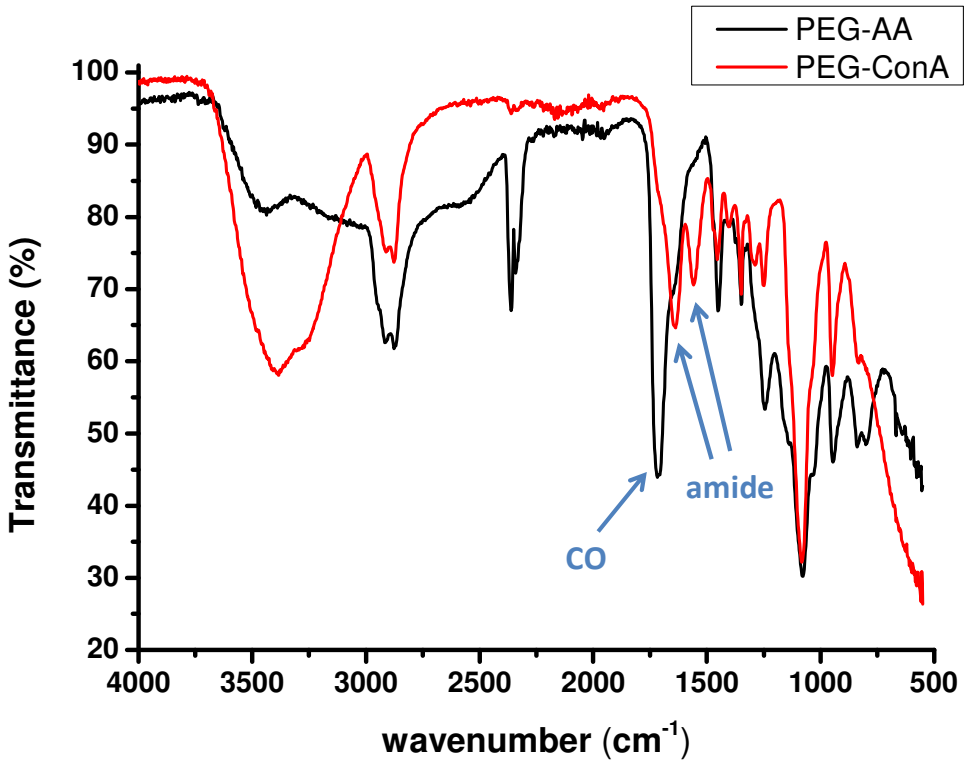

Figure 26: Infrared spectra of PEG-AA and PEG-ConA SCPs.

To prove that the ConA is covalently bound to the SCPs, fluorescence microscopy was used in combination with the labeling of the protein with FITC. The FITC molecule has an isothiocyanate moiety which is reactive towards nucleophiles including amine and sulfhydryl groups on proteins. After binding of FITC on one of these groups, the SCP should be fluorescent thus showing successful conjugation of ConA to the SCPs. On the confocal image (**Figure 27**) the whole SCP is fluorescent indicating the binding of FITC to the protein. The surface showed the strongest fluorescence signal. As the FITC is a small molecule it can diffuse into the SCP and therefore the whole SCP is fluorescent. Further washing steps would decrease the signal intensity.

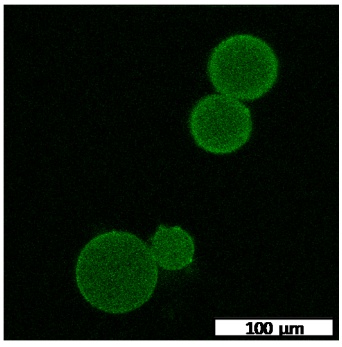

Figure 27: Confocal microscope image of PEG-ConA SCPs labeled with FITC.

ConA functionalized SCPs were analyzed for their ConA content by amino acid analysis as described above. As the PEG-ConA SCPs are analyzed from solution, there is the possibility of unbound ConA left in solution. The free protein in solution could act as an inhibitor in the carbohydrate mediated surface interaction measurements and thus interfere with the binding of the covalently attached ConA molecules on the SCP. Therefore, the supernatant was also analyzed to show that ConA is covalently bound to the substrate rather than in the solution. The surface density of ConA was then calculated. With the known amount of ConA in the sample, the surface can be calculated that the protein captures. Therefore, this method allows evaluating the amount of Con A that is bound on the SCP and allows an estimate of the number of sugar ligands attached to the flat surface that can later take part in the surface adhesion studies. The amino acid analyzer showed closely packed ConA on the SCPs with a density of $3.57 \cdot 10^{16}$ ConA/m^2. To obtain the surface area of the SCPs the volume of the surface was measured by measuring the SCP radius of all particles in a known amount of suspension (1 µL) with an optical microscope.

In conclusion, a straightforward synthesis route towards versatile functionalized hydrogel SCPs was established. The functionalization *via* radical surface chemistry of readily prepared PEG SCPs allows for an easy and highly versatile preparation of functionalized SCPs. With this method in hand, SCPs with tailored ligand densities can be prepared thus giving the opportunity to study the dependence of ligand density on adhesion at soft interfaces. Furthermore, the attached functional groups (amines and carboxy groups) allow for the post-modification with (bio)molecules giving stable amide bonds. Two biomolecules, that play an important role in this thesis, mannose and ConA, could be successfully attached to the SCPs. These functionalized SCPs now allow for the measurement of specific ligand/receptor interactions at the interface. The following chapter will describe the use of these SCPs for adhesion measurements.

5. Adhesion Measurements *via* RICM Using SCPs as Sensors

In order to measure adhesion at soft surfaces, in the previous chapters the synthesis of soft PEG SCPs and their versatile functionalization was presented. With the benzophenone-mediated introduction of various monomers as coupling group, a convenient route towards homogeneously functionalized PEG SCPs was established. The functional groups on the SCPs allow for the post-modification with a variety of molecules such as dendrimers, sugar ligands and protein receptors. As the physical properties of the SCPs are tunable, probes with different Young's moduli and functionalization degrees could be prepared to measure the influence of flexibility and ligand density on adhesion giving new insights into the correlation of these factors. Special focus will be devoted to ligand/receptor mediated adhesion processes, more specifically on sugar ligand/protein receptor interactions as studied for the model system mannose-ConA.

Thus, the previously synthesized and characterized SCPs will now be applied as sensors for adhesion measurements studying the effect of ligand/receptor mediated surface adhesion. Therefore, three methods will be presented: First a direct binding assay, where the influence of the ligand density and probe flexibility will be evaluated for their influence on the adhesion process *via* RICM. Second, the inhibition of the previously studied direct binding of mannose/ConA with different monosaccharides will be evaluated. Therefore, a new inhibition/competition assay based on the adhesion induced elastic deformation of the SCPs will be developed. This method allows for inhibition measurements and gives fast and straightforward access to relative affinities of a variety of sugar ligands. Third, RICM based methods will be combined with AFM to study the effect of a loading force on the carbohydrate mediated adhesion and how it effects the binding of analytes to the receptor.

The ability to quantify ligand/receptor mediated surface adhesion is crucial for advances in such rapidly developing fields as nanotechnology or biomedicine. In order to quantify and further understand the underlying principles of such surface interactions and apply this knowledge for the rational design *e.g.* of new coatings or cell growth scaffolds, several methods were developed to measure interaction forces, like surface force apparatus (SFA) and atomic force microscopy (AFM).[35,99–102] These methods usually quantify adhesion in terms of the mechanical work required to detach adherent surfaces and are therefore

dependent on the complex detachment mechanism as well as the uniformity and size of the examined contact area. Methods employing very small or uneven contact areas thus limit the precision and detection level of adhesion measurements.

A major step towards solving these problems is presented by methods employing µm-sized probes with well-defined geometry such as colloidal probe AFM.[35] Recently, the colloidal probe technique was extended by using elastomer based particles as soft colloidal probes (SCPs).[64,103] The use of soft, deformable probes enables larger contact areas as well as a direct measurement of the contact area *via* RICM further improving the sensitivity of adhesion measurements. This approach is based on the JKR theory, that allows to extract the adhesion energy from the induced mechanical deformation of the SCP[46] without the need to consider the complex detachment mechanisms. The JKR approach has been successfully applied for adhesion energy measurements by different experimental methods, *e.g.* the so called JKR apparatus[104] or the above mentioned soft colloidal probe AFM technique[64] as well as by simply measuring the elastic deformation of adhered particles using RICM.[105] However, those methods only measured non-specific interactions at interfaces and thus have only little biological context. Furthermore, they do not allow studying the proposed interconnection of all three factors - affinity, ligand density and elasticity due to their low variability.

In the first part of this chapter, the previously developed SCPs will therefore be used as probes for direct adhesion studies. Therefore, first the principle of the direct adhesion measurements will be explained followed by the measurements of electrostatic interactions at interfaces as a proof of principle. Afterwards, special focus is devoted to the carbohydrate/lectin interactions, specifically the interactions of mannose and ConA as well-established model system. Here, the surface functionalization with both mannose and ConA will be described. Then, the influences of flexibility and ligand density will be explained by means of the example of the mannose/ConA interaction. Finally, the inhibition by addition of specific inhibitors interfering with the adhesion of the SCP will be described. This leads to a new inhibition competition assay that will be applied for the screening of various analytes and their relative affinities towards ConA.

Figure 28 shows an example for a direct binding experiment. Besides the functionalized SCPs, a flat substrate is required to function as the second surface the SCP will adhere to. This flat substrate should meet a minimum of requirements such as high transparency, rigidity, non-porosity and easy functionalization.[106] All these requirements are met by glass

cover slides, a cost efficient material, transparent, resistant to heat, which can easily be chemically modified and will be used exclusively in this thesis.

In a typical adhesion measurement, the SCPs will be dispersed in water and placed on the surface of a transparent glass slide. The SCPs sediment onto the surface and since they are soft, they can form a distinct contact area. This contact area and the particle size will be determined with an inverted light microscope in RICM mode and, respectively, in transmission mode.

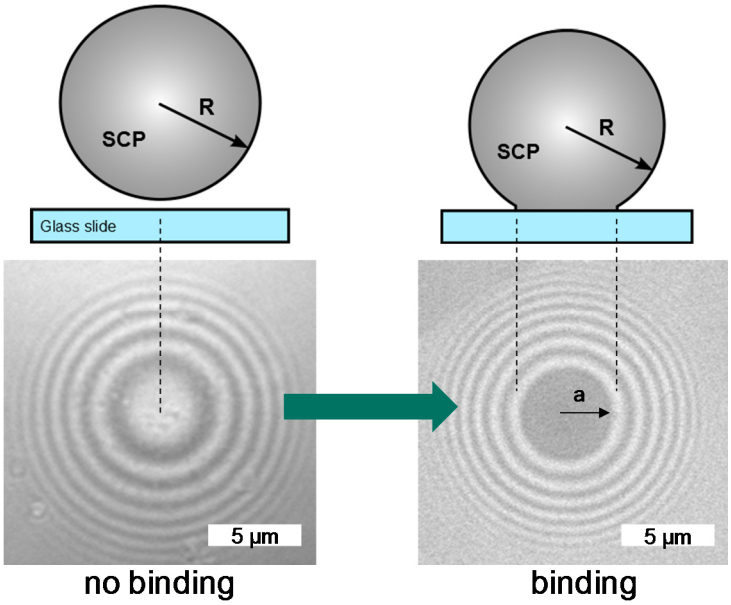

Figure 28: Contact area measurements of soft colloidal probe microparticles *via* RICM. The contact area is imaged by a light microscope and shows the typical interference pattern.

The calculation of adhesion energies is based on the JKR model, relating the adhesion energy to the induced deformation of the elastic sample.[46] The JKR theory is valid when describing large adhesion areas and soft samples, which is the case here.

To determine the contact radius, a RICM based method developed by J. Erath et al was adopted[64] as described in the following section. RICM reveals the contact radius formed by the SCP resting on the functionalized glass coverslip[107] (**Figure 28**). To get the intensity distribution over the distance *r* from raw data, the average of intensity profiles over an angle φ, as shown in **Figure 29**A, is taken. For analysis of the intensity distribution, a simple model with correction factors for finite aperture and geometry effects is used (**Figure 29**, **Table 4**). To obtain the correction factors, glass beads on a glass surface in RICM mode (**Figure 29**A) are imaged. Five glass beads were recorded with a diameter in the range of 10-20 µm and the intensity profile was extracted (**Figure 29**B). Using the profiles, the shape of the beads can be reconstructed and compared to the known spherical shapes of the glass beads (glass

bead radius *R* measured by light microscopy), and the correction factors c_l corresponding to our experimental setup **Figure 29**C can be determined. The correction factors as determined for the first six local minima and maxima are shown in **Table 4**.

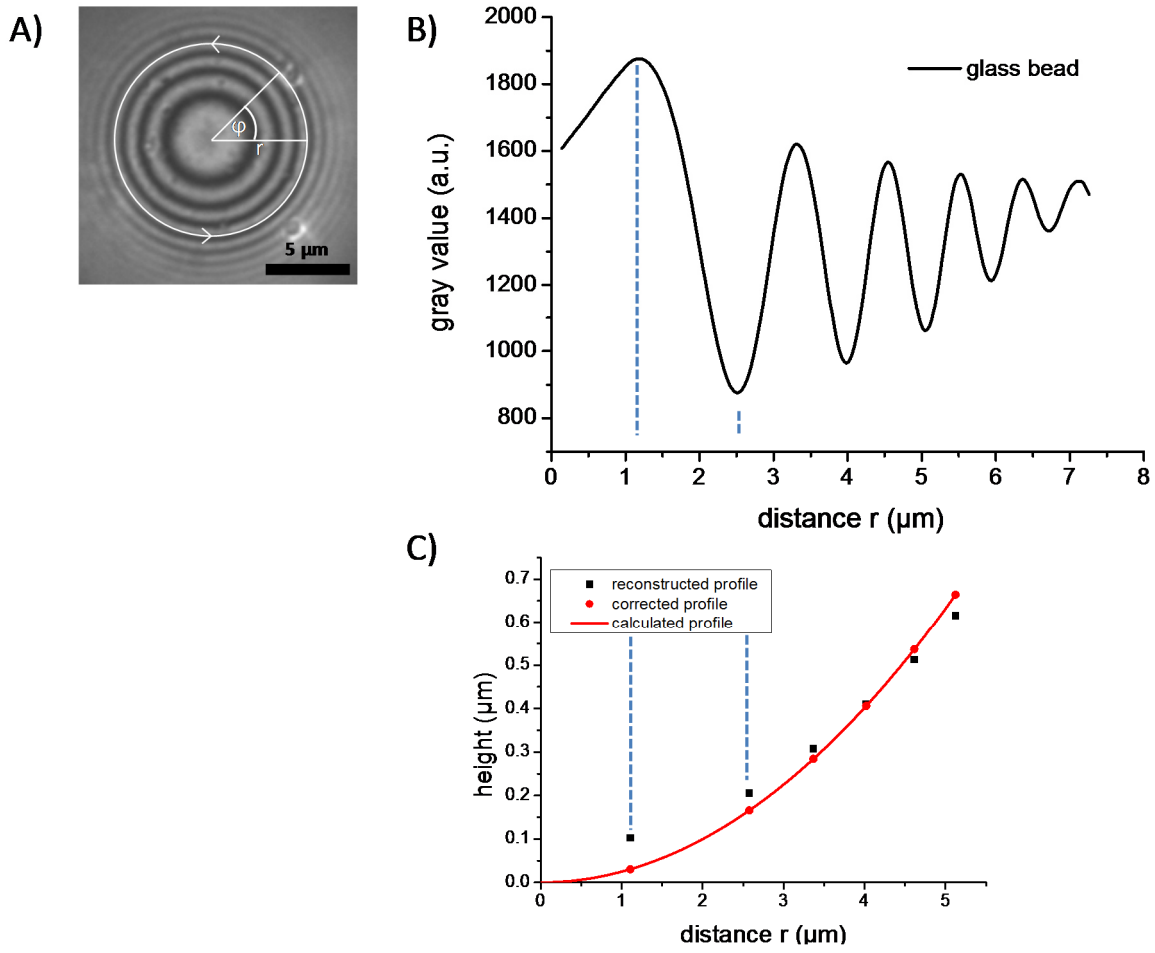

Figure 29: Reconstruction of the height profile of the object from the RICM images, A) RICM image of a glass bead on a glass surface, B) extracted intensity profile and C) reconstruction of the profile

Table 4: Correction factors cl for the RICM setup: (c_1: 1st maximum, c_2: 1st minimum, c_3: 2nd maximum, $c4$: 2nd minimum, c_5: 3rd maximum, c_6: 3rd minimum)

c_l	c_1	c_2	c_3	c_4	c_5	c_6
nm	-72	-39	-24	-4	24	48

To determine the contact area of the SCP on the functionalized glass surface, the height profile of the particles has to be reconstructed from the RICM images (**Figure 30**).

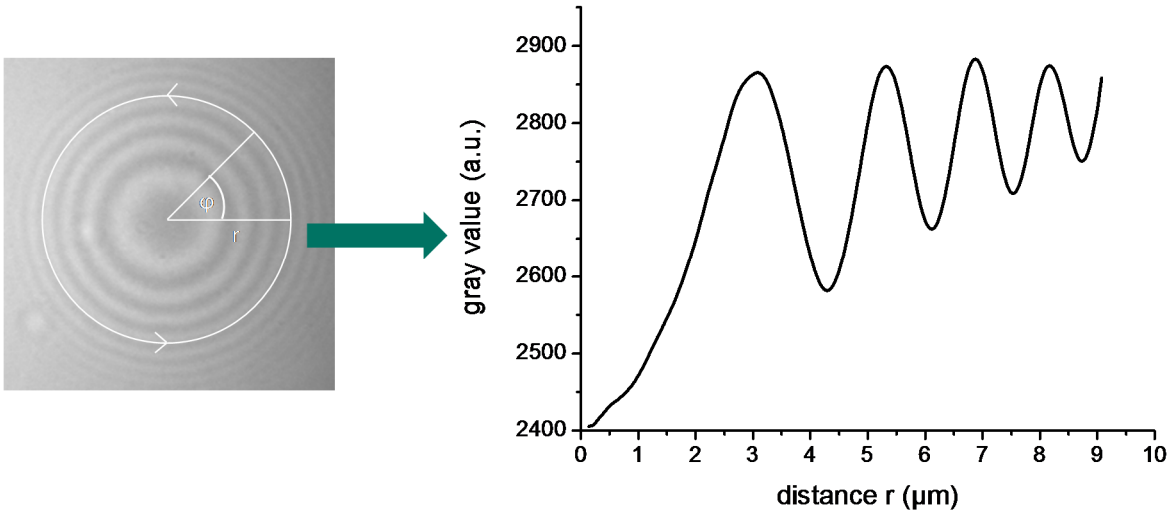

Figure 30: Interference pattern of a mannose functionalized SCPs (PEG-Man) on a ConA surface and the extracted intensity profile

In the region of contact, corresponding to $h(x) = 0$, equation (1) will be simplified to

$$I(x) = I_1 + I_2 - 2\sqrt{I_1 I_2} \tag{17}$$

and the intensity of the image is at its minimum. The optical path difference and vertical distance between adjacent maximum and minimum intensity points can be calculated from simple optical theory.

$$\delta = \frac{l\lambda}{2n} \tag{18}$$

$$\Delta h(x) = \frac{\delta(l)}{2} = \frac{l\lambda}{4n} \tag{19}$$

The contact radius a can be then calculated according to the Pythagoras theorem to the obtained height profile and by equation (8).

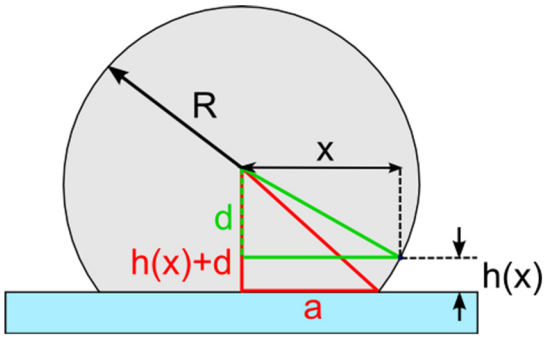

Figure 31: Mathematical description for the calculation of the contact radius a

$$a = \sqrt{\mathrm{R}^2 - \left(\mathrm{d} + \mathrm{h(x)}\right)^2} = \sqrt{R^2 - \left(\sqrt{R^2 - x^2} + h(x)\right)^2} = \sqrt{R^2 - \left(\sqrt{R^2 - x^2} + \left(\frac{l\lambda}{4n} + c_l\right)\right)^2} \tag{20}$$

where R is the particle radius, x are positions of the local minima and maxima, l is the index of the maxima/minima, n the refractive index of the solvent and c_l the correction factor.

The radius of the particle is determined in the same way with the difference that as the radial profile height the minimum was taken (**Figure 32**) The set of SCPs, with their known mechanical properties *via* AFM and their contact radii using the RICM technique now allows for the measurements of energies and thus adhesion energies *via* the JKR approach presented in chapter 1.3.

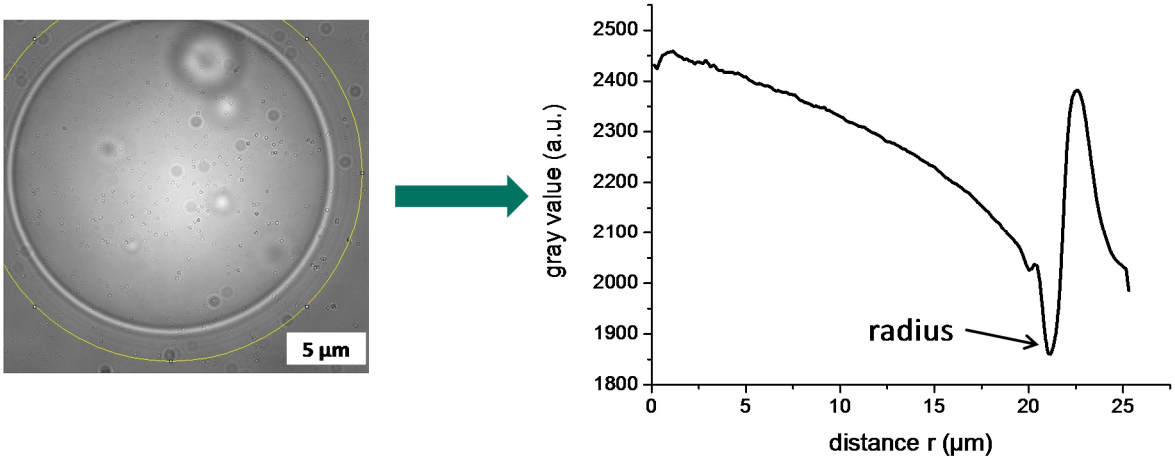

Figure 32: Determination of SCP radius. The left picture shows the phase contrast image of the SCP and its corresponding profile height on the right determined with ImageJ. The radius of the SCP was defined as the minimum of this height profile.

5.1. Electrostatic Interactions

In a first set of experiments, adhesion due to acid–base and electrostatic interactions of three differently functionalized PEG SCPs carrying cationic amine groups against negatively charged silanol groups on glass coverslips (**Figure 33**) was studied. The coverslips were plasma cleaned to obtain a silicon oxide surface with high density of silanol groups in water that deprotonate above pH 2 to form negatively charged species. All samples used for the following adhesion measurements were prepared by irradiating one time for 90 s followed by a second step, the addition reactions for fabrication the PEG-EDA, PEG-SUC and PEG-dendrimer systems as described in chapter 4. The degree of functionalization was determined by TNBS titrations according to chapter 4.2 (**Table 5**). Here a Young's modulus of E = 32 ± 5 kPa (as measured by AFM force-deformation) and a Poisson ratio of $\nu = 0.5$ were applied for all PEG SCPs.

Table 5: Characterization of the functionalized microparticles for their degree of functionalization and resulting adhesion energies

	Functionalized SCPS	Functionalization degree [µmol/g]	Adhesion energy [mJ/m^2]
⊖	PEG-AA	42 ± 5[a]	0.15 ± 0.01
	PEG-SUC	26 ± 5[b]	0.07 ± 0.01
⊕	PEG-EDA	42 ± 5	1.20 ± 0.04
	PEG-dendrimer	27 ± 5	0.83 ± 0.12
	PEG-AMEA	26 ± 5	0.26 ± 0.02

a) Concentration was measured after reaction with EDA. b) Concentration of previous amine particles (PEG-AMEA)

As expected, attractive interactions between amine SCPs and the glass surfaces in water were observed. Upon contact between SCPs and the coverslip, a distinct contact area forms that can be readily imaged *via* RICM as depicted in **Figure 33** (insets). The Newton fringes of the images showed sufficient contrast to evaluate the contact area. Their homogeneity also suggests that the SCP surfaces are very smooth as indicated by AFM measurements of the SCP surface topography with a root mean square surface roughness of only 2.5 nm. The amine SCPs differ in their degree of functionalization and, consequently, in the resulting adhesion energies on the glass slides (**Table 5**). As a negative control, unmodified PEG SCPs were imaged, showing no adhesion on the coverslips. As expected, the PEG-EDA SCPs with

the highest degree of functionalization (42 µmol/g) show a five times higher adhesion energy when compared to PEG-AMEA SCPs (26 µmol/g)(**Figure 33**). This can be attributed to the higher concentration of amine groups of PEG-EDA SCPs resulting in increased interactions with the glass surface. If the PEG-AMEA SCPs with the PEG-dendrimer SCPs are compared, a stronger adhesion energy for the dendrimer functionalized probes, even with the same number of amine groups, can be seen.

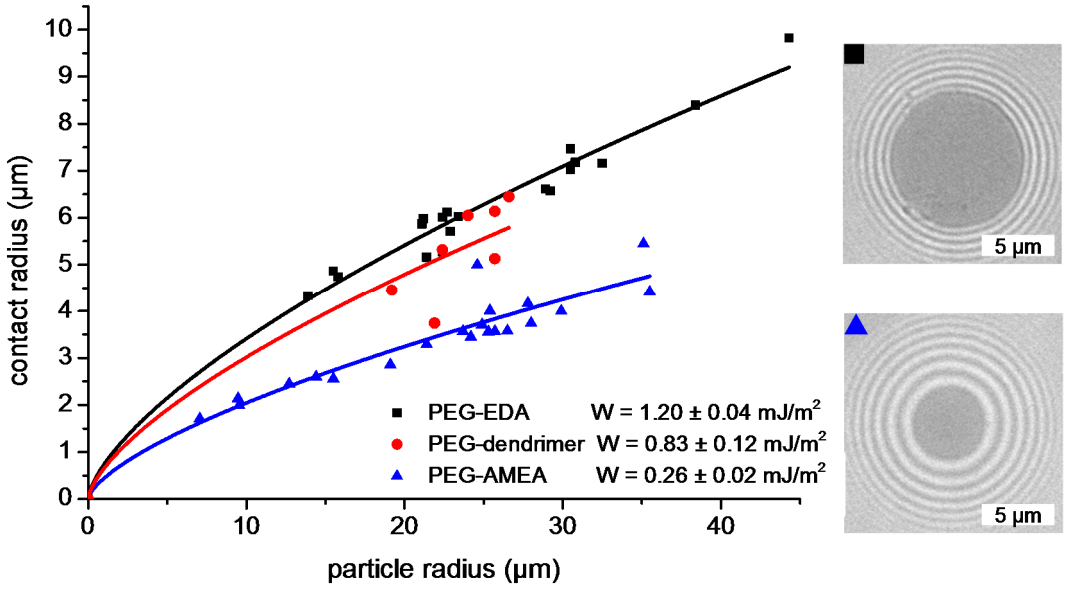

Figure 33: Contact radius versus particle radius of amine functionalized SCPs on a glass surface in water. The contact radii of these SCPs were determined *via* RICM. The typical interference patterns with the adhesion area (grey circle) of PEG-EDA and PEG-AMEA are shown on the right. Adhesion energies *W* were calculated by fitting the data points with the JKR model (eq. 12) using an elastic modulus of the particles of 32 kPa.

The dendrimers present two different amine groups that might show statistical hindrance when binding to silanol surfaces and the reduced surface energy for PEG-dendrimer observations could be attributed to this effect. From the calculated adhesion energies between silica and the amine functionalized SCPs, now the number of molecular contacts can be estimated. In close contact, at intermolecular distances of 0.2-0.4 nm the adhesion is mainly due to acid–base interaction.[108] Formation of acid–base bonds in aqueous solution is exothermic, and the interaction energy amounts to 10-40 kJ/mol.[108] In the neutral pH regime the interaction between silanol (SiOH) and amine (NH_2) groups is on the order of 25 kJ/mol[109], assuming no additional electrostatic and unspecific interactions. For an adhesion energy of 1.2 mJ/m^2 that is measured for the PEG-EDA SCPs gives $3 \cdot 10^{16}$ NH_2-SiOH contacts per square meter corresponding to the amine surface concentration. This

amine surface concentration can be roughly compared to values from the TNBS tests on PEG-EDA SCPs, where a degree of functionalization of 0.34 amines bound to each PEG-dAAm (8000 Da) chain was obtained. A mesh size of 9-13 nm[110,111] of PEG-dAAm (8000 Da) networks then gives ~$1 \cdot 10^{16}$ NH_2-groups per square meter, three times smaller, but of the same magnitude as estimated from the adhesion energy measurement. A similar agreement was achieved, when the adhesion measurement and TNBS tests of AMEA and dendrimer functionalized SCPs were compared. However, the estimation of the amine surface concentration from adhesion measurements did not consider additional unspecific electrostatic interactions. As a result, the adhesion measurements overestimate the number of amines on the particle surface which also may explain the discrepancy with the TNBS measurements.

In order to test the assumption of additional electrostatic contributions to adhesion for these systems, measurements of PEG-EDA SCPs on negatively charged glass surfaces in sodium chloride solutions of different concentrations were carried out (**Figure 34**). These SCPs had a moderate ζ potential of +16 mV. As expected the adhesion energy decreases with increasing salt concentration. This can be attributed to the screening of charges described in the DLVO theory. The residual adhesion energies at high salt concentrations could then be attributed to interactions between SiOH and NH_2-groups.

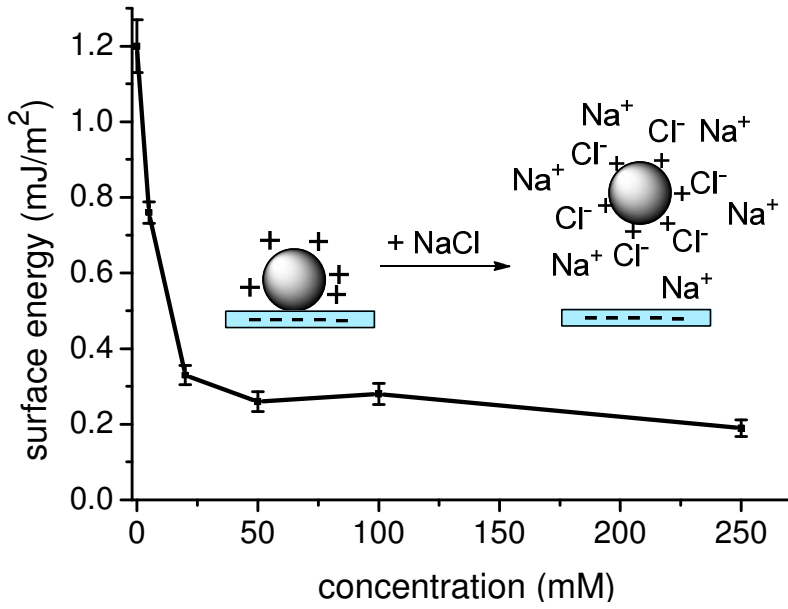

Figure 34: Adhesion energies of PEG-EDA SCPs on a silica surface as a function of sodium chloride concentration. The energy for each data point was calculated from the measured contact radius and the corresponding particle radius obtained by using the JKR model with an elastic modulus of the particles of 32 kPa.

In a second set of experiments, electrostatic interactions of anionic SCPs (PEG-AA and PEG-SUC) against positively charged surfaces were studied. PDADMAC, a cationic charge polyelectrolyte, was dip-coated on glass slides to obtain positively charged surfaces. PEG-AA and PEG-SUC differ in their degree of functionalization by a factor of two, having the same absolute values as the cationic PEG-EDA and PEG-AMEA systems

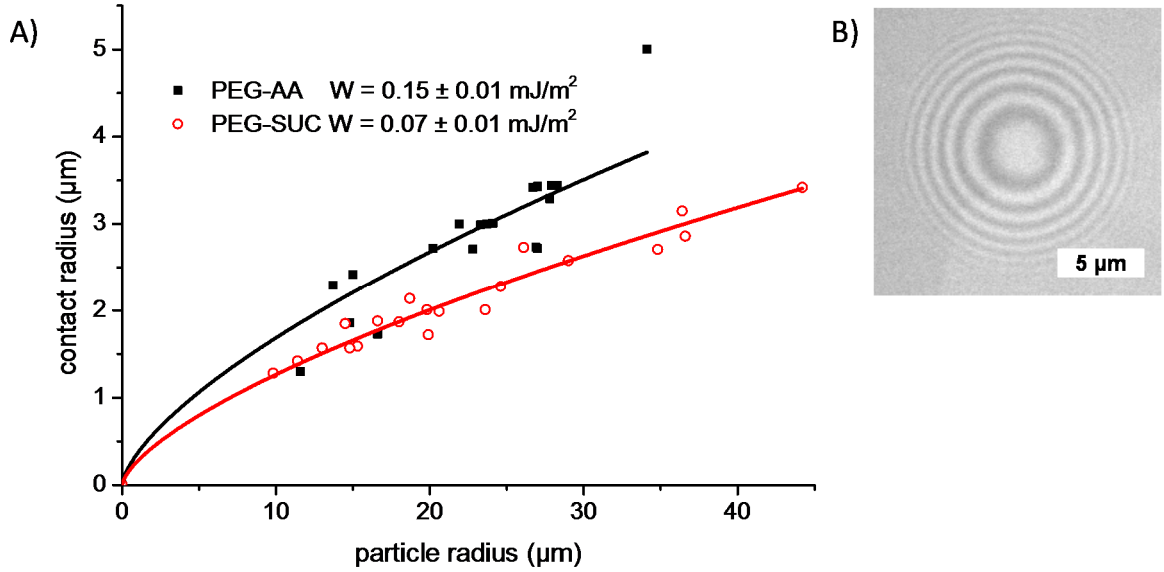

Figure 35: A) Contact radius versus particle radius of carboxylate functionalized SCPs (PEG-AA and PEG-SUC) on a PDADMAC coated glass surface in water. The contact radii of these SCPs were determined *via* RICM. The data points were fitted with the JKR model (eq. 12) to obtain the adhesion energies *W*. B) Interference pattern of positively charged PEG-EDA on PDADAMC functionalized slides.

In comparison with the interactions between the amine SCPs and the silica surfaces, the overall adhesion energy as well as the difference between the two SCPs with carboxylic acid groups is lower. This effect was attributed to the coverslip modification by adsorption of only a single polycation layer. It is known that such initial polyelectrolyte layers form ill-defined and rough surfaces,[112] thus lower adhesion energies with the carboxylic acid SCPs could be expected. As negative control positively charged PEG-EDA SCPs were tested on the PDADMAC slides, and no adhesion was observable due to the repulsive forces of the like-charged surfaces.

The electrostatic interaction measurements at the surface showed that the functionalized SCPs are useful for adhesion measurements. Due to their elastic properties, they strongly deform thus creating a large contact area which can be detected *via* RICM. This now allows focusing on specific interactions mediated by mannose and ConA.

5.2. Carbohydrate-Protein Interactions

So far the SCP technique has been used to measure surface energies arising from electrostatic interactions. Here, the setup will be extended in order to now screen biomolecular interactions of various carbohydrate compounds. Carbohydrates play an important role in many biological recognition events such as cell signaling, inflammation and viral infections.[113,114] The adhesion processes are controlled by interfacial interactions mediated by specific carbohydrate-protein interactions. In general, carbohydrates bind only very weakly to their corresponding proteins but with high specificity. To achieve biologically relevant binding, multivalency is often involved in natural carbohydrate recognition events allowing cells to attach strongly to other biological surfaces.[115] Because of the importance of these adhesion processes mediated by multivalent carbohydrate-protein interactions, the development of techniques to examine, evaluate and quantify these interactions has become more important.

Label free biosensors based on surface plasmon resonance (SPR), impedance spectroscopy or quartz crystal microbalance (QCM) have become standard screening methods in the pharmaceutical industry and in research settings.[116,117] The advantage of these techniques lies in their ability to probe biomolecular interactions with high selectivity without the risk of altering the binding affinity of the analyte molecules e.g. by fluorescent labeling. The developments in this field are directed towards more affordable sensors with increased throughput and enhanced selectivity and sensitivity. Selectivity and sensitivity are still limited in particular for analyte molecules having dielectric constants close to water as the measured signals, e.g. changes in the refractive index (SPR), become very small. Carbohydrates belong to this class of analytes and are exceptionally difficult to analyze because they also exhibit low affinity to their receptors.[118] Direct force-based detection *via* atomic force microscope (AFM), optical traps or the like offer increased sensitivity and also precise information on the nature of the interaction, e.g. discrimination between specific and unspecific binding.[119] Affinity biosensors could therefore take advantage of force-based detection.

The SCP-RICM technique based on force detection can be easily adapted to construct various biosensors for high throughput applications. The SCPs' adhesion energy serves as physical detection signal and is analogous to the resonance frequencies measured with SPR or QCM biosensors. In the following, the well-known mannose/ConA interactions will be

used as a model binding pair and the influences of flexibility and ligand density will be evaluated.

5.2.1. Schematic Discussion of Cooperative Surface Binding

The ligand and receptor molecules participating in the interactions are in general anchored to different interfaces such as membranes. These membranes are composed of lipid bilayers, which undergo thermal fluctuations and deformation due to low binding energies and their high elasticity. The balance between the fluctuating mechanical deformation of the membranes and the affinity of the interacting molecules controls the strength of the adhesion process. In this system, a cooperative binding phenomenon may result due to the smoothing of the rough membranes upon binding to a surface presenting the binding partners.[62] This phenomenon is illustrated in **Figure 36**. Here, the initial binding of the interacting molecules reduces the distances between the interfaces, thereby incrementing the probability of binding of the molecules located in the vicinity of the already existing bonds. In addition, the formation of new bonds induces an elastic deformation of the membrane, which assists in synergic fashion to the creation of new bonds.[62,120] Therefore, the numbers of bonds between the interacting interfaces will depend on the concentration of molecules, their affinity and the elastic properties of the membrane.

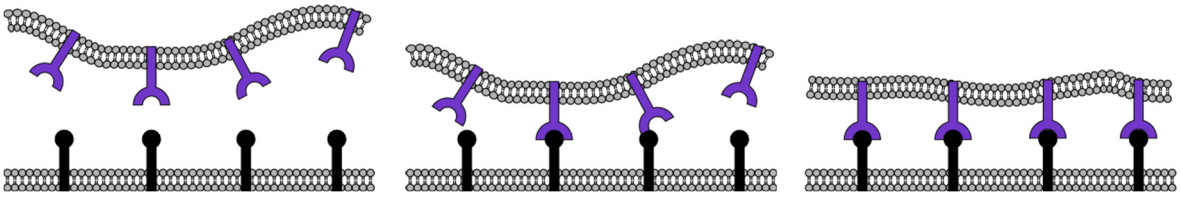

Figure 36: Schematic drawing of membrane flattening when two membranes with their ligands or receptors adhere. The first bond formation increases the probability of a second bond formation as the ligand/receptor pair is in closer proximity. Due to the formation of new bonds the membrane is flattened this in turn increases the probability again of creating a new bond, thus binding cooperativity takes place.

By theoretical studies it was postulated that the thermal fluctuations of the membrane permit the formation of the first bonds between the interfaces.[62,121] The stability and subsequent extension of the adhesion zone depends on the affinity and concentration of the interactive molecules as well as on the deformation of the cell membrane. For instance,

ligands and receptors with high affinity are more effective on pulling and keeping the membrane into the bond distance level, and a high density of the interacting molecules promotes the extension of the adhesion zone by suppressing the thermal fluctuation of the membrane and producing its deformation. Conversely, the adhesion process would be disfavored when the concentration or affinity of the ligand and receptor molecules are low, because the thermal fluctuation of the membrane generates unbinding of the primary bonds. In addition, experimental approaches have confirmed that the concentration of the interacting molecules has a profound effect on the adhesion processes. Albersdorfer et al.[122] established that the adhesion of giant vesicles on planar surfaces is governed by the concentration of receptors in the domains. In such a way, at low concentration of receptors, the domains remain separated for hours, whereas at higher concentrations they form strong adhesion patches in few minutes. In the following the influence of the elasticity and ligand concentration will be studied for the adhesion energy measurements *via* the SCP-RICM approach.

5.2.2. Surface Functionalization and Characterization

In order to determine the adhesion energies between the functionalized PEG-Man SCPs and ConA functionalized glass slides or PEG-ConA SCPs and mannose functionalized glass slides, the glass surfaces were prepared *via* standard surface chemistry using organosilanes.

In general, the functionalization of the glass surfaces is achieved by the reaction of their silanols groups with organosilane reagents. Depending on the organosilane reagent employed, different functional groups such as hydroxyl, amino, aldehyde, expoxy or thiol groups can be introduced to the surfaces. These functional groups serve then as anchoring points for the attachment of the biomolecules, which may be inserted by a wide variety of mechanisms, ranging from covalent to non-covalent interactions, *via* specific parts or specific functional groups of their molecular structure.[123] Importantly, the selected mechanism for the attachment of the biomolecules should not cause conformational changes and should promote a homogenous distribution of the biomolecules in the treated area. In addition, the formation of smooth surfaces during the functionalization process is preferred, as the surface roughness has a profound effect on the adhesion process, mainly by creating a physical barrier between the interacting molecules.[124]

Here, the biomolecule of interest, Concanavalin A (ConA), has been immobilized on the glass surface *via* covalent interactions by the condensation of its primary amino groups (e.g. lysine residues) with the aldehydes or epoxy groups on the glass surface. Both, aldehyde or epoxy coupling, are evaluated for their ability to give smooth surfaces and even distributions of ConA or mannose on the glass slides.

The functionalization of the glass surfaces with aldehyde groups is based on a process consisting of three steps: in the first step, the glass surface is washed with piranha solution (see chapter 8.1) to remove the impurities and to activate the silanol groups (SiOH) on the surface. Subsequently, the silanol groups react with APTES to generate amino functionalities.

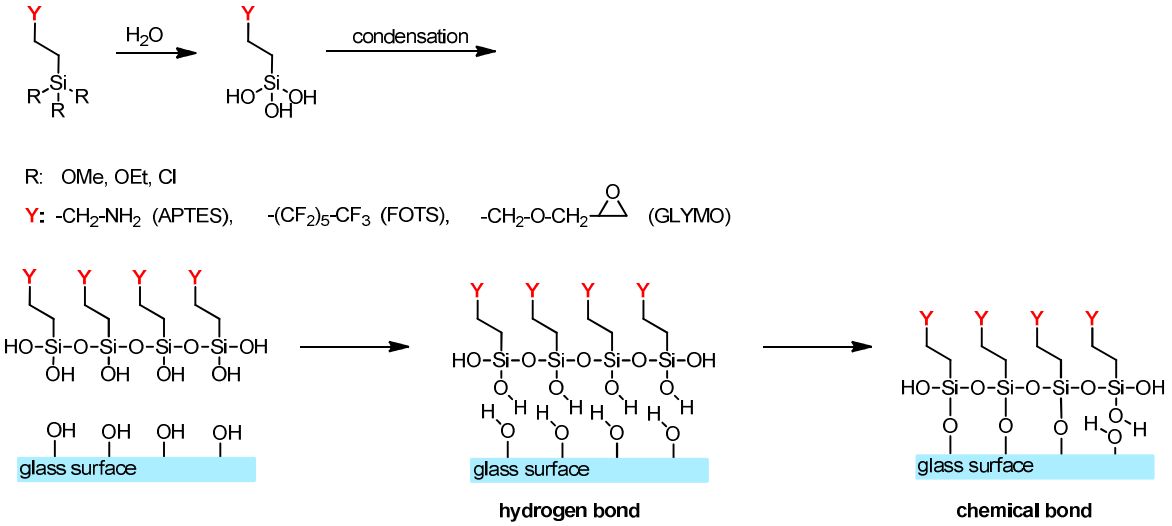

Scheme 11: Functionalization of glass slides with organosilanes giving surfaces with functional groups like amines and epoxides.

Next, the incorporation of the aldehyde groups to the surface is achieved by the reaction of the already available amino groups with glutaraldehyde. The bi-functional glutaraldehyde reacts rapidly with amine groups at around neutral pH. It is the most efficient aldehyde for generating thermally and chemically stable cross-links with amines.[125] The presence of the aldehyde functionalities on the surface then allows the binding of the Con A as it reacts with several functional groups of proteins like amines, thiols, phenol and imidazole. It should be noted that the structure of glutaraldehyde in aqueous solutions is rather complex. It can be present in at least 13 different forms depending on pH, concentration, temperature etc.[126] A small overview of the structures of glutaraldehyde in solution is given in **Scheme 12**A. For simplicity, the cross-linking *via* Schiff's base formation is shown but they are unstable under

acidic conditions. Glutaraldehyde reacts reversibly with amino groups over a wide pH range (≥pH 3), except between pH 7 to 9 where only little reversibility is observed.[126] The cross-linking of proteins generally implies ε-amino groups like lysyl residues.[127] The unprotonated amino groups are very reactive as nucleophiles. It should be noted that lysyl groups have a pKa > 9.5, but it is presumed that the small percentage of amines present in their unprotonated form at lower pH is sufficient to react with glutaraldehyde, driving the acid-base equilibrium to deprotonation of these groups for further reaction.[126]

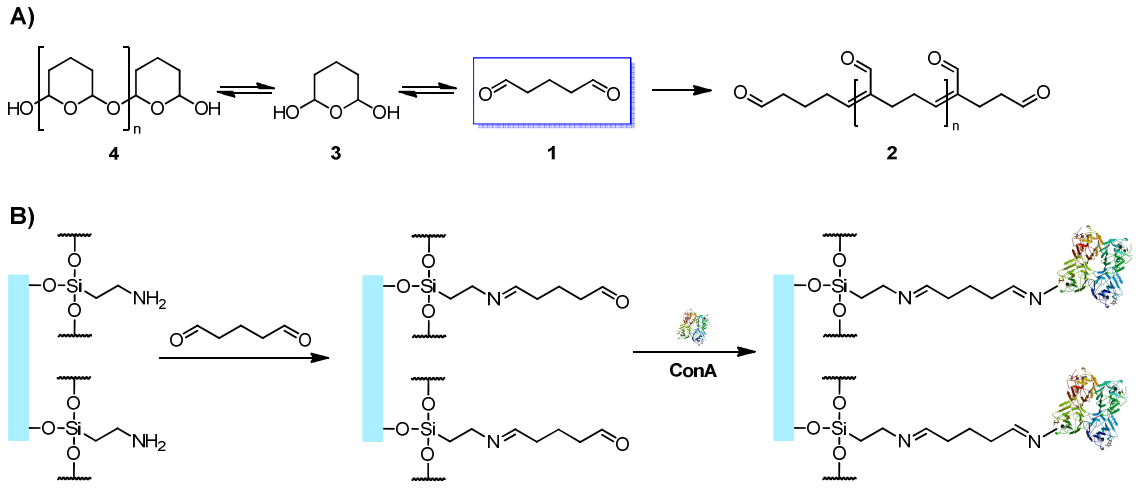

Scheme 12: A) Possible forms of glutaraldehyde (1) in aqueous solution. B) Functionalization of amine slides with glutaraldehyde and further reaction with ConA. For simplicity the reaction with monomeric glutaraldehyde is shown which gives a Schiff's base.

The reaction of the silano groups present on the glass surface with the epoxysilane 3-Glycidoxypropyltrimethoxysilane (GLYMO), permit the functionalization of the surface with reactive epoxy groups (**Scheme 11**). The presence of these groups allows the subsequent binding of α-thioethyl-mannose by the nucleophilic ring-opening of the epoxide by thiols.

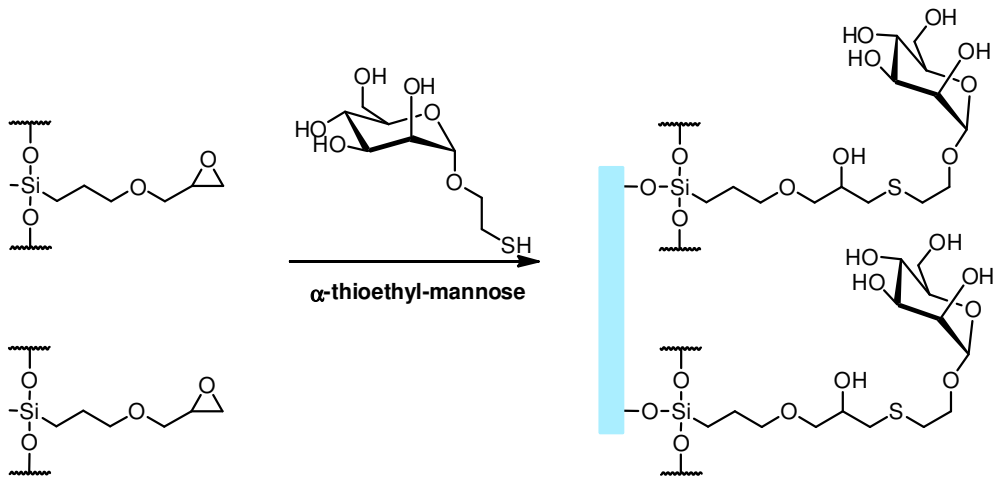

Scheme 13: Reaction of epoxy functionalized glass slides with α-thioethyl-mannose

The homogeneity and the roughness of the glass surface functionalized with ConA were studied *via* AFM by Dr. Stephan Schmidt. Here, the surface properties were evaluated at the same conditions that will be used for the adhesion measurements (functionalized glass surfaces immersed in lectin buffer), in order to avoid possible changes of the conformation of the protein e.g. by performing the measurements in air. The surface properties were evaluated in tapping mode to prevent the detachment of the proteins by a prolonged contact with the cantilever.

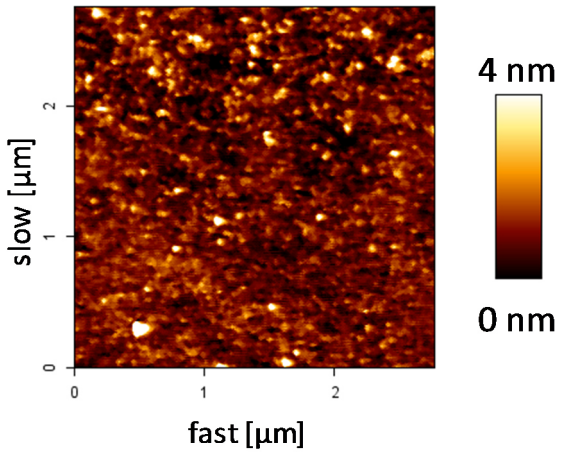

Figure 37: Topographical AFM images of glass surfaces functionalized with aldehyde/ConA obtained by tapping mode under lectin buffer. The image shows a smooth functionalized surface.

Figure 37 presents the AFM images of glass surfaces functionalized with APTES/Glutaraldehyde/ConA. The surface properties were evaluated on different spots in order to probe that the surface properties do not vary in different areas of the glass slide. It

shows a homogenous distribution of the ConA with an average roughness of 0.75 nm. The surface density of the ConA and Man-surfaces almost reached close packing ($1.03 \cdot 10^{16}$ and $1.27 \cdot 10^{16}$ ConA per m^2), as measured by amino acid analysis. Overall these results show that the functionalized glass surfaces are suitable for the measurements between the functionalized SCPs and the corresponding surface in a so called direct binding assay.

5.2.3. Direct Binding Assay *via* SCP Adhesion

The direct binding assay follows the same principle as explained in chapter 5.1. Here the measurement principle is based on the adhesion induced deformation of a ligand bearing SCP on a receptor surface or vice versa that can be related to the surface energy by the JKR theory. In analogy to affinity biosensors like SPR, this technique now allows for direct binding assays, where the signal is read out after binding of ligands and receptors. In case of the SCP measurement the signal was obtained by reading out the adhesion energies between mannose and ConA coated surfaces. Taking into account the surface densities of these binding partners, the specific ligand/receptor binding energy can be determined.

With this setup and using the 32 kPa PEG-Man SCPs (see chapter 4.3.1), first the direct binding assay was performed and two experimental options were compared: a) Man-SCP on ConA surface; and b) ConA-SCP on Man-surface (**Figure 38**). The surface energies of the SCPs were obtained measuring the SCP radii and contact area with the glass surface by RICM. The data was then fitted with Equation (12), yielding the surface energy W of the SCPs.

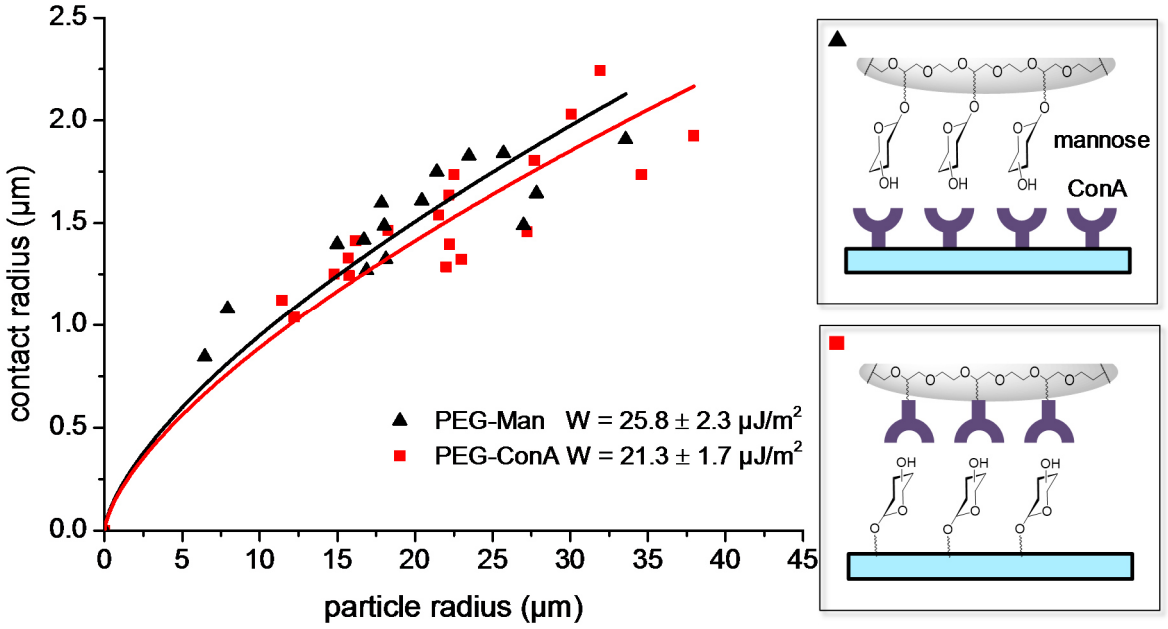

Figure 38: Contact radius versus particle radius for the different experimental configurations: ▲) SCPs with mannose ligands and a ConA functionalized glass surface; ■) SCPs with ConA and a Man-functionalized glass surface. The solid lines correspond to the adhesion energy *W* fitted with the JKR model (eq. 12). Both fit curves give similar results of the adhesion energy.

The surface energy obtained in direct binding of the Man-SCPs on ConA was 25.8 ± 2.3 µJ/m^2 and 21.3 ± 1.7 µJ/m^2 for the ConA-SCPs adhered to the Man-surface, respectively. Both systems show similar surface energies indicating similar densities of the binding partners as also shown by amino acid analysis as well as the independence of the binding partner's location (either on SCP or glass slide). The experimental data can be put into context with the theoretical upper limit of the adhesion energy between ConA and mannose. The upper limit assumes the ideal situation in which all ConA binding pockets on the surface bind to a mannose ligand with 5.2 kcal/mol contribution to the surface energy. With the ConA densities as measured by amino acid analysis, the upper surface energy limit would be 290 µJ/m^2 and thus 10 times larger than the measured values. The stark difference between upper theoretical limit and measured value can be explained by the surface roughness on the order of 3 nm and non-ideal distribution of binding partners: The mannose-ligands have a similar but random spacing compared to the ConA binding sites. Therefore the positions of most binding partners do not match entirely, overall reducing the probability of specific Man/ConA interactions (**Figure 39**).

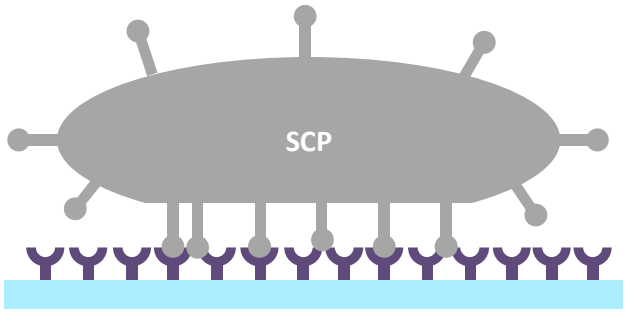

Figure 39: Schematic drawing of the random distribution of ligands that do not entirely match with the receptor binding partners causing a reduction in adhesion energy.

The specificity of the SCP adhesion was tested by addition of competitively binding sugar ligands into the measurement cell, for example, 10 mM α-methyl-D-mannose. At a critical level of competitive ligands, the SCP contact areas and surface energies completely vanish, thus indicating the specificity of the SCP-glass slide adhesion (**Figure 44**). Importantly, when adding α-methyl-D-mannose at lower concentrations up to 1 mM, the probes are still in contact with the glass surface and the surface energy gradually decreases with increasing concentration of competitive sugar ligands. Therefore, depending on their concentration and affinity, the ConA receptors are inhibited only partially by the added sugar ligands. This can be directly visualized by the decreasing SCP contact areas upon sugar addition and quantified in terms of surface energy by the JKR approach. Owing to the specificity of the interaction and the concentration-dependent response of added sugar ligands, the SCP measurements can be used to perform inhibition/competition assays. This procedure involves variation of the analyte concentration and measurement of the respective SCP surface energies. Generally, these assays yield the half-maximal inhibitory concentration (IC_{50}) of the analyte as a measure of the analyte affinity (chapter 5.2.4). The resolution in direct binding measurements for adhesion energy determination is limited by the inability of the method to differentiate between contact radius shifts smaller than 0.5 µm (this is dependent on the used wavelength, here 546 nm). However, the resolution limit can be significantly enhanced by using softer SCPs.

5.2.3.1. Variation of the Young's Modulus

Substrate stiffness is being perceived as an important physical factor in the response of many cell types to the substrate surface.[128,129] As of yet, the mechanism for this mechano-sensitve behavior of cells is still under debate. Most likely, the lack of information regarding

this factor stems from the fact that studies on the adhesion processes so far have been focused on the employment of giant vesicles or various cell systems.[130,131] In this respect, the modulation of the elastic properties of the vesicles cannot be achieved easily as their interior is not supported by the three dimensional network. The use of cells for the elucidation of the effect of elasticity is also not the best option, due to the involvement of multiple parameters that cannot be controlled or deconvoluted easily.

In order to study the effect of material stiffness on ligand/receptor interactions with a simplified measurement system, ConA modified coverslips (see chapter 5.2.2) and mannose functionalized PEG-SCPs (chapter 4.3.1) with different mechanical properties (chapter 3.1) were used. The SCPs with a Young's modulus of 4 and 15 kPa were prepared with PEG-dAAm with a molecular weight of 20000 Da, whereas the 32 kPa SCPs were prepared with PEG-dAAm with 8000 Da. **Figure 40** presents the adhesion energy of PEG-Man SCPs with varying Young´s modulus on ConA surfaces (PEG-Man (32 kPa), PEG-Man (15 kPa) and PEG-Man (4 kPa), respectively).

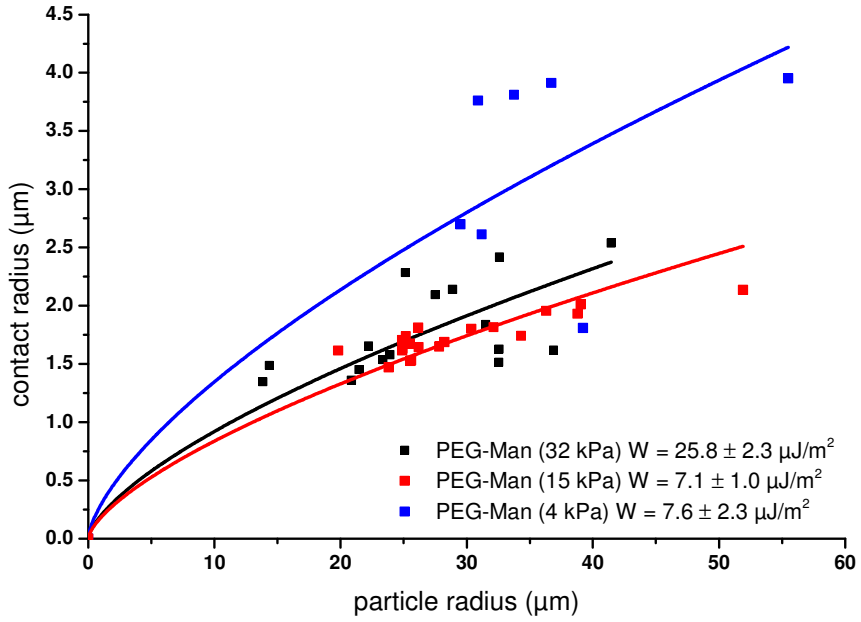

Figure 40: Influence of the backbone flexibility of PEG SCPs on the adhesion measurements. The functionalization degree is equal in all cases. Lowering the Young's modulus from 32 kPa to 4 kPa lead to an increase in the contact radii.

All SCPs showed a similar functionalization degree of mannose groups of around 56 µmol/g (**Table 6**). When the molecular weight of the PEG is increased from 8000 to 20000 Da, the Young's modulus is decreased from 32 kPa to 15 kPa. This was attributed to

the longer, more flexible chains of PEG 20000 Da. It is interesting to note, that with the same functionalization degree of 56 µmol/g the contact areas of PEG-Man (15 kPa) are equal to the contact areas of PEG-Man (32 kPa). Here, the ligand density is lower compared to the 32 kPa SCPs as they are spread over a larger backbone, so that the distance between two mannose groups is expected to be larger. In general, a lower ligand density would lead to smaller contact areas but the softness of the SCPs enhances the deformation leading to similar contact areas. A further decrease in the elasticity to 4 kPa and equal functionalization degree of 54 µmol/g lead to an increase in the contact areas. Here, the more flexible chains enhance the deformation of the SCPs again leading to larger contact areas (**Figure 41**).

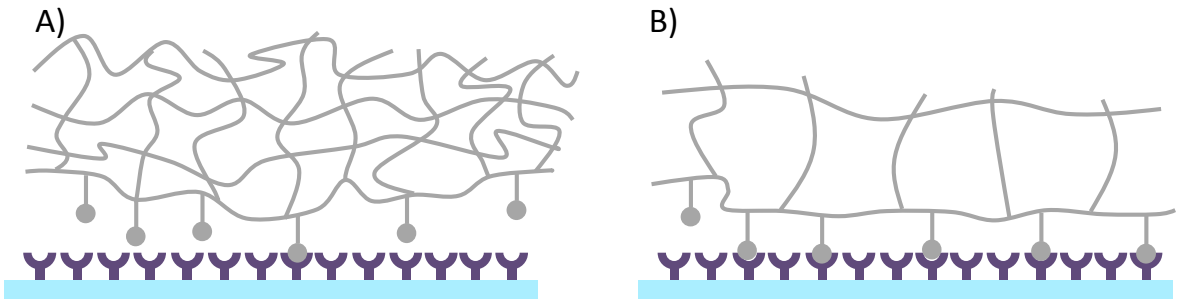

Figure 41: Schematic drawing of the binding of ligands to receptors for A) a 32 kPa SCP and B) a 4 kPa SCP with the same functionalization degree. The contact area increases when the Young's modulus decreases.

Table 6: Adhesion energies of PEG-Man SCPs with different Young's modulus

Sample	Mannose functionalization [µmol/g]	Adhesion energy [µJ/m^2]
PEG-Man (32 kPa)	56 ± 14	25.8 ± 2.3
PEG-Man (15 kPa)	56 ± 25	7.1 ± 1.0
PEG-Man (4 kPa)	54 ± 14	7.6 ± 2.3

The adhesion energy decreases for SCPs with similar contact radii but different Young's moduli (PEG-Man (32 kPa) and PEG-Man (15 kPa)). As the adhesion energy W is proportional to the Young's modulus E (Equation (3)) the adhesion energy will be decreased given similar contact areas. Comparing now the 4 kPa and 15 kPa SCPs the adhesion energy is similar. This can be explained by the increase in the contact areas while decreasing the Young's modulus. In general, softer SCPs increase the sensitivity of the measurements as they form larger contact areas and thus allow the measurements of weak interactions. In the following the influence of the ligand density will be discussed.

In terms of adhesion energy as a function of SCP stiffness, no clear trend could be observed. This could be the consequence of two contributions, the chain entropy and chain bending rigidity that may oppose each other when varying the stiffness of PEG-SCP: On the one hand, one could expect an increase of the adhesion energy when increasing the stiffness of the SCP due to entropic reasons. Increasing the stiffness would decrease the chain flexibility, therefore the entropic cost by immobilizing the PEG chains due to adhesion on the substrate would be reduced, hence *larger* adhesion energies could be observed. On the other hand, when increasing the elastic modulus of the PEG SCPs the bending rigidity of the polymer increases. This may *reduce* the adhesion as the enthalpic cost to bend the polymer chains such that the same amounts of ligands and receptors bind is increased. This interplay between chain entropy and bending rigidity on polymer interactions has been theoretically analyzed by Forrey *et. al.*[132] As of yet, the presented measurements give only a crude experimental insight into these phenomena, one would need to vary the elastic properties over a much larger range in order to completely ascertain the effect of surface stiffness on specific adhesion.

5.2.3.2. Variation of Acid Ligands and Ligand Density

Cell adhesion mediated by ligand/receptor interaction is expected to be strongly influenced by ligand and receptor density.[133] The density would influence both, the rate at which ligand/receptor bonds form and the final density of ligand/receptor bonds between the cell and the adhesion surface. The number of bonds between the cell and surface directly influences the strength of cell adhesion. The ability to design biomimetic substrates with known and quantifiable densities thus allows studying the influence of ligand density on adhesion phenomena.

In the following chapters, first the effect of the mannose group concentration on PEG-CA SCPs will be evaluated. Therefore, PEG-CA probes with three different functionalization degrees will be tested for their influence in adhesion experiments (**Figure 42**). Then, the effect of the grafting type of PEG-AA and PEG-MAA SCPs with similar mannose group concentrations will be tested for its effect on the adhesion on ConA functionalized surfaces.

PEG-CA probes were synthesized by Hanging Wang, MPI KGF, Golm, with three different functionalization degrees (low, middle and high). The probes were then further functionalized with aminoethyl-mannose and the influence of the ligand density on adhesion

was studied. In principle, a higher functionalization degree should increase the surface interactions due to multiple binding events thus deforming the SCP stronger (**Figure 42**).

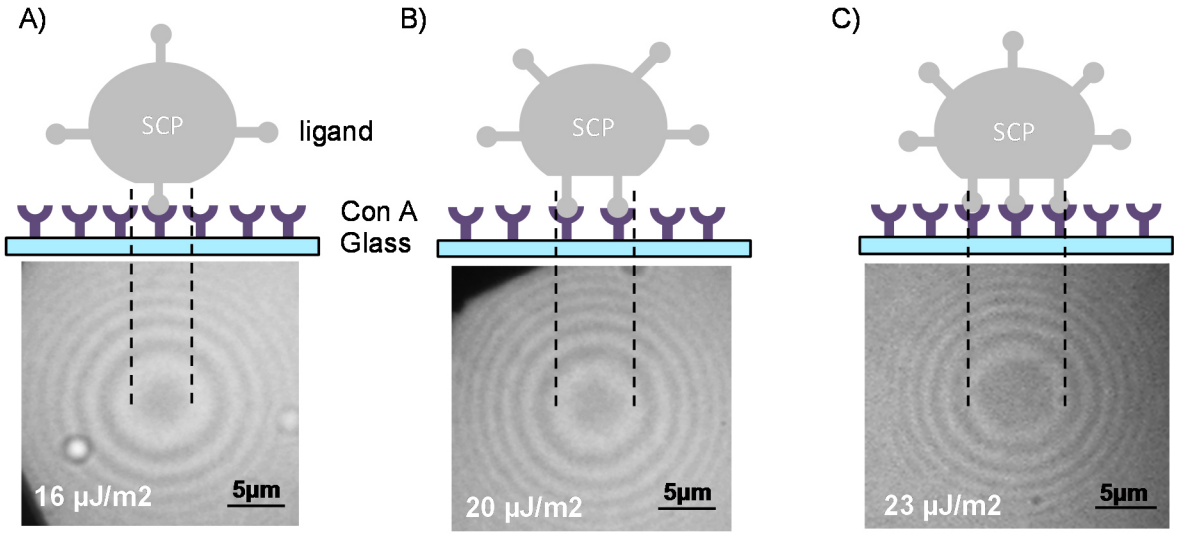

Figure 42: Schematic representation of the ligand density on A) low functionalized SCPs (PEG-CA_{low}); medium functionalized SCPs (PEG-CA_{middle}) and C) highly functionalized SCPs (PEG-CA_{high}) and the corresponding contact areas.

The results in **Figure 43** and **Table 7** show that a higher ligand density on the PEG-CA probes leads to higher values for adhesion energies. The increase in adhesion energy can be explained by the higher ligand/receptor bond formation at higher mannose concentrations. Moreover, it was found that with a mannose concentration of 22 ± 6 µmol/g, an adhesion energy of 16 ± 2 µJ/m^2, and with a twofold increase to 44 ± 8 µmol/g an 1.2-fold increase of the adhesion energy of 20 ± 2 µJ/m^2 was obtained. Another twofold increase of 89 ± 9 µmol/g leads again to a 1.2-fold increase of the adhesion energy (23 ± 2 µJ/m^2).

Table 7: PEG SCPs with different carboxylic acid ligands and its corresponding mannose functionalization. Adhesion energies obtained with these SCPs

Sample	Concentration of mannose groups (µmol/g)	Adhesion energy per square meter (µJ/m^2)
PEG-CA_{low}	22 ± 6	16 ± 2
PEG-CA_{middle}	44 ± 8	20 ± 2
PEG-CA_{high}	89 ± 9	23 ± 2
PEG-AA	56 ± 14	24 ± 2
PEG-MAA	193 ± 29	47 ± 5

The ligand density influences the adhesion of the SCPs to the surface. Besides the possibility to increase the ligand density on the probes by increase of functionalities, the ligand density can be also increased by different graftings on the SCPs. Attaching a polymer due to grafting of a polymerizable monomer to the SCP surface leads to multivalent presentation of the ligand. This was achieved through the grafting of AA and MAA to the SCPs, and the influence of the grafting type on the adhesion was studied. Here, the polymer chains on the SCPs should present the mannose in a highly multivalent fashion which should increase the possibility of binding of the ligands to the receptors. The flexibility of the polymers should be higher compared to the flexibility of the scaffold and thus the adhesion should increase in comparison to PEG-CA probes. An effect for the different grafting types was indeed observed (**Figure 43**B). It can be seen that the adhesion energy of PEG-AA with a polyacid chain is 23 ± 2 µJ/m^2 at a functionalization degree of 56 ± 14 µmol/g, whereas similar adhesion energy of 23 ± 2 µJ/m^2 for PEG-CA$_{high}$ but with a higher functionalization degree of 89 ± 9 µmol/g was obtained.

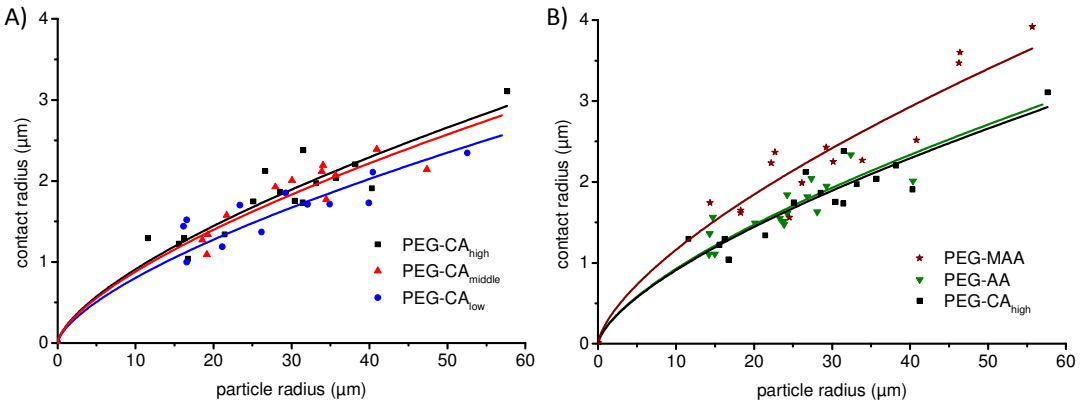

Figure 43: Contact versus particle radius plotted for A) the different ligand densities and B) different grafting types of PEG SCPs

Considering the mannose group concentration of PEG-AA which is almost half of the PEG-CA$_{high}$ concentration, one can conclude that polyacid chains grafted on the particles are more efficient in the adhesion processes than single mannose ligands presented by PEG-CA. Also, for a twofold increase in the concentration from PEG-CA$_{high}$ (89 ± 9 µmol/g) to PEG-MAA (193 ± 29 µmol/g) the adhesion energy increases also twofold from 23 ± 2 µJ/m^2 to 47 ± 5 µJ/m^2 compared to an increase of 1.2-fold for a monomeric grafted molecule.

The increase in adhesion energies for polyacid grafted SCPs can be explained by the grafted polymer chains that are flexible, which dramatically increases the probability of

finding its target compared to ligands firmly anchored on the surface. Therefore they can bind to the binding pockets of ConA, even when the mannose group concentration e.g. of PEG-AA is lower compared to PEG-CA_{high}. The thermal fluctuations of grafted chains also produce a spring-like force that pulls bridged surfaces together once the ligand/receptor bond is formed.[134] This same entropic effect is responsible for repulsive steric forces as the grafted polymer is compressed. The net achievement is a long-range attraction and a shorter-range repulsion between two surfaces.[135] These forces may extend beyond the influence of attractive van der Waals or repulsive electrostatic forces and thus dictate the adhesive properties of surfaces, as well as the strength of the adhesion between the probes and the receptor surface. In all cases, some unreacted carboxyl groups are present which can have repulsive forces with the negatively charged ConA as the pI is in the range 4.5-5.5.[136] The PMAA chains have a more hydrophobic character compared to PAA which can positively contribute to the adhesion due to some attractive hydrophobic forces resulting in higher adhesion energy. Overall, higher ligand densities on the SCPs lead to higher adhesion energies. Polymeric chains on the SCP increase in turn the adhesion energy due to their multivalent fashion and flexibility to find the corresponding binding partner. This higher ligand/receptor bond formation at higher mannose concentrations is responsible for the larger adhesion energies.

5.2.4. Inhibition/Competition Binding Assay

The direct binding assays as performed so far allow for the characterization of soft (bio)-interfaces but are not well suited for high-throughput screening applications, as each analyte would need to be conjugated to either of the two surfaces. Alternatively, the SCP-RICM can be used for an inhibition/competition assay that gives fast and straightforward access to affinities of added analytes that bind to either receptors or ligands. Upon addition of such additional analytes, they compete with the bonds that were formed upon adhesion of the SCP to the receptor surface (direct binding assay) and thereby inhibit the interaction between the SCP and the surface. Depending on the concentration and the affinity of the analyte, the contact area and surface energy will decrease. If all of the binding sites are occupied, the SCP detaches from the surface. Consequently, detection of contact area changes upon analyte addition yields the inhibitory concentration and thus the binding affinity of the analyte (**Figure 44**).

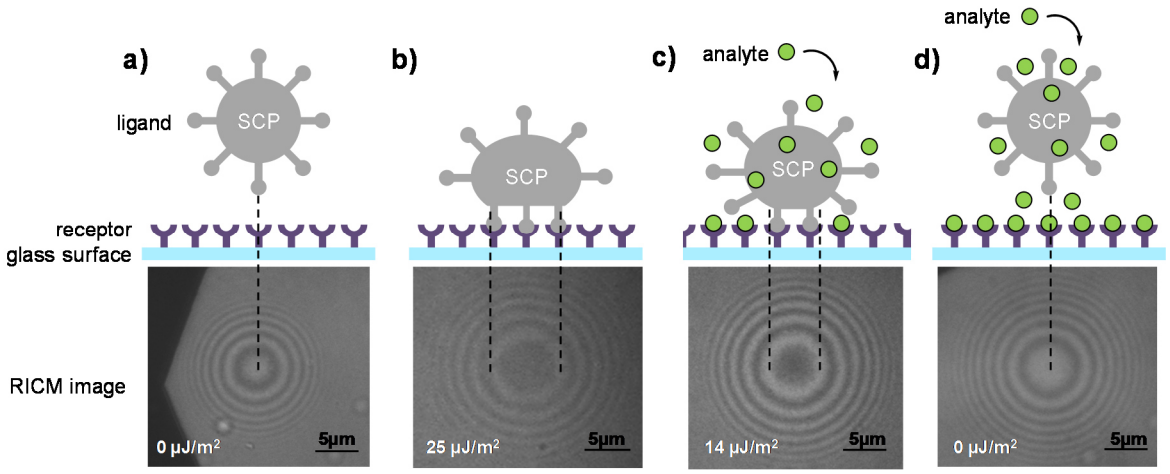

Figure 44: General principle: a) the ligand-functionalized probe comes into contact with the functionalized receptor surface, and b) upon contact with the receptor surface, ligand/receptor complexes form and induce mechanical deformation of the SCPs. c) Inhibition affinity assays by addition of analytes and detection of contact area until d) the probe detaches from the receptor surface. The RICM images show the contact area between the probe and the receptor surface, where the dark area in the center signifies the contact area. The upper sketch is not to scale, and the geometrical match between ligand and receptor surface is visually idealized.

As analytes, various monosaccharides were used: α-methyl-D-mannose, D-mannose (D-Man) and D-glucose (D-Glu) with different binding affinities to ConA. All of the measurements were conducted with the PEG_{8k}-Man SCPs and ConA glass surfaces. Furthermore, the SCP elastic modulus (4, 15, and 32 kPa) was varied to study the effect of PEG flexibility on the IC_{50}. With the direct binding between PEG-Man SCPs and ConA surface as a reference, the different analytes were added, and for each concentration the decrease in surface energy was determined until the SCPs were detached completely. **Figure 45** shows the surface energy normalized direct binding experiment as a function of the inhibitor concentrations.

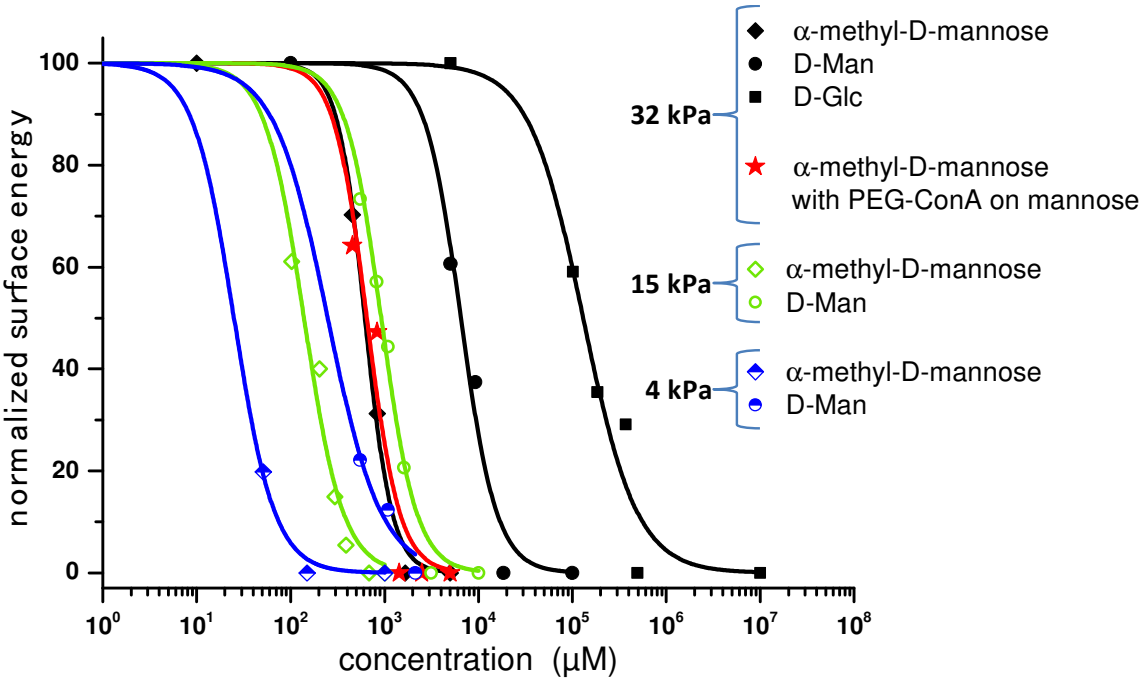

Figure 45: IC_{50} curves for various monosaccharides as analytes inhibiting the Man/ConA interaction

The normalized surface energy data showed a characteristic sigmoidal shape that was fitted with the Hill equation to obtain the IC_{50} values *k*:

$$y = Start + (End - Start)\frac{x^n}{k^n + x^n} \tag{21}$$

where *Start* is the value at 100% binding and equals 100, *End* is the value where the SCP is detached and no binding is observed anymore and equals 0, *x* corresponds to the concentration and *n* describes the cooperativity.

To compare the IC_{50} obtained with the different SCPs a 'relative activity" was used that relates every analyte to the IC_{50} of α-methyl-D-mannose (**Table 8**) (e.g. for Man(1,3,5)-5: 620 µM/((IC_{50} value) µM · (number of Man residues) = 620 µM/(0.8 µM · 3) = 258). Clearly, all of the carbohydrate inhibitors reduced the surface energy of the SCP owing to binding and inhibition of ConA. As expected, the monosaccharides show decreasing relative affinity from α-methyl-D-mannose, D-Man, to D-Glu, in agreement with calorimetric studies in solution.[137]

Table 8: IC_{50} values and relative activities normalized per Man unit of sugar analyte as measured by SCP-RICM

Inhibitor	SCP-RICM IC50 [µM]	Relative activity/Man
D-Glc	$1.3 \cdot 10^5 \pm 1.9 \cdot 10^4$	0.005
D-Man	6490 ± 500 (32 kPa)	0.1
	920 ± 36 (15 kPa)	0.15
	248 ± 81 (4 kPa)	0.1
α-methyl-D-mannose	620 ± 20 (32 kPa)	1
	140 ± 12 (15 kPa)	1
	25 ± 2 (4 kPa)	1
α-methyl-D-mannose[a]	650 ± 80	1
Man(3)-5	6.1 ± 0.7	101
Man(1,5)-5	3.4 ± 0.5	91
Man(1,2)-5	3.9 ± 0.3	80
Man(1,3,5)-5	0.8 ± 0.1	258
Man(all)-5	0.4 ± 0.1 (32 kPa)	248
	0.12 ± 0.02 (15 kPa)	234
	<0.05 (4 kPa)	>100
Man(all)-10	0.3 ± 0.1	207
Man(2,4,6,8,10)-10	0.09 ± 0.01	1378
oligo(amidoamine) backbone	n.b.	-

a) Inverted system PEG-ConA SCPs on Man functionalized glass slides; n.b.: not binding

It can be seen that it does not matter what system is used to measure the IC_{50} values (PEG-Man/ConA or PEG-ConA/Man, see **Figure 38**) as with both systems similar IC_{50} for α-methyl-D-mannose were obtained (620 ± 20 and 650 ± 80 µM, respectively). The similarity between values can be attributed to exclusively specific interaction between Man and ConA and to the similar coverage of the SCPs and surfaces by the ligands and receptors like it was shown in the amino acid analysis (see chapter 4.3 and 5.2.2).

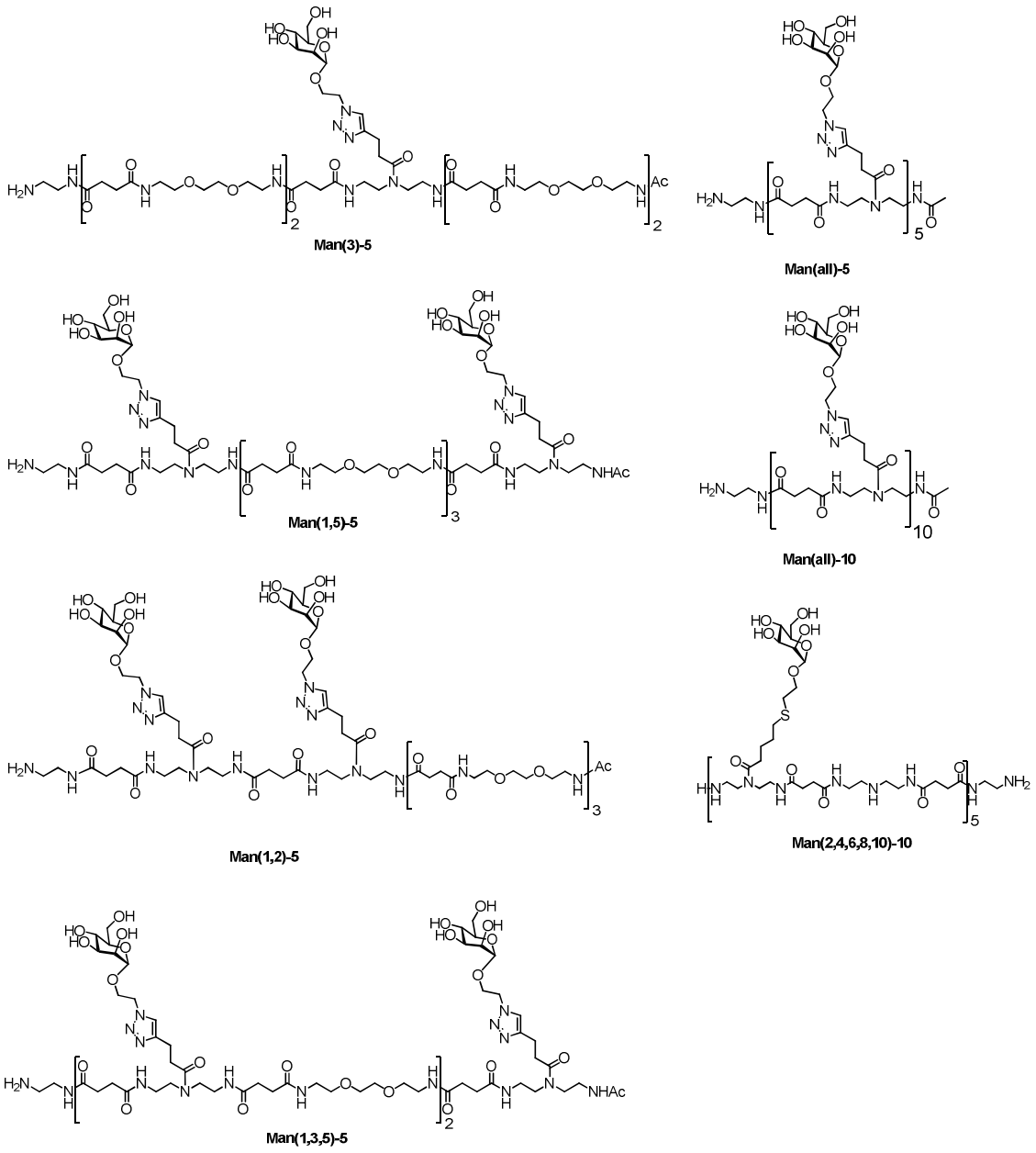

Scheme 14: Structures of the sequence-defined oligoamidoamines

Furthermore, the IC_{50} decreases by a factor of 4 when the Young's modulus is reduced by half from 32 kPa to 15 kPa and by a factor of 25 when reducing the elastic modulus from 32 kPa to 4 kPa. This is likely to be due to an increased entropic gain upon unbinding the softer, more flexible PEG chains from the receptor surface.[115,138] But it is important to note that the relative activities are similar regardless of the probes elastic modulus, meaning that the SCP method is quite robust. The SCP screening assay is able to identify the analyte affinity even though the SCPs may differ in elastic modulus.

To show that the assay is also suitable for structurally and chemically different model drugs, a set of multivalent glycooligomers based on monodisperse sequence defined

oligo(amidoamine) scaffolds with a molecular weight of 2 kDa were synthesized by Daniela Ponader and studied in inhibition/competition assays.[139] The oligo(amidoamines) carry up to five Man groups on a single chain of the same length (Man(3)-5, Man(1,5)-5, Man(1,2)-5 and Man(1,3,5)-5, Man(all)-5). To test longer oligo(amidoamines) a molecule of ten repeating units was synthesized (Man(all)-10). The nomenclature for the glycooligomers is as follows: Man defines the sugar that is bound on the backbone; the number in brackets defines the position where the sugars are placed on the backbone; and the last number defines the number of units of the backbone.

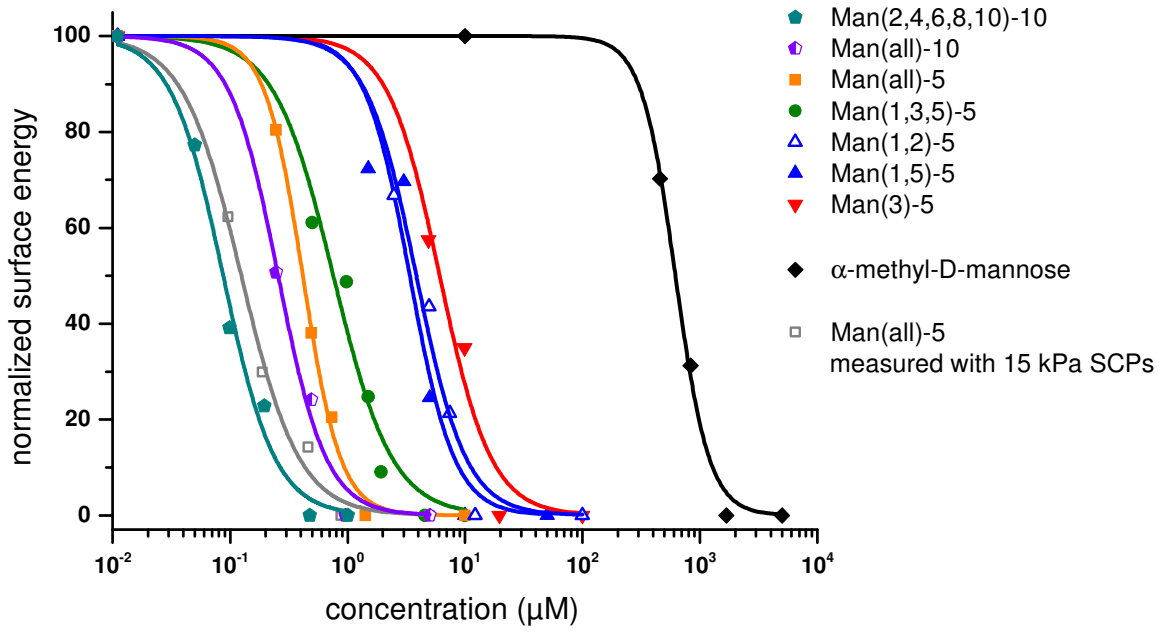

Figure 46: IC_{50} curves for various homomultivalent oligo(amidoamines) as analytes inhibiting the Man/ConA interaction

All oligomeric structures show strong inhibition of ConA surfaces with IC_{50} values in the micromolar range and the same structural dependence as was previously observed by a comparable SPR study.[139] The oligo(amidoamine) backbone shows no affinity to Con A thus confirming no non-specific interactions of either scaffold or non-binding ligands. The monovalent Man(3)-5 showed the lowest binding affinity but a high increase of 100-fold compared to α-methyl-D-mannose. The high affinity of Man(3)-5 is possibly due to the hydrophilic ethylene glycol spacer in its backbone. It is known that ethylene glycol is highly hydrated when dissolved in water. Upon binding of the molecule to the receptor the water molecules can be released resulting in a gain in entropy.[115,139] The divalent Man(1,2)-5 and Man(1,5)-5 showed enhanced affinity compared to monovalent Man(3)-5. Surprisingly the

symmetric divalent Man(1,5)-5, which might be able to bridge two binding pockets of ConA (chelate), and the asymmetric Man(1,2)-5, not able to bind two binding sites simultaneously, showed similar binding affinity. A chelate binding of two binding sites by one molecule would drastically increase the binding affinity due to the enthalpic gain of binding a second site in combination with the reduced entropic cost of binding the second site.[115] Thus, since both Man(1,5)-5 and Man(1,2)-5 showed a similar affinity one can conclude that Man(1,5)-5 does not undergo chelate binding, but both molecules show enhanced statistical rebinding to ConA when compared to the monovalent Man(3)-5. Furthermore, the so-called steric shielding effect of receptor binding sites[138] due to the bulky backbone might also lead to an increase in affinity (**Figure 47**). The trivalent Man(1,3,5)-5 glycooligomer presented a significantly enhanced relative activity of 258 compared to the mono- and divalent molecules. Man(all)-5 and Man(all)-10 show further increased binding affinity due to an increase in the number of mannose residues but the relative activity per mannose stayed equal to the trivalent molecule, although an increased statistical rebinding effect could be expected for higher multivalency. Even though the 10mer has the probability for chelating the binding pockets, the SCP-RICM approach does not show the effect of the additional Man sub-units because they hinder each other in binding. To test this assumption a 10mer was synthesized by Felix Wojcik (Man(2,4,6,8,10)-10) which has 5 Man residues on the backbone but with an additional spacing unit that differs from the previous ethylene glycol unit. Here, the relative activity increases one order of magnitude to 1378 compared to Man(all)-10 or Man(all)-5 with a relative activity of around 200. This high increase in the relative activity can potentially be attributed to chelate binding of the molecule, as the longer distance between the Man residues and the more flexible structure promotes this binding mode. But one has to note that this structure differs in its coupling of the sugar residues compared to the Man(2,4,6,8,10)-10 molecule as the sugar was introduced *via* the thiol-ene chemistry, which may also have an effect on the overall binding affinity due to the different linker chemistry.

Besides different oligomers presenting only mannose ligands along the scaffold (‘homomultivalent ligands’) also so called 'heteromultivalent' constructs were investigated.[140] Here, starting from the all Man(1,3,5)-5 ligand, the mannose residues were replaced stepwise towards galactose or glucose ligands. Galactose shows no affinity towards ConA while glucose shows a slightly reduced affinity to ConA when compared to mannose.[141]

Table 9: IC_{50} of the heteromultivalent glycooligomers measured by SCP-RICM

Inhibitor	SCP-RICM IC50 [µM]
Man(1,3,5)-5	0.8 ± 0.1
Glc(1,3,5)-5	2.1 ± 0.1
Gal(1,3,5)-5	n.b.
GalManGal(1,3,5)-5	1.0 ± 0.1
ManGalMan(1,3,5)-5	0.8 ± 0.1
ManManGal(,1,3,5)-5	0.7 ± 0.1
GlcManGlc(1,3,5)-5	0.4 ± 0.1
ManGlcMan(1,3,5)-5	0.5 ± 0.1

n.b.: not binding

The non-binding galactose on Gal(1,3,5)-5 showed no binding to the ConA surface as expected. Replacing the mannose residues with glucose (Glc(1,3,5)-5) showed a three time lower IC_{50} value compared to the Man(1,3,5)-5. It is known in literature that glucose binds 4 times less than mannose to ConA[142] which also explains the lower affinity. The IC_{50} values obtained for three trivalent structures with galactose but different ligand composition, GalManGal(1,3,5)-5, ManManGal(1,3,5)-5 and ManGalMan(1,3,5)-5 show IC_{50} values in the same range as Man(1,3,5)-5. A decrease in the affinity would be expected by exchanging the binding mannose ligands towards non-binding galactose ligands due to a decrease in statistical probability of one or more mannose ligands to bind to the ConA receptor. This indicates that all trivalent systems undergo monovalent binding while the other residues, binding or non-binding, promote steric shielding of the unbound binding pockets of ConA. Replacing the galactose residues with glucose should show the same relative affinities but instead a decrease in the IC_{50} value to $0.4 \pm 0.1\ \mu M$ is observed which is half of Man(1,3,5)-5.

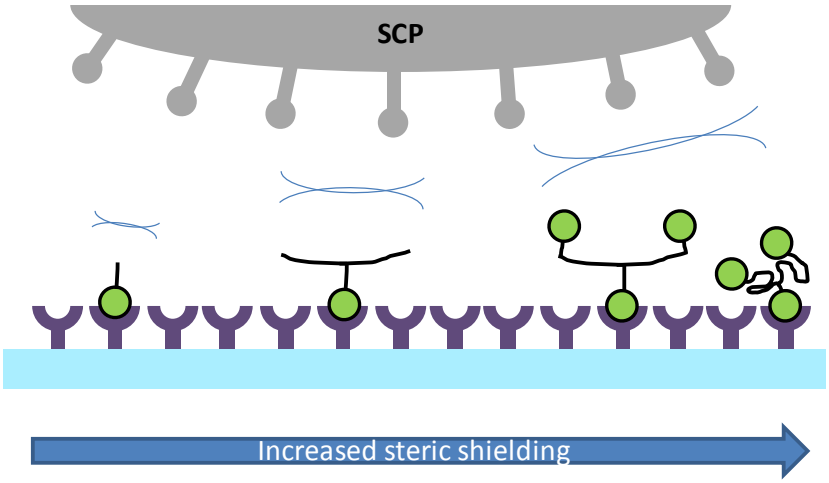

Figure 47: Schematic drawing of the steric shielding of the glycooligomers during the SCP-RICM measurements. Monovalent molecules have a smaller steric shielding compared to multivalent molecules.

Another parameter that can be read out from the Hill plots is the cooperative binding of the multivalent analytes. Interestingly, all of the curves exhibit a slope on the order of two, regardless of mono- or multivalent mannose presentation. The fact that the slope values were invariant for different inhibitors suggests that the process that defines the Hill-plot slopes was the adhesion of the SCP to the surface, rather than the binding of the inhibitor to the receptor. This could mean that the presence of an analyte not only inhibits a single receptor but also enhances the probability of unbinding adjacent receptors at the SCP surface. Thus, the observed cooperative inhibition is due to surface unbinding rather than binding cooperativity of the analytes themselves. A similar observation was made by Whitesides *et. al.* where the inhibition between microspheres and erythrocytes was studied by optically controlled collision using optical tweezers.[143]

Furthermore, for practical reasons it was tested if the surface can be easily regenerated by repeating the formation and inhibition of the PEG-Man and ConA interaction *via* washing cycles with lectin binding buffer and inhibition with α-methyl-D-mannose. This gave reproducible results and thus allowed the measurement of different molecules on the same surface highlighting the possibility to regenerate the measurement cells for a high throughput screening with a large number of analytes.

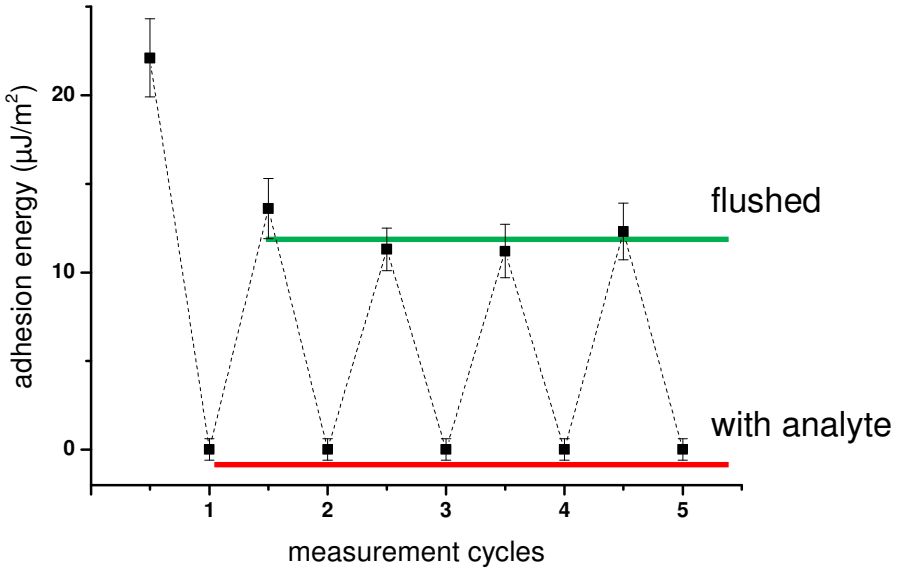

Figure 48: Surface recovery experiments with several washing and loading steps

Overall, the SCP-RICM method is highly sensitive and shows reproducible results in carbohydrate screening assays, without the need of expensive instrumentation. Inhibition assays were conducted to study carbohydrate–lectin interactions using non-labeled analytes yielding relative affinities that agreed well with those obtained from SPR measurements. Thus the method has several useful characteristics especially for the characterization of analytes with low molecular mass and refractive indices close to water such as carbohydrates.

Furthermore, decreasing the stiffness of the PEG SCP scaffold affects the adhesion of the SCPs to the receptor surface as the contact zones changes and lower adhesion energies could be detected, i.e. the measurement became more sensitive. Similarly, the increase of the ligand density also increases the adhesion of the SCP to the surface. In principle, the binding of SCPs to a receptor surface represents a drastically reduced cell-matrix model system that can be used to study a range of physiochemical parameters of the hydrogels on their specific adhesion.

6. SCP-AFM Measurements

The previous results showed that direct adhesion measurements of carbohydrate mediated surface interactions based on the PEG SCPs are possible. The developed methods allowed the evaluation of two factors - flexibility and ligand density - during adhesion measurements and gave first insights into the complex interplay of SCP properties and resulting surface interactions. Furthermore, the SCP adhesion measurement can be performed as an inhibition/competition assay and to determine the affinity of a large variety of ligands.

In the next and final chapter, the previously established setup will be further advanced by combining the optical detection of SCPs with AFM force spectroscopy. Attaching the SCP to a tipless cantilever allows for the direct measurement of adhesion forces between ligand-modified SCPs and receptor-modified surfaces, studying the effect of external force on ligand/receptor interactions as well as analyzing the displacement kinetics of initially bound ligands. On the one hand, this presents another step towards a model system for cell-cell interactions as in nature cells always experience external forces e.g. in a tissue through neighboring cells. On the other hand, this allows for the investigation of ligand inhibition and competition on a more detailed level as now the AFM will also give insights into the interfacial phenomena during ligand displacement (**Figure 49**).

So far, soft AFM probes have only been used to study non-specific interactions.[64,103,144] Specific carbohydrate ConA interactions have been determined using hard, inorganic AFM probes,[33,145] but not yet with soft and flexible probes. Therefore the combination of the previously introduced soft colloidal probes with RICM and AFM presents for the first time the opportunity to directly link the information from the force experiments and the advantages of soft probes, e.g. simultaneous measurement and visualization of binding and resulting surface energies *via* RICM.

In the following, the novel SCP-AFM approach will be applied for: 1) PEG SCPs as biomimetic AFM colloidal probes by analyzing the work of adhesion between PEG-Man SCPs and ConA surface under variation of loading rate and loading force (**Figure 49**A). Therefore, the SCP is brought into contact with the surface (**Figure 49**A1) and the contact area is detected *via* RICM. Here, the adhesion energy (W_{JKR}) can be detected *via* the JKR model with the contact radius under variation of the loading force (F) and known elastic modulus (E), Poisson ratio (ν) and radius of the SCP (R). The grey circle corresponds to the contact area. Then, the SCP is retracted and force curves are collected (**Figure 49**A2) and analyzed. The greyed area in the force curve depicts the work of adhesion (W_{pull}), which is

determined *via* AFM force spectroscopy. 2) Analyzing the displacement of receptor bound ligands upon competitive binding of SCPs under variation of the ligand valency (**Figure 49**B). After addition of inhibitors (1) the SCP was pressed on the surface (2). The inhibitors are replaced over time by the ligands presented on the SCP (3). The displacement of the inhibitors from ConA (4) was measured by W_{pull} at different contact times.

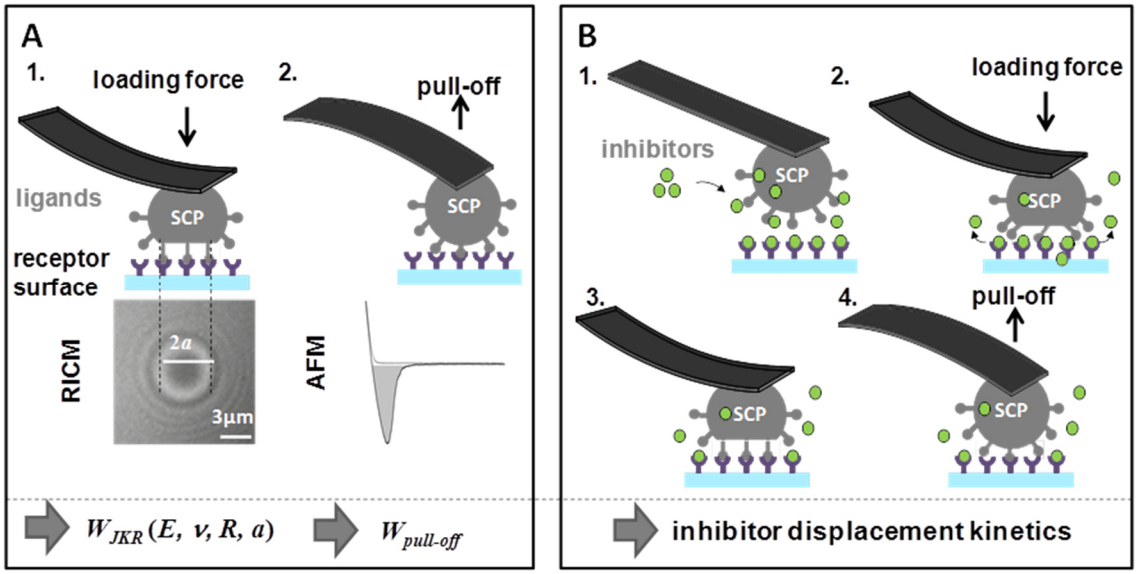

Figure 49: Schematic SCP-AFM measurement modes. PEG-Man SCPs are attached to a tipless cantilever and the adhesion on a ConA glass slide is determined. A) Determination of W_{JKR} (1) *via* detection of the contact radius under variation of the loading force (F) and known elastic modulus (E), Poisson ratio (ν) and radius of the SCP (R). The grey circle corresponds to the contact area. Determination of W_{pull} (2) *via* AFM force spectroscopy. First the SCP is brought into contact with the surface (1) and the contact area is detected *via* RICM. Then retraction force curves are collected (2) and analyzed, where the greyed area in the force curve depicts W_{pull}. B) Analysis of the inhibitor displacement due to competition with SCP. After addition of inhibitors (1), and initial pressing with the SCPs on the surface (2) the inhibitors are replaced over time by the ligands presented by the SCP (3). Measurement of W_{pull} at different contact times reveals the displacement of the inhibitors from ConA (4).

In order to verify the experimental set-up, a series of experiments varying different parameters such as loading forces, loading rates and contact time were performed. Furthermore, adhesion measurements based on the JKR theory with AFM pull-off measurements were performed. With these experiments at hand the unbinding kinetics of mono- and multivalent inhibitors form a pre-incubated ConA surface can be studied.

6.1. Direct Binding Assay

The combination of SCPs and AFM for adhesion measurements is shown in a schematic diagram in **Figure 49**. The PEG_{8k}-Man SCPs are attached to AFM cantilevers and ConA functionalized glass slides are used as receptor-presenting surfaces. The Young's modulus of the SCPs was tested again as this time the SCPs are glued on a substrate which might influence the mechanical properties. The Young's modulus was measured directly on the probes that were attached to the cantilever. This means that no glass bead was used to deform the SCP, instead the glued SCP on the cantilever was directly pressed against the ConA surface (see chapter 3.2.2) and from the deformation the Young's modulus was calculated. An increased Young's modulus of 330 ± 30 kPa compared to 32 ± 5 kPa was determined. This difference of one order of magnitude can be explained by the gluing process. To ensure that the probe deformation took place mainly at the substrate/probe interface, a large contact area between cantilever and probe was established when gluing. Thus the network is on the one hand previously stretched and on the other hand it is fixed on one side so that no deformation can take place in that direction.

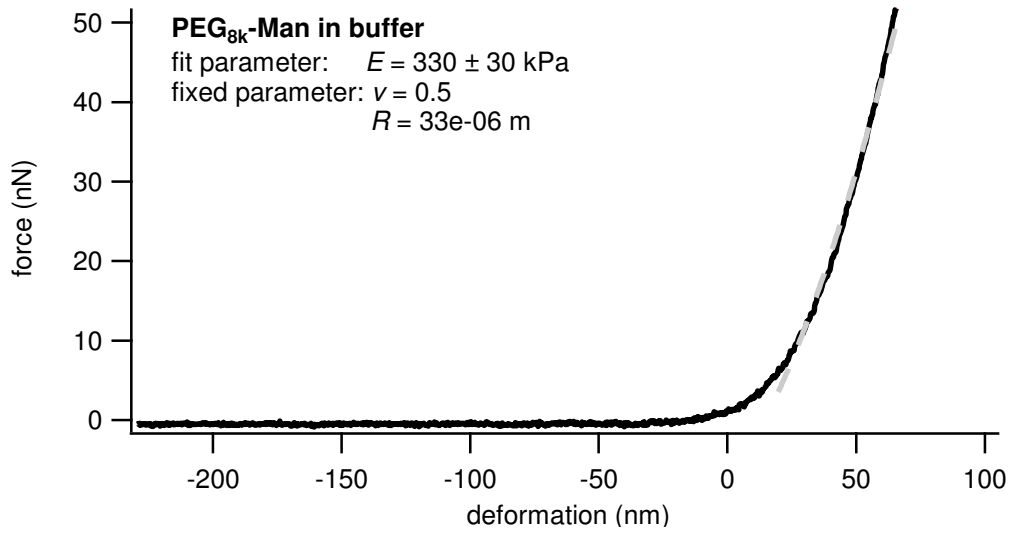

Figure 50: Young's modulus of PEG-Man glued on the cantilever of an AFM. The dashed line represents the Hertz fit.

The use of such new soft AFM probes requires careful assessment of the cantilever optical lever sensitivity (OLS) that was conducted two times for comparison. First, after determination of the spring constant and before attachment of the PEG-Man SCPs and second, after the measurements were finished the probes were removed again mechanically

from the cantilever, and the OLS was determined again directly in the measurement cell. If the difference between the OLS was less than 20% the obtained data was used for further processing. The attachment of the probe proved to be non-trivial since the SCPs are composed of a soft hydrogel material. For example, it was impossible to attach SCPs in dry state to the cantilever, as in the dried state it attaches strongly to the substrate it is dried on. Furthermore, the probes would not swell as before due to the gluing. Therefore, the SCPs were attached to the cantilever directly in the AFM liquid cell containing the measurement buffer. It was important that the glue at the cantilever was viscous when attaching the hydrated PEG SCPs in solution. The best results were obtained if the two component epoxy mixture was pre-cured for about 4 min in air before immersing it in the solution and attaching the probes.

Due to the combination with RICM, the SCP-AFM method has the ability to determine the contact area between the probes and the substrate. One advantage is that the obtained work of adhesion data measured *via* AFM pull-off curves (W_{pull}) can be normalized per unit area and compared to static JKR adhesion measurements (W_{JKR}). The method allows for studying carbohydrate interactions close to the biological context and without the need of using hard glass or plastic beads as colloidal probes. Therefore, a series of AFM based adhesion measurements were performed and the influence of different parameters such as contact time, force and loading were determined on the interaction between mannose ligands and ConA receptors.

6.1.1. Dependence of Adhesion Force and Work of Adhesion on Unloading Rate

In a first experiment, force-distance curves were measured with the PEG-Man as AFM force probe and ConA coated coverslips as substrate.[146] The SCP mounted on the cantilever was brought into contact with the ConA surface and held at constant loading force (10-100 nN) on the surface for a certain contact time (t = 10 s) before retracting the probes at a distinct unloading velocity of 0.01-10 µm/s (circa $1 \cdot 10^2$-$1 \cdot 10^5$ nN/s depending on the cantilever spring constant). From the retraction curves, the pull-off force (F_{pull}) and the work of adhesion (W_{pull}) could be obtained (**Figure 51**A). F_{pull} is the force that is needed to remove the probe from the surface. In order to test the specificity of the obtained adhesion data, an excess of α-methyl-D-mannose (2 mM) was added into the measurement cell, thereby

blocking the ConA receptor binding sites. The addition of α-methyl-D-mannose led to a decrease of F_{pull} and W_{pull} as can be seen from the force curve (**Figure 51**B). This suggests that specific interactions between the mannose SCP and the ConA surface were present.

The loading rate was varied to study the behavior of the SCP adhesion. The effect of loading rate on F_{pull} was determined for different loading forces (**Figure 51**C). All force spectra show two linear regimes: a slow-loading regime of 130 to 6480 nN/s and a fast-loading regime of 6480 to 130000 nN/s. The two loading rate regimes are usually associated with the dissociation of ligand/receptor complexes that have to overcome multiple energy barriers in order to separate.[147] A similar behavior was shown by Siedlecki *et al.* for protein (fibrinogen) coated colloidal probes and model surfaces.[148] Theoretically this could be used to determine the dissociation constants[149] of mannose units and ConA. However, it is not applicable here, because it is related to the dissociation of single ligand/receptor complexes only. The specificity of this interaction was again confirmed by the reduced adhesion forces in presence of α-methyl-D-mannose as inhibitor (**Figure 51**B, open symbols).

Overall F_{pull} as well as W_{pull} were shown to be loading rate dependent. The fact that the adhesion of mannose functionalized SCPs with ConA surface was rate dependent can be explained due the specific interaction between ligand- and receptor-modified surfaces that are non-covalent and possess dynamic, time dependent properties, e.g. increasing the SCP loading rate increases the force required to separate the ligand/receptor complex.[147,149] Due to the high loading rate dependence, all subsequent measurements were conducted at a constant unloading rate of 10000 nN/s.

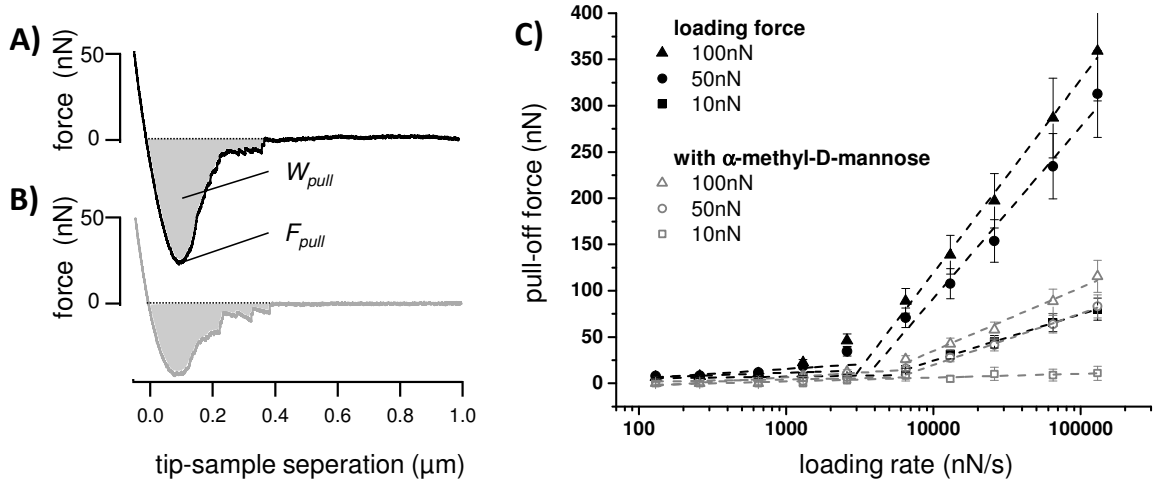

Figure 51: A) Typical AFM retraction curve for PEG-Man (radius 25 µm, loading force 50 nN contact time 10 s) from a ConA surface without inhibitor. The grey area show the work of adhesion of the SCP (W_{pull}), the minimum of the curve signifies the adhesion force (F_{pull}). B) Retraction curve after addition of 2 mM under the

same conditions. C) Pull-off forces of PEG-Man on ConA functionalized glass surface at different loading rates (contact time = 10 s) and with varying loading forces (100 nN, 50 nN and 10 nN). After addition of 2 mM α-methyl-D-mannose (complete saturation of ConA[97]) a decrease of the adhesion force is observed.

6.1.2. Dependence of the Work of Adhesion on Loading Force

A dependence of the adhesion force on the unloading rate was shown before. In the following, the SCP adhesion behavior under different loading forces (F) will be discussed. In **Figure 51**C it can be also seen that F_{pull} increases with increased loading force. Therefore, adhesion depends also on the loading force that was applied before retracting the AFM cantilever. For example, Vakarelski *et al.* could show that F_{pull} or W_{pull} increase for increasing loading force and reach a maximum constant value if the load becomes large enough.[150] Here the dependence of the energy W_{pull} on the loading force will be discussed. Additionally the W_{pull} which describes the energy in a non-equilibrium can be compared to the equilibrium adhesion energy (W_{JKR}) that can be determined optically *via* the contact radius a:

$$W_{JKR} = \frac{(a^3K - FR)^2}{6\pi a^3 K R^2} \tag{22}$$

where F is the loading force, R the radius of the colloidal probe and K=[4E/3(1-ν^2)] its effective elastic modulus, with v the Poisson ratio and E the elastic modulus. W_{JKR} can be considered to reflect the equilibrium adhesion energies because the measurement is conducted without moving the SCP from the surface. W_{JKR} can be then calculated from the deformation of the hydrogel SCP under a constant loading force on the ConA surface (**Figure 52**).

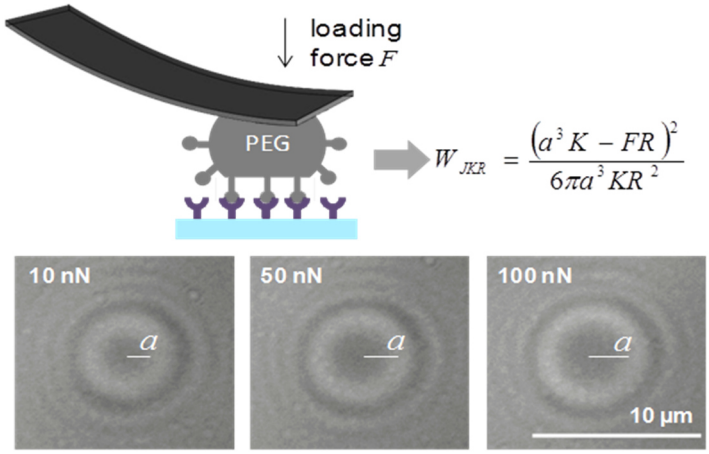

Figure 52: Determination of W_{JKR} involves determination of the contact radius *a via* optical microscopy at a well-defined loading force *F*.

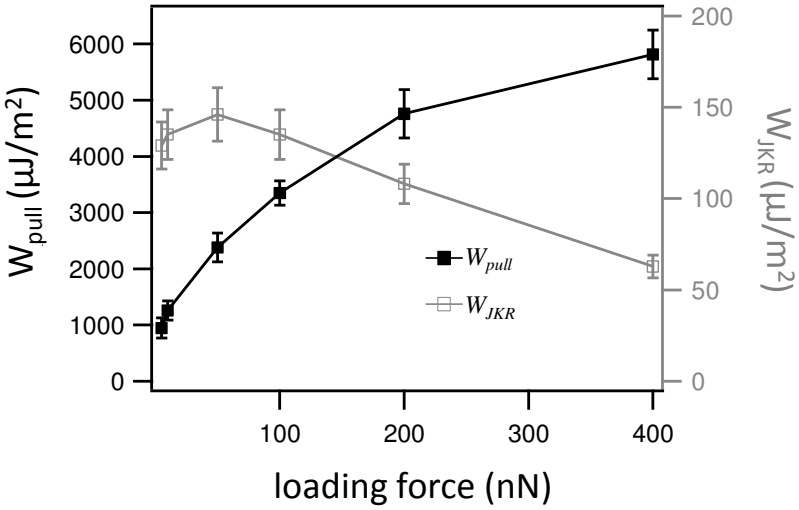

Figure 53: W_{pull} and W_{JKR} as a function of the loading force. The unloading rate for W_{pull} measurements was $1 \cdot 10^5$ nN/s.

W_{pull} and W_{JKR} were determined at different loading forces in a range of 10-400 nN (**Figure 53**). W_{pull} increased with the loading force and leveled off at forces larger than 400 nN, whereas W_{JKR} decreased slightly with the loading force. An increase of W_{pull} with increasing loading force appears to be a common phenomenon in dynamic measurements.[150] The five-fold increase of W_{pull} from 10 nN to 400 nN is due to improvements of the contact of the SCP to the surface and thus an increase of the number of ligand/receptor interactions. This in turn increases the work of adhesion (W_{pull}) at increased loading force due to larger contact areas. The reduction of W_{JKR} with the loading force from (50 nN to 400 nN) was not expected, as the JKR theory does not describe a dependence of

the adhesion energy on loading force.[38] Plotting of the contact radius as function of loading force reveals a mismatch of the JKR theory with the experimental data at high loading force (**Figure 54**).

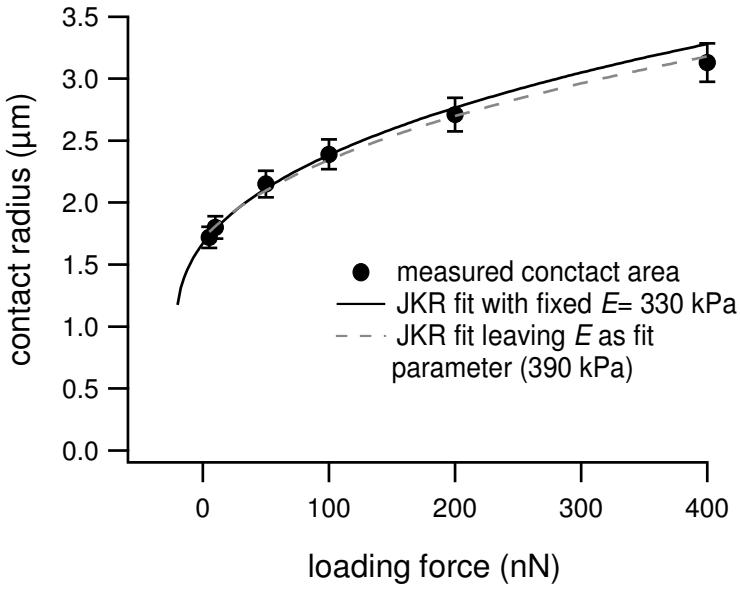

Figure 54: Contact radius as a function of applied load. The lines are fits according to the JKR equation 3. The full line represents a JKR fit with a fixed elastic modulus E=330 kPa. The dashed line represents a fit with E as free fit parameter.

The plot shows that at higher loading forces the JKR fit deviates from the JKR model with the experimentally determined E. Leaving E as free fit parameter gave a considerably larger elastic modulus of 390 kPa. The independence of the adhesion energy on the applied load holds only when the deformation is purely elastic. Here, the SCP shows non-elastic deformation at higher loading forces. This could be due to strong compression of the SCPs at high loads resulting in a decrease in volume due to water displacement.

The dynamic W_{pull} measurement was one order of magnitude higher when compared to the static W_{JKR} measurement. This is caused by e.g. viscoelastic deformation that may serve to increase the adhesion strength by several orders of magnitude,[49] and therefore W_{pull} most likely overestimates the surface binding energy. However, due to practical considerations, in the following contact time-dependent measurements W_{pull} will be determined instead of W_{JKR}. This is because the exact moment of contact between SCP and ConA surface could not be precisely determined optically, whereas *via* AFM approach-retract curves the contact time is well-defined.

6.2. Inhibition Kinetics

As the ligand/receptor mediated binding to a substrate is a dynamic process, it can be assumed that the adhesion energy would be dependent also on the contact time between PEG-Man SCPs and ConA surfaces. W_{pull} was measured under variation of the contact time range of 0-60 s and at constant load force of 50 nN (**Figure 55**). Large changes in W_{pull} were observed in the range of 0-30 s that then leveled off. Such comparatively slow increase in adhesion energy with contact time is rather typical for 'soft contacts',[103,150] and suggests that upon binding conformational changes of the polymer matrix and protein layer are involved. The contact area does not increase over time which results from the applied constant load.

In biological systems like cell surfaces, the interactions between cells are often affected by competing ligands. This situation can be mimicked by introducing freely dissolved mannose glycooligomers as inhibitors (**Scheme 14**) before bringing the SCP in contact with the ConA surface (**Figure 49**B). When the PEG-Man SCPs come into contact with the ConA surface with already bound inhibitors, the SCP competes with the inhibitors for ConA binding pockets thereby replacing them from the ConA layer. Generally, in presence of carbohydrate inhibitors, W_{pull} is reduced. The evaluation of W_{pull} over time should depend also on the inhibitor concentration and their binding affinity to ConA. In terms of concentration dependence it can be observed that larger concentration of α-methyl-D-mannose as inhibitor decreased W_{pull} due to blocking of the ConA surface (**Figure 55**).

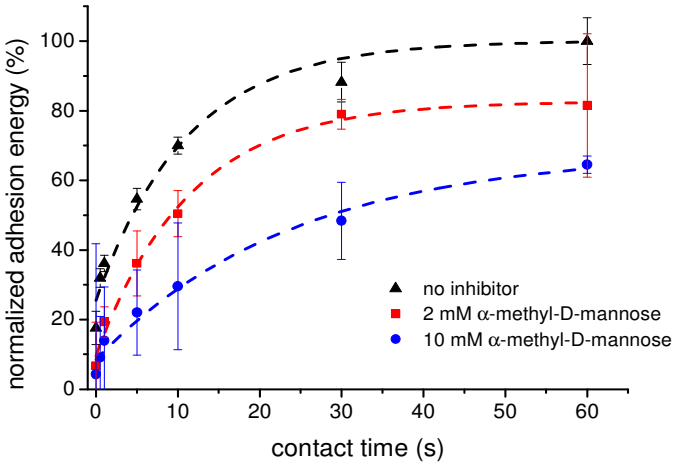

Figure 55: Concentration dependency of the adhesion after addition of α-methyl-D-mannose at different concentrations.

For example, at a contact time of 0 s an adhesion energy of 0.56 mJ/m^2 can be found if no inhibitor is present and a reduction of the W_{pull} by a factor of 2.6 and 2.9 for 2 mM and 10 mM added α-methyl-D-mannose, respectively.

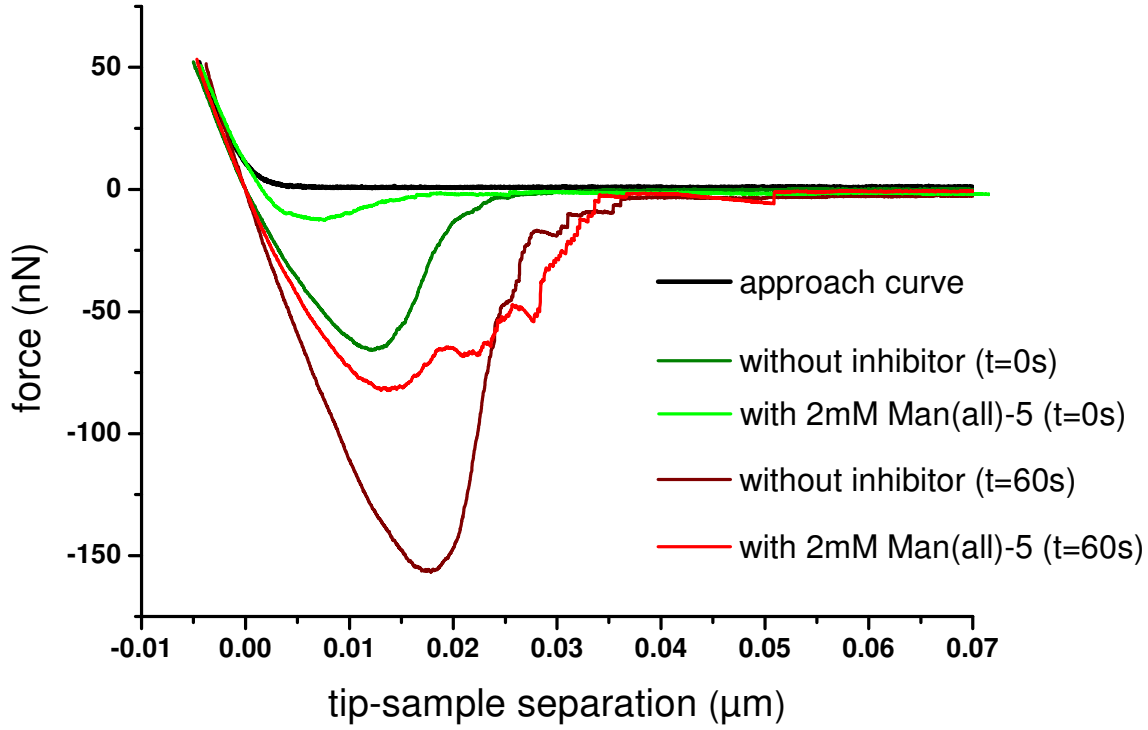

Figure 56: Typical force curves at t=0 s and t=60 s with and without inhibitor (2 mM Man(all)-5). The relative increase in work of adhesion in case no inhibitor is present is much larger when compared to measurements with inhibitor.

W_{pull} increases, however, for larger contact times due to both, time dependent binding of the SCP on the ConA surface, and displacement of the inhibitors from the surface (**Figure 56**). The extent to which W_{pull} increases due to inhibitor replacement can be shown by comparing the relative increase of W_{pull} in presence and absence of inhibitor. The relative increase of W_{pull} from the initial (t=0 s) to maximum contact time (t=60 s) was calculated as $[W_{pull}(t)-W_{pull}(t_0)]/W_{pull}(t_0)$. The relative increase of W_{pull} is much larger if inhibitors are present: from t=0 s to t=60 s the increase was only a factor of 2.5 for the non-inhibited ConA surface, but a factor of 10 to 20 for the inhibited samples (**Figure 57**). This indicates that the mannose presenting inhibitors were displaced from the ConA surface upon the adhesion of the SCPs. Displacement of the inhibitors by the SCP enables formation of specific interactions between SCP and ConA surface and results in the strong increase of W_{pull} over time.

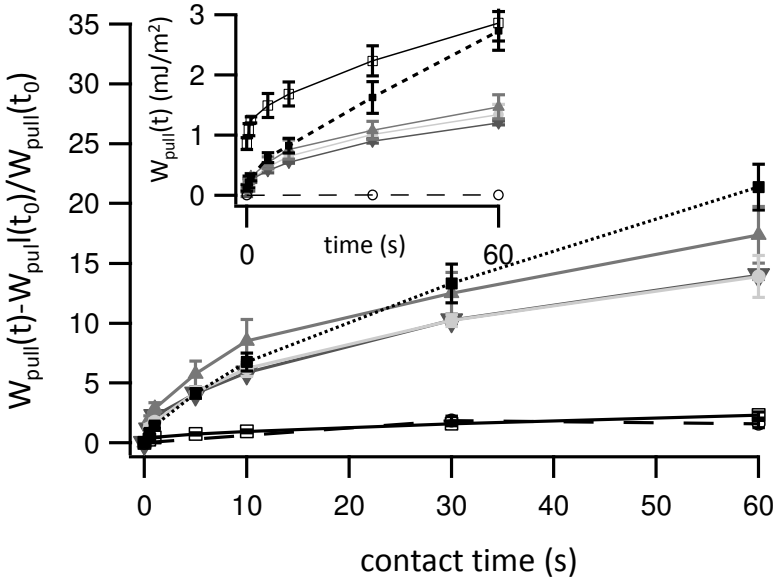

Figure 57: W_{pull} depends on contact time (t) and shows displacement of the inhibitor from the ConA surface. Labels: empty symbols denote measurements without inhibitor; □-PEG-Man, ○-nonfunctionalized PEG SCPs (dashed line); filled symbols denote measurements with inhibitor; ▼-(α-methyl-D-mannose, ▲-Man(1,2)-5, ●-Man(all)-5 and ■-galactose (dotted line). Inset: Measurement of W_{pull} between PEG-Man and ConA surface as a function of t. Main graph: The relative increment of W_{pull} from $t = 0$ [$W_{pull}(t)$ - $W(t_0)$] / $W_{pull}(t_0)$ is much larger if an inhibitor is present (filled symbols) than without inhibitor (empty symbols).

6.2.1. Effect of Multivalency on ConA Surface Inhibition

The carbohydrate-binding protein ConA exists as a tetramer at physiological pH, thus in comparison to monovalent mannose units such as α-methyl-D-mannose ConA achieves drastically larger functional affinity when binding to multivalent mannose species.[139] Here again multivalent glycooligomers (α-methyl-D-mannose, Man(1,2)-5 and Man(all)-5) as well as a nonbinding sugar galactose were used as inhibitors to study the displacement of such multivalent interactions due to the competing ligands attached to the SCPs. For comparison, the total concentration of carbohydrate units maintained constant, e.g. the monovalent α-methyl-D-mannose and galactose concentration were adjusted to 10 mM, Man(1,2)-5 to 5 mM and Man(all)-5 to 2 mM, respectively.

The relative increase of W_{pull} (**Figure 57**) in presence of the carbohydrate ligand shows that the galactose inhibited ConA surface undergoes faster recovery of SCP adhesion when

compared to mannose-ligand inhibited ConA surfaces. It is known that galactose does not bind to ConA thus the SCP adhesion is recovered faster. The comparison of the pentavalent Man(all)-5 and monovalent α-methyl-D-mannose shows that both ligands have a similar inhibitory potential with regard to the adhesion of the mannose-functionalized SCPs. This is rather surprising, as the IC_{50} affinity measurements *via* SCP-RICM showed two orders of magnitude smaller IC_{50} values for the multivalent glycooligomers compared to monovalent α-methyl-D-mannose. Therefore, from the SCP-RICM assay one would expect a higher inhibitory potential for the multivalent glycooligomer in comparison to the monovalent mannose. The bivalent glycooligomer (Man(1,2)-5) even shows a larger relative increase of W_{pull} when compared to the monovalent mannose. This could be explained with the fact that the binding site spacing of the tetrameric ConA is about ~10 nm, thus exceeding the spacing of the mannose units on the bivalent oligomer backbone. As a result, only one mannose unit can bind to ConA at a time, reducing the effective concentration of mannose units by a factor of two when compared to the monovalent or pentavalent ligands.

Nevertheless, the comparison between monovalent and pentavalent mannose ligands showed that the inhibitory potential with regard to adhesion upon forced contact was quite independent on the valency of the inhibitor. This appears to contradict previous affinity measurements *via* SCP-RICM that showed that the inhibitor affinity increased by orders of magnitude in case of a multivalent scaffold. This is most likely due the fact that the SCP-AFM inhibitor displacement assay is not sensitive to the steric shielding of receptors. Steric shielding is observed in classic inhibition affinity assays, e.g. SPR and leads to large binding constants for macromolecular ligands because they can block receptor binding sites without actually binding to them.[138] The displacement of the glycooligomer ligands from the receptor as measured by the increase of W_{pull} is not sensitive to steric shielding of adjacent receptor sites, which explains why the mannose ligands behaved similarly. Therefore, the results obtained by SCP-AFM indicate that the high affinity of multivalent glycooligomers measured in inhibition affinity assays is mainly due to steric shielding effects, whereas the association of sugar units on the scaffold to the receptor is statistical and not due to chelate binding effects.

The results also indicate that binding of even pentavalent glycooligomers to protein receptors is highly reversible as indicated by the 10-fold increase of W_{pull} after 60 s contact time. The exact molecular mechanism of the dissociation of these compounds is assumed to be stepwise and should be relatively fast for the individual binding units.[59] The phenomenon of reversibility of binding is also known in nature which is used to improve

specificity. Even cell communication is reversible, though it is multivalent, therefore the fast replacement of multivalent sugar ligands allows for reversibility if the wrong cell or pathogen binds initially.[151] Such a forced contact between surfaces could be relevant in physiological cell/cell or cell/bacteria interactions. Therefore this analytical method has a potential in pharmaceutical sciences to test the applicability of multivalent carbohydrate drug molecules inhibiting the interaction of viral or bacterial adhesion receptors in order to prevent infection.

Overall, the reduced cell model system as represented by ConA surfaces and PEG-Man SCPs showed that the displacement of multivalent sugars from receptor molecules is reversible. It should be noted, however, that due to technical reasons the physiological context could not be mimicked correctly. For example, the receptors were covalently bound on glass, and the forces upon contact were rather large. Mimicking a true cell/cell contact would require even softer materials, mobile membrane anchored receptors that exhibit lateral mobility and can undergo clustering, higher density of carbohydrates on the PEG SCP and possibly also lower forces upon contact.

7. Conclusion and Perspectives

In this thesis, an experimental platform of sensors based on soft colloidal probes (SCPs) was developed and their potential in a variety of assays such as direct adhesion measurements, inhibition assays and force spectroscopy was shown. Through the control of the SCP properties and functionalization, the interplay of affinity, ligand density and elasticity as a mechanism to regulate biomolecular interactions at interfaces was investigated. Special focus was devoted to sugar ligand/lectin receptor interactions as they are known to play an important role in many cell-adhesion mediated phenomena but their multivalent interactions at interfaces were not yet well understood.

To achieve this aim, in the first part, hydrogel microparticles based on polyethylene glycol (PEG) were synthesized. PEG is known as a suitable material for many biological applications due to its biocompatibility and its low non-specific interaction with (bio)surfaces. To ensure well-defined interfacial properties of the probes, a surfactant free synthesis of PEG SCPs using kosmotropic sodium sulfate salt was performed. This approach allowed both, controlling the particle size and adjusting the elastic properties of the PEG probes by varying the molecular weight of the PEG macromonomers from 1450 to 20000 Da. With the help of the different elastic properties of the probes, the influences of flexibility of the scaffold could now be evaluated on adhesion. Reaction conditions were optimized for probes in a size range of 10-50 µm. By varying the PEG macromonomer and the initiator concentration, the Young's modulus could be tuned in the range of 0.3-80 kPa.

In order to use the hydrogel probes for the analysis of specific interfacial interactions, radical surface chemistry was introduced in the second part by using benzophenone as photoinitiator to graft polymerizable monomers such as acrylic acid to the SCPs. With this highly versatile method, various functionalities such as carboxylic or amine groups could be directly attached to the PEG network. By using different carboxylic acids (methacrylic acid, acrylic acid and crotonic acid), different grafting types were obtained. Methacrylic acid grafts on PEG SCPs resulting in long poly(methacrylic acid) chain, acrylic acid gives shorter oligo(acrylic acid) chain, and crotonic acid grafts in the form of single crotonic acid molecules. This now opened the opportunity to study the influences of the ligand density on soft adhesion. Titration, fluorescence microscopy and IR-spectroscopy proved that the monomers were covalently attached to the probes and the functionalization degree could be varied from 30-260 µmol/g. Confocal laser scanning microscopy and Raman spectroscopy showed the distribution of functional groups within the probes to be homogeneous. The

functional groups are accessible and could be further modified with more complex structures such as dendrimers or proteins. Through the control of the SCP properties and functionalization, new insights into the interplay of affinity, ligand density and elasticity as a mechanism to regulate biomolecular interactions at interfaces could be expected. Special emphasize was devoted to the functionalization of PEG SCPs with mannose ligands and ConA protein as receptor.

Therefore, in the third part of the thesis, three methods were explored to study the influences of the three factors: elasticity, ligand density and affinity on adhesion measurements using the newly developed SCPs: a direct binding assay and an inhibition/competition assay were performed by using SCPs in combination with reflection interference contrast microscopy (RICM) allowing for the quantification of adhesion energies. Furthermore, a combined approach using RICM and AFM was realized also quantifying the kinetics of ligand displacement.

In a first set of adhesion measurements, non-specific electrostatic interactions were measured in a direct binding assay between amine functionalized SCPs and anionically charged glass slides *via* RICM. Increasing the charge density of amine functionalized SCPs resulted in increasing the adhesion energy from 0.26 ± 0.01 mJ/m^2 to 0.83 ± 0.12 mJ/m^2.

The SCP method showed to be reproducible and highly sensitive and therefore also suitable to study weaker interactions such as ligand-receptor interactions at soft interfaces. With the well-known ligand/receptor pair mannose/ConA, the influence of three factors – elasticity, ligand density and affinity on the specific ligand-receptor mediated adhesion process could be evaluated. By decreasing the elasticity of the SCP from 30 kPa to 4 kPa, while keeping the functionalization degree constant, an increase in contact area and thus adhesion energy resulted. Furthermore, the influence of the ligand density on adhesion was studied. A high ligand concentration on the SCPs generally leads to high adhesion energies. A 1.2-fold increase in the adhesion energy by doubling the mannose concentration was observed. Subsequently, SCPs with long grafted chains like PEG-MAA and PEG-AA led to an increase in ligand/receptor binding as the longer chains are more flexible. Thus with similar mannose group concentrations, the SCPs with long grafted chains have a comparably higher adhesion energy. The SCPs and the optical set-up used in this thesis allowed for the detection of adhesion energies with a detection limit of a few μJ/m^2 exceeding the sensitivity limit of the SFA or colloidal probe AFM.

Besides the direct adhesion measurements, the SPC-RICM set-up can also study inhibition processes, specifically the inhibition of ligand/receptor mediated adhesion by the

addition of inhibitors. Thereby, a new inhibition assay was conducted to study carbohydrate/lectin interactions using e.g. sequence-defined glycooligomers as inhibitors, yielding relative affinities. Strong inhibition on the ConA surfaces with IC_{50} values in the µM range were observed and they agreed well with previous SPR measurements.[139] Furthermore the IC_{50} values decreased by a factor of 25 when reducing the Young's modulus from 32 to 4 kPa. The studies suggested that most likely statistical binding and sterical shielding were involved in the binding of the glycooligomers to the receptor surface. In general, this method has several useful benefits such as high sensitivity, robustness, cost efficiency and is especially suitable for the characterization of analytes with low molecular mass and refractive indices close to water which are often difficult to characterize with standard methods such as SPR or QCM. Furthermore, the binding of SCPs to a receptor surface represents a drastically reduced cell-matrix model system potentially giving more insights into cell-cell interactions.

Finally, the combination of RICM and AFM was presented as a technique to measure forces and in the same time detecting the contact area of the adhered object. This method was used to study mannose/ConA interactions at different loading forces and contact times. By increasing the loading forces, the adhesion forces increased due to the enlargement of the contact area. When incubating the ConA surfaces with mannose ligands as inhibitors the overall adhesion energies drastically decreased, but the time-dependent adhesion energies increased faster over time. These measurements indicated a displacement of mannose inhibitors by the competing ligands of the SCP, an absence of multivalency effects and the reversibility of the carbohydrate interactions as part of their comparatively high specificity. Consequently, the method allows for studying the carbohydrate interactions close to the biological context that involves compliant materials such as the extracellular matrix and soft cell membranes.

Future work will therefore focus on the application of the hydrogel probes as extracellular matrix model for direct cell interaction studies *via* AFM. This will give for the first time the opportunity to directly link the information from the force experiments and the advantages of soft probes e.g. simultaneous measurement and visualization of binding and resulting surface energies *via* RICM. Due to the technical advantages of the SCP-RICM set-up such as its high sensitivity while using a simple optical detection method, these techniques will be expanded to further ligand/receptor pairs and developed for high throughput screenings as a new method to determine ligand affinities.

8. Appendix

8.1. Experimental Part

8.1.1. Materials

Standard commercial grade reagents and solvents were used without further purification. 2-Aminoethyl methacrylate hydrochloride (AEMA), benzophenone and succinic anhydride (SUC) were purchased from Acros Organics, benzotriazole-1-yl-oxy-tris-pyrrolidinophosphonium hexafluorophosphate (PyBOP) and 1-hydroxybenzotriazole (HOBt) from IRIS. All other chemicals were purchased from Sigma Aldrich and used without further purifications.

8.1.2. Methods

Nuclear Magnetic Resonance Spectroscopy (NMR). ^{1}H-NMR spectra were measured with a Varian 400-MR spectrometer. All chemical shifts are reported in part per million (ppm). The proton signal of residual, non-deuterated solvent (δ 7.26 ppm for $CHCl_3$) was used as an internal reference for ^{1}H spectra. Coupling constants (*J*) are reported in Hertz [Hz]. The following abbreviations are used to indicate the multiplicities: s, singlet, d, doublet; t, triplet; m, multiple.

Reversed-phase HPLC (RP-HPLC) was performed with 214 nm UV detection on a C18 (Agilent Eclipse, 4.6 × 100 mm) analytical column at 60°C and a flow rate of 1 mL min^{-1}, if not indicated differently. Eluent: (A) water + 0.1% TFA; (B) acetonitrile + 0.1% TFA.

Fourier Transform Infrared Spectroscopy was measured on a Varian 1000 FT-IR with an ATR (attenuated total reflectance) unit in the range of 4000–500 cm^{-1}.

Turbidity Measurements were done on a turbidimetric photomer TP1 (Elmar Tepper, Germany) at a heating rate of 1 K min^{-1}.

Ultraviolet-Visible Spectrophotometry (**UV/Vis**) was recorded on an Agilent G1103A 8453 UV-VIS Photometer 190-1100 nm Quartz cuvettes with a layer thickness of 1 cm^{-1} were used.

Scanning Electron Microscopy (SEM) images were obtained with a GEMINI LEO 1550 microscope operating at 3 kV.

Reflection Interference Contrast Microscopy (RICM). RICM on an inverted microscope (Olympus IX71, Germany) was used to obtain the contact area between the microparticles and a hard glass surface. For illumination a Hg-vapor lamp was used with a green monochromator (546 nm). A Zeiss Antiflex 63 x NO 1.25 oil-immersion objective, additional polarizers to avoid internal reflections and a Zeiss AxiocamHRm camera were used to image the RICM patterns. To conduct the JKR measurements of the adhesion energies, both the contact radius and the particle radius were measured. Image processing and data analysis were done using the image analysis software ImageJ (public domain NIH) and the mathematical software OriginPro (OriginLab, USA).

Atomic Force Microscopy (AFM). All experiments were performed on a NanoWizard III AFM (JPK Instruments AG, Germany) installed on an inverted optical microscope (Olympus IX71, Germany). The thermal noise method was used to calculate the spring constant of the cantilever (CSC 12 and NSC 12, µMash, Germany).

8.1.3. Experimental Procedures

Poly(ethylene glycol)-Dimesylate (PEG-dimesylate).

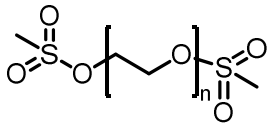

PEG (100 g) was dissolved in 200 mL toluene and water was removed by azeotropic distillation in vacuum. PEG was redissolved in 1 L dry THF. 3 eq. triethylamine (TEA) was added, followed by the dropwise addition of 3 eq. mesyl chloride in THF. The solution was stirred for 24 h at RT. A white precipitate formed and the reaction solution turned slightly yellow. The resulting salt was the TEA-HCl salt that was filtered. The volume of the THF filtrate was then reduced under vacuum. The THF solution was poured into cold diethyl ether where the product, PEG-dimesylate, precipitated. The product was collected by filtration and dried under vacuum. A white solid in quantitative yield was obtained.

^{1}H-NMR(400 MHz; CDCl3): δ(ppm) = 4.38 (m, 4 H, MsO-*CH*$_2$-), 3.76 (m, 4 H, MsO-CH$_2$-*CH*$_2$), 3.64 (m, 434 H, PEG), 3.08 (s, 6 H, Me).

IR: ν = 2883 (C-H), 1466 (C-H), 1174 (S-O), 1106 (C-O-C) cm^{-1}.

Table 10: Equivalents used for the mesylation of PEG

M_n PEG [Da]	n (=3 eq.) [mmol]	TEA [mL]	Ms-Cl [mL]
1450	414	58	32
4600	130	18	10
8000	75	11	6
20000	30	4	2

Poly(ethylene glycol)-Diamine (PEG-diamine).

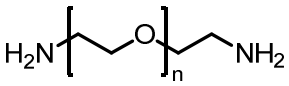

The PEG-dimesylate was dissolved in 300 mL 25% aqueous ammonia solution and the flask was closed with a stopper and secured with parafilm. The orange solution was vigorously stirred for 4 days at RT. The stopper was removed and the ammonia was allowed to evaporate for 3 days. The pH of the solution was raised to 13 with 1 N NaOH and saturated with NaCl (>20 g). The solution was extracted with dichloromethane 3 times. During the extraction the mixture forms an emulsion due to the interaction of the polymer with both, the aqueous and the organic phase. The combined organic phases were dried over $MgSO_4$. Magnesium sulfate was filtrated and the filtrate containing the PEG-diamine was concentrated in vacuum. The product was precipitated in cold diethyl ether. The white powder, PEG-diamine, was filtrated and dried under vacuum. PEG-diamine was obtained as white solid.

^{1}H-NMR(400 MHz; $CDCl_3$): δ(ppm) = 3.64 (m, 517 H, PEG), 2.93 (t, J=5.2 Hz, 4 H, -CH_2-*CH_2*-NH_2).

IR: ν = 2882 (C-H), 1579 (N-H), 1466 (C-H), 1101 (C-O-C) cm^{-1}.

Table 11: Yields of the PEG-diamine synthesis

M_n PEG [Da]	Yield [%]
1450	43
4600	81
8000	91
20000	90

Poly(ethylene glycol)-Diacrylamide (PEG-dAAm).

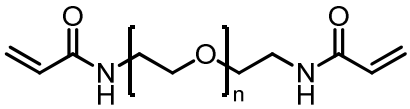

PEG-diamine was dissolved in 500 mL dry THF. 2.5 eq. triethylamine was added, followed by dropwise addition of 2.5 eq. acryloyl chloride in THF over 30 min. The solution was stirred for 24 h at RT. A white precipitate formed which was the TEA-salt that was filtered. The volume of the THF filtrate was then reduced under vacuum. The THF solution was poured into cold diethyl ether where the product, PEG-diacrylamide, precipitated. PEG-diacrylamide was obtained as white solid.

^{1}H-NMR(400 MHz; $CDCl_3$): δ(ppm) = 6.57 (NH), 6.29, 6.15 (dd, 4H, CH_2=CH-CON-), 5.62 (dd, 2 H, CH_2=*CH*-CON-), 3.64 (m, 534 H, PEG).

IR: ν = 2882 (C-H), 1663 (CO-NH, Amide I), 1547 (N-H, Amide II), 1466 (C-H), 1101 (C-O-C) cm^{-1}.

Table 12: Used equivalents for acrylation

M_n PEG [Da]	n (=2.5 eq.) [mmol]	TEA [mL]	Acryl-Cl [mL]	Yield [%]
1450 (15 g)	124 (6 eq.)	17 (6 eq.)	6.7 (4 eq.)	39
4600 (35 g)	38	5	3	66
8000 (35 g)	22	3	2	87
20000 (35 g)	9	1	1	80

The product of PEG M_n = 1450 Da was not pure, therefore it was dissolved in 200 mL deionized water. The pH was raised to pH 6 with 1 M NaOH. The solution was saturated with NaCl, and extracted with dichloromethane 3 times. The organic phase was dried with $MgSO_4$ and concentrated in vacuum. The product was precipitated in cold diethyl ether and dried under vacuum.

General Procedure for the Synthesis of PEG SCPs

To a 1 M sodium sulfate solution (10 mL) PEG dAAm was added at a concentration of 0.5 wt-% and vigorously shaken until a homogeneous dispersion was formed. The UV photoinitiator Irgacure 2959 was added at a concentration of 0.01 wt-% and the dispersion was photopolymerized for 90 s using a Heraeus HiLite Power curing unit (Heraeus Kulzer, Germany). The resulting microparticles were poured to 30 mL MilliQ water and were centrifuged at 5000 rpm for 10 min. They were washed 3 times with MilliQ water to remove salts.

The effect of initiator concentration on the synthesis of PEG SCPs was studied on polymer dispersions prepared with 0.75 wt-% PEG-dAAm (M_n = 20000 Da) in 0.75 M Na_2SO_4 solution. In these polymer dispersions, the concentration of the initiator Irgacure 2959 was varied as $3.00 \cdot 10^{-2}$ wt-%, $1.50 \cdot 10^{-}2$ wt-%, $7.50 \cdot 10^{-}3$ wt-% and $3.75 \cdot 10^{-3}$ wt-%. The polymerization and purification processes of the samples were done according to the standard procedure.

Swelling Ratio

The swelling degree of PEG-dAAm SCPs was determined by measuring the particle volume in the dry and the swollen states by light microscopy. The swelling ratio (Q) was then obtained by dividing the swollen gel volume (V_1) by the dried gel volume (V_0), $Q = V_1/V_0$.

Determination of Young's modulus

The Young's modulus of PEG–dAAm particles was determined by AFM force distance measurements (Nanowizard I, JPK Instruments AG, Germany). Here, a tipless cantilever was first calibrated by measuring the spring constant with the thermal noise method and then a glass bead with a diameter of 5 µm was attached on the cantilever. Several force-deformation measurements were performed at the apex of the SCPs followed by evaluation of the elastic moduli using the Hertz model.[45]

General Procedure for the Functionalization of PEG SCPs

2 Step process. Water was exchanged by ethanol through several washing steps and the microparticles were left in 10 mL of ethanol. Benzophenone was added at a concentration of 3 wt-% (250 mg) and the probes were irradiated with UV for 90 s. The dispersion was washed with ethanol 4 times and then with water. 10 mL water was left and AA or AMEA was added to the suspension at a concentration of 15 vol-% (0.5 wt-%). The mixture was shaken and irradiated with UV for 90 s. The particles were washed first with a 1:1 mixture of water and ethanol, then with MilliQ water.

1 step process. PEG_{8k} SCPs (50 mg, 6.3 µmol) were washed with ethanol (10 mL) to exchange the solution. Benzophenone (250 mg, 1.4 mmol) and an unsaturated carboxylic acid (acrylic acid (1.2 mL, 17.7 mmol), methacrylic acid (1.5 mL, 17.7 mmol) or crotonic acid (1.5 g, 17.7 mmol) or AMEA (15 wt-%) were added and the mixture was flushed with argon for 30 s. The dispersion was photopolymerized for 90 s. To obtain a higher functionalization, the irradiation of 90 s was repeated several times and the suspension was flushed with argon for 10 s between each irradiation cycle. A total irradiation of 10x90 s was accomplished. The probes were washed with ethanol 3 times and left again in ethanol.

Quantification of the Functional Groups on the SCPs

Amines. The functionalization degree of the amine functionalized microparticles was determined by using the reaction of 2,4,6-trinitrobenzenesulfonic acid (TNBS) with free amino groups.[152] First, the solid content of the microparticle dispersion was determined gravimetrically by drying 500 mL of the dispersion at 100 °C for 3 h. Subsequently, 1 mL of the dispersion was diluted with 3 mL of 0.1 M borate buffer (pH 9.3) and 2 mL of 1 mM TNBS solution was added. The mixture was allowed to react for 2 h at 37 °C. Then, the microparticles were separated from the solution by centrifugation at 5000 rpm for 5 min, using a centrifugal filter with a pore size of 0.20 µm. The absorption of the supernatant was measured at 350 nm to determine the amount of unreacted TNBS. A blank sample was prepared in the same manner, using pure water instead of the microparticle dispersion. The concentration of the amino groups on the microparticles was determined from the difference of the absorption between the blank and the sample. A calibration curve was established with solutions of TNBS at different concentrations (0.5 mM, 0.33 mM, 0.25 mM and 0.1 mM).

Carboxylic Groups. Carboxyl groups were titrated with the toluidine blue O (TBO) dye adsorption assay.[91] The microparticles were dispersed in an aqueous solution of

$5x10^{-4}$ mol/L TBO adjusted to pH 10 with NaOH and incubated for 5 h at RT. The microparticles were then rinsed five times with NaOH solution (pH 10) to remove the non-complexed TBO molecules and centrifuged. Desorption of the dye was performed in 50% acetic acid solution. The concentration of released TBO was measured from the adsorption at 633 nm and the amount of COOH groups was calculated with the assumption that 1 mol of TBO had complexed with 1 mol of carboxylates. An equivalent sample was dried under vacuum and its dry mass was measured to calculate the mass concentration of COOH groups.

Post-functionalization of the Carboxylate SCPs

With ethylenediamine (EDA). Water was exchanged with DMF through several washing steps and the carboxylate functionalized microparticles were left in 10 mL of DMF. 0.73 g (1.4 mmol) PyBOP, 0.09 g (0.7 mmol) HOBt and 195 mL (1.4 mmol) triethylamine (TEA) were added to activate the carboxylic groups. This suspension was shaken for 1 h at RT, then 100 mL (1.5 mmol) EDA were added. The mixture was allowed to react for 3 h at RT. Then, the microparticles were centrifuged at 5000 rpm for 10 minutes and washed 3 times with DMF, 3 times with a 1:1 mixture of DMF and water and with MilliQ water.

With an oligo(amidoamine) dendrimer. The dendrimer was prepared by Dr. Muriel Behra following the synthesis route published by Hartmann et al.[96] Water was exchanged with DMF through several washing steps and the carboxylate functionalized microparticles were left in 4 mL of DMF. 0.052 g (0.1 mmol) PyBOP, 0.015 mg (0.1 mmol) HOBt and 250 mL (1.8 mmol) TEA were added to the dispersion and allowed to react for 2.5 h at RT. Then 0.18 g (0.1 mmol) dendrimer in 1 mL DMF was added. The mixture was allowed to react overnight at RT. Then the microparticles were centrifuged at 5000 rpm for 10 min, washed 3 times with DMF, 3 times with a 1:1 mixture of DMF and water followed by MilliQ water.

With aminoethyl-linked mannose. Ethanol was exchanged with DMF through several washing steps and the carboxylate functionalized microparticles (0.05 g) were left in 10 mL of DMF. 0.728 g (1.40 mmol) PyBOP, 0.097 g (0.70 mmol) HOBt and 195 µL (1.40 mmol) TEA were added to activate the carboxylic groups. This suspension was shaken for 15 min at RT, then 0.050 g (0.12 mmol) aminoethyl-linked mannose was added. The mixture was

allowed to react for 3 h at RT. The microparticles were washed 3 times with DMF and 3 times with methanol. 0.004 g (0.08 mmol) sodium methoxide was added and reacted for 1 h at RT.[153,154] Then, the microparticles were centrifuged at 5000 rpm for 10 min and washed 3 times with methanol and 3 times with MilliQ water. The particles were stored with 0.01 wt-% NaN_3.

With Concanavalin A (ConA). PEG-AA microparticles were washed with a 0.1 M phosphate buffer pH 6.5. Activation of the carboxyl groups were carried out by addition of 0.1 M EDC (2.5 mL) and 0.1 M NHS (2.5 mL) in phosphate buffer pH 6.5.[155] The particles were incubated for 4 h at RT and excess coupling agent was removed by washing with phosphate buffer pH 6.5. 5 mL of ConA in phosphate buffer pH 6.5 (0.2 mg/mL) was added and reacted for 12 h. The microparticles were centrifuged and washed first with PBST buffer pH 7.4 and subsequently with lectin binding buffer and stored with 0.01 wt-% NaN_3.

Post-functionalization of the Amino SCPs

The amine functionalized microparticles were dispersed in 10 mL DMF and 56 mL (0.4 mmol) TEA and 0.04 g (0.4 mmol) succinic anhydride (SUC) were added. The mixture was allowed to react for 2 h at RT. The microparticles were then centrifuged at 5000 rpm for 10 min and washed 3 times with DMF, 3 times with a 1:1 mixture of DMF and water and with MilliQ water.

Fluorescence Labeling of Amino Groups

A stock solution of NaH_2PO_4 (10 mM, pH 9) was prepared. 0.5 mg of fluorescein isothiocyanate (FITC) was dissolved in 20 mL of the buffer. To a sample of amino SCPs in water (2 mL), 10 mL of the FITC solution was added. A blank sample with nonfunctionalized PEG SCPs was prepared in the same way. The reaction tubes were covered with aluminium foil and stirred for 2 h at RT The excess solution was centrifuged and the SCPs were washed with MilliQ water. The resulting microparticles were measured on a confocal microscope (LEICA DM IRBE).

Labeling of PEG-Man SCPs with FITC-ConA

200 µL mannose bearing PEG-Man SCPs were added in an eppendorf tube and centrifuged. The supernatant was decanted and 100 µL lectin binding buffer pH 6 (50 mM NaCl, 1 mM $MnCl_2$, 1 mM $CaCl_2$, 10 mM HEPES) and 10 µL FITC labeled Concanavalin A solution (5 mg/mL) were added to the SCPs. The tube was coated in aluminum foil and incubated for 1 h. The excess solution was centrifuged and the particles were washed with lectin binding buffer 3 times. The resulted microparticles were measured on a confocal microscope (LEICA DM IRBE).

Inhibition of the interaction was done by adding of α-methyl-D-mannose (100 µL) (10 mg/mL) in lectin binding buffer pH 6.5 to the fluorescence labeled mannose SCPs and it was shaken for 10 min. The particles were washed with lectin binding buffer 3 times and the resulted microparticles were measured on a confocal microscope.

Labeling of the PEG-ConA SCPs

PEG-ConA particles were labeled with fluorescein isothiocyanate (FITC). Therefore 200 µL of the particle suspension was centrifuged and decanted. Than 1 mL of FITC (0.1 mg/ml) in a NaH_2PO_4 buffer (10 mM, pH 9) was added, covered with aluminium foil and reacted for 12 h. The excess solution was centrifuged and the particles were washed with MilliQ water. The resulting particles were measured on a confocal microscope.

Amino Acid Analysis

The samples were first lyophilized and then conc. HCl solution was added to cleave the amino acids from the peptide. Subsequently, the samples were dissolved in SDB buffer and analyzed on a Sykam amino acid analyzer S433 (Sykam, Germany).

Glass Surface Preparation for Electrostatic and Hydrophobic Measurements

Lab-Tek chambered coverglass was used as glass surface (Thermo scientific, Germany) and cleaned prior to use by piranha solution (96% H_2SO_4 and 30% H_2O_2, 3:1) followed by plasma cleaning on a Harrick plasma cleaner. Positively charged surfaces were prepared by incubating with polydiallyldimethylammonium chloride (PDADMAC). For this a stock solution of 250 µL of 20% PDADMAC solution in 40 mL of a 0.5 M NaCl solution was prepared and 200 µL of the solution was filled into the chambers. The solution was incubated for 1 h and the surface was washed with water.

Hydrophobic surfaces were obtained by vapor deposition of trichloro (1*H*,1*H*,2*H*,2*H*-perfluorooctyl) silane (FOTS) on glass coverslips and by coating PEI (poly(ethylene imine)) due to electrostatic interactions (1mg/mL). The glass coverslips were previously washed with isopropanol and piranha solution.

Glass Surface Preparation for Biological Studies

Coverslips (Ø 24 mm) were used as glass surface (Thermo scientific, Germany) and cleaned prior to use by washing with isopropanol and piranha solution (96% H_2SO_4 and 30% H_2O_2, 3:1). The coverslips were rinsed with MilliQ water and dried in a nitrogen stream. Amine surfaces were prepared via chemical vapor deposition.[156] Here, the coverslips and 3-aminopropyltriethoxysilane (APTES) (50 µL) on a freshly cleaned coverslip were placed in a desiccator and vacuum was applied for 1 min. The desiccator was sealed and the coverslips were left for 1 h to react with the vapor. The coverslips were rinsed with MilliQ water and dried with nitrogen. Then, the coverslips were placed in PBS buffer pH 7.4 containing 2.5% glutaraldehyde for 30 min[157] followed by washing with MilliQ water and drying. ConA (0.2 mg/mL) in PBS buffer pH 7.4 was placed on the aldehyde functionalized surfaces for 1 h[157] and prior to the measurements washed with lectin binding buffer pH 6.

Mannose surfaces were prepared by preparing first epoxy functionalized coverslips. Therefore, the Piranha cleaned coverslips were placed in a solution of ethanol (114 mL), MilliQ water (6 mL), acetic acid (120 µL) and 3-glycidoxypropyltrimethoxysilane (GLYMO) (3 mL) for 2 h. Additionally, the coverslips were washed with isopropanol and dried under a N_2-stream and placed in an oven for 12 h at 150°C. A solution of α-thioethyl-mannose (1 mg/mL) in PBS buffer pH 7.4 was placed on the slides for 12 h. The mannose surfaces were washed with PBST buffer pH 7.4 three times and subsequently with lectin binding buffer pH 6.

Reflection Interference Contrast Microscopy (RICM) Measurements

RICM on an inverted microscope (Olympus IX71, Germany) was used to obtain the contact area between the microparticles and a hard glass surface. For illumination a Hg-vapor lamp was used with a green monochromator (546 nm). A Zeiss Antiflex 63 x NO 1.25 oil-immersion objective, additional polarizers to avoid internal reflections and a Zeiss AxiocamHRm camera were used to image the RICM patterns. To conduct the JKR measurements of the adhesion energies, both the contact radius and the particle radius were measured. Image processing and data analysis were done using the image analysis software Image-J (public domain NIH) and the mathematical software OriginPro (OriginLab, USA).

Inhibition/Competition Measurements *via* RICM

1 mL of lectin binding buffer pH 6 was added to the ConA functionalized surface and PEG-Man SCPs were spread into the solution. The particles were sedimented and the contact radius and the particle radius were measured. For inhibition measurements, the inhibitors Man(all)-10, Man(all)-5, Man(1,3,5)-5, Man(1,5)-5, Man(1,2)-5 Man(3)-5, *α*-Me-D-Man, D-Man, D-Glc, Glc(1,3,5)-5, Gal(1,3,5)-5 and all heteromultivalent inhibitora were dissolved in water with a known concentration. A known amount of inhibitor solution was added into the solution and well mixed so that all bound particles were detached from the surface. As the particle sedimented, they were equilibrated for 30 min and the contact radius and the particle radius were measured again. This procedure was repeated stepwise to obtain data points at different concentrations of the inhibitor. To determine the IC_{50} values, the data points were analyzed in OriginPro using the Hill1 equation.

Surface Recovery Experiments

PEG-Man SCPs were added to ConA functionalized coverslips and the contact radius and particle radius was measured. The interaction was inhibited with α-methyl-D-mannose (200 µL) (10 mg/mL) so that the particles were detached from the surface. Afterwards, the surfaces were carefully washed with lectin binding buffer so that the SCPs were not washed out and the contact radii and particle radii were measured. The interaction was inhibited again with *α*-methyl-D-mannose and the cycle was repeated 5 times. A shift from the initial measurement to the first washing cycle is observed as the surface could not be fully

recovered. Since all measurements were normalized with respect to the blank signal the slight shift on the adhesion energy did not affect the reproducibility of the analysis.

AFM Force Spectroscopy

All experiments were performed on a NanoWizard III AFM (JPK Instruments AG, Germany) installed on an inverted optical microscope (Olympus IX71, Germany). The thermal noise method was used to calculate the spring constant of the cantilever (9-26 N/m). The soft colloidal probes (radius: 25-44 µm) were glued with epoxy resin (UHU Plus Schnellfest 5 min, UHU GmbH & Co. KG, Bühl, Germany) to the cantilever. First, a small drop of epoxy resin was spread on a glass surface and the end of the cantilever was dipped into the epoxy and then retracted. The glue was allowed to pre-cure for 4 min on the cantilever. In 10 µL of dispersion containing the PEG-Man probes were placed on the ConA surfaces in 1 mL lectin binding buffer pH 6. An optical microscope was used to position the cantilever over a single particle and the cantilever was then brought into contact with the particle. The epoxy resin was then cured for 20 min in the buffer solution before collecting the first force curves. The loading rate (r_f) measurements were accomplished at 3 different forces (10 nN, 50 nN and 100 nN) with a contact time of the probe at the surface of 10 s varying the retraction velocity (0.001-10 µm/s) for each measurement. A solution of α-methyl-D-mannose was added to obtain a final concentration of 2 mM, for loading rate measurements in presence of an inhibitor. To study the effect of contact time force measurements were performed with delay times upon contact ranging from 0 to 60 s at load of 50 nN and retraction speed of 0.5 µm/s. At least ten force-distance curves on different spots were recorded for each contact time. The adhesion energies were obtained by calculating the work of adhesion from the measured force-distance curves and normalized by the contact area (see RICM). Inhibition measurements were done with two different concentrations (2 mM and 10 mM) of α-methyl-D-mannose, D-galactose at 10mM and multivalent glycooligomers (Man(1,2)-5 and Man(all)-5) at a constant overall concentration with respect to mannose residues at the di- and pentamer scaffolds (5 mM and 2 mM respectively).

8.2. List of Abbreviations

AA	Acrylic Acid
AFM	Atomic Force Microscopy
AMEA	2-Aminoethyl methacrylate hydrochloride
APTES	3-Aminopropyltriethoxysilane
ATR	Attenuated Total Reflectance
CA	Crotonic Acid
ConA	Concanavalin A
DMF	*N*,*N*-Dimethylformamide
EDA	Ethylenediamine
EDC	3-(Ethyliminomethyleneamino)-*N*,*N*-dimethylpropan-1-amine
FITC	Fluorescein Isothiocyanate
FOTS	Trichloro (1*H*,1*H*,2*H*,2*H*-perfluorooctyl) Silane
FTIR	Fourier Transform Infrared
Gal	Galactose
Glc	Glucose
GLYMO	3-Glycidoxypropyltrimethoxysilane
HEPES	4-(2-Hydroxyethyl)-1-piperazineethanesulfonic acid
HOBt	1-Hydroxybenzotriazole
JKR	Johnson Kendall Roberts
LCST	Lower Critical Solution Temperature
MAA	Methacrylic Acid
Man	Mannose
M_n	Number Average Molecular Mass
NHS	*N*-Hydroxysuccinimide
PBS	Phosphate Buffered Saline
PBST	Phosphate Buffered Saline with Tween 20
PDADMAC	Polydiallyldimethylammonium Chloride
PEG	Poly(ethylene glycol)
PEG-dAAm	Poly(ethylene glycol)-diacrylamide
PEI	Poly(ethylene imine)
PNIPAm	Poly(*N*-isopropylacrylamide)

PyBOP	Benzotriazole-1-yl-oxy-tris-pyrrolidinophosphonium hexafluorophosphate
RICM	Reflection Interference Contrast Microscopy
RT	Room Temperature
SCP	Soft Colloidal Probe
SDB	Sperm Dilution Buffer
SEM	Scanning Electron Microscopy
SFA	Surface Force Apparatus
SUC	Succinic Anhydride
TBO	Toluidine Blue O
TEA	Triethylamine
THF	Terahydrofuran
TNBS	2,4,6-Trinitrobenzenesulfonic acid

9. References

[1] O. Wichterle, D. Lim, *Nature* **1960**, *185*, 117–118.

[2] J. K. Oh, R. Drumright, D. J. Siegwart, K. Matyjaszewski, *Prog. Polym. Sci.* **2008**, *33*, 448–477.

[3] H. Kawaguchi, *Prog. Polym. Sci.* **2000**, *25*, 1171–1210.

[4] a. K. Bajpai, J. Bajpai, R. Saini, R. Gupta, *Polym. Rev.* **2011**, *51*, 53–97.

[5] B. R. Saunders, H. M. Crowther, B. Vincent, *Macromolecules* **1997**, *30*, 482–487.

[6] M. Heskins, J. E. Guillet, *J. Macromol. Sci. Part A - Chem.* **1968**, *2*, 1441–1455.

[7] X. Zhou, B. Liu, X. Yu, X. Zha, X. Zhang, Y. Chen, X. Wang, Y. Jin, Y. Wu, Y. Chen, et al., *J. Control. Release* **2007**, *121*, 200–7.

[8] A. Schoubben, P. Blasi, S. Giovagnoli, C. Rossi, M. Ricci, *Chem. Eng. J.* **2010**, *160*, 363–369.

[9] R. Arshady, M. H. George, *Polym. Eng. Sci.* **1993**, *33*, 865–876.

[10] D. Duracher, A. Elaissari, C. Pichot, *J. Polym. Sci. Part A Polym. Chem.* **1999**, *37*, 1823–1837.

[11] R. Arshady, *Colloid & Polym. Sci.* **1992**, *270*, 717–732.

[12] S. Seiffert, D. A. Weitz, *Soft Matter* **2010**, *6*, 3184.

[13] A. Elaissari, Ed., *Colloidal Polymers: Synthesis and Characterization*, CRC Press, **2003**.

[14] P. Dowding, B. Vincent, E. Williams, *J. Colloid Interface Sci.* **2000**, *221*, 268–272.

[15] G. R. Hendrickson, M. H. Smith, A. B. South, L. A. Lyon, *Adv. Funct. Mater.* **2010**, *20*, 1697–1712.

[16] K. L. Prime, G. M. Whitesides, *J. Am. Chem. Soc.* **1993**, *115*, 10714–10721.

[17] C. Pale-Grosdemange, E. S. Simon, K. L. Prime, G. M. Whitesides, *J. Am. Chem. Soc.* **1991**, *113*, 12–20.

[18] J. M. Harris, Ed., *Poly(Ethylene Glycol) Chemistry: Biotechnical and Biomedical Applications*, Plenum Press, New York, **1992**.

[19] F. E. Bailey, R. W. Callard, *J. Appl. Polym. Sci.* **1959**, *1*, 56–62.

[20] K. Knop, R. Hoogenboom, D. Fischer, U. S. Schubert, *Angew. Chem. Int. Ed.* **2010**, *49*, 6288–308.

[21] S. Zalipsky, C. Gilon, A. Zilkha, *Eur. Polym. J.* **1983**, *19*, 1177–1183.

[22] J. B. Thorne, G. J. Vine, M. J. Snowden, *Colloid Polym. Sci.* **2011**, *289*, 625–646.

[23] D. A. Hammer, D. E. Discher, *Annu. Rev. Mater. Res.* **2001**, *31*, 387–404.

[24] M. Behra, N. Azzouz, S. Schmidt, D. V Volodkin, S. Mosca, M. Chanana, P. H. Seeberger, L. Hartmann, *Biomacromolecules* **2013**, DOI 10.1021/bm400301v.

[25] A. Elaissari, P. Cros, C. Pichot, V. Laurent, B. Mandrand, *Colloids Surfaces A Physicochem. Eng. Asp.* **1994**, *83*, 25–31.

[26] Y. Inomata, H. Kawaguchi, M. Hiramoto, T. Wada, H. Handa, *Anal. Biochem.* **1992**, *206*, 109–114.

[27] J. T. Kadonaga, R. Tjian, *Proc. Natl. Acad. Sci.* **1986**, *83*, 5889–5893.

[28] K. Tsukagoshi, R. Kawasaki, M. Maeda, M. Takagi, *Anal. Sci.* **1996**, *12*, 721–726.

[29] M. Behra, S. Schmidt, J. Hartmann, D. V Volodkin, L. Hartmann, *Macromol. Rapid Commun.* **2012**, 1–6.

[30] P. Kowallik, R. Schulz, B. D. Guth, A. Schade, W. Paffhausen, R. Gross, G. Heusch, *Circulation* **1991**, *83*, 974–982.

[31] Q. Luo, P. Liu, Y. Guan, Y. Zhang, *ACS Appl. Mater. Interfaces* **2010**, *2*, 760–7.

[32] B.-Y. Kim, J. H. Jeong, K. Park, J.-D. Kim, *J. Control. Release* **2005**, *102*, 525–38.

[33] L. B. R. Castro, M. Kappl, D. F. S. Petri, *Langmuir* **2006**, *22*, 3757–62.

[34] G. Binnig, C. Quate, C. Gerber, *Phys. Rev. Lett.* **1986**, *56*.

[35] H.-J. Butt, B. Cappella, M. Kappl, *Surf. Sci. Rep.* **2005**, *59*, 1–152.

[36] H.-J. Butt, *Biophys. J.* **1991**, *60*, 1438–1444.

[37] W. Ducker, T. Senden, R. Pashley, *Nature* **1991**.

[38] M. Kappl, H.-J. Butt, *Part. Part. Syst. Charact.* **2002**, *19*, 129.

[39] M. Glaubitz, N. Medvedev, D. Pussak, L. Hartmann, S. Schmidt, C. A. Helm, M. Delcea, *Soft Matter* **2014**.

[40] "Aspire Conical Tapping Mode AFM Probes - Nanoscience Instruments," can be found under http://store.nanoscience.com/store/pc/viewPrd.asp?idproduct=2556&idcategory=0, **2014**.

[41] G. Meyer, N. M. Amer, *Appl. Phys. Lett.* **1988**, *53*, 2400.

[42] A. Torii, M. Sasaki, K. Hane, S. Okuma, *Meas. Sci. Technol.* **1996**, *7*, 179–184.

[43] J. L. Hutter, J. Bechhoefer, *Rev. Sci. Instrum.* **1993**, *64*, 1868.

[44] B. Derjaguin, *Kolloid-Zeitschrift* **1934**, *69*, 155–164.

[45] H. Hertz, *J. für die reine und Angew. Math.* **1882**, *1882*, 156–171.

[46] K. L. Johnson, K. Kendall, A. D. Roberts, T. R. Society, R. Society, P. Sciences, *Proc. R. Soc. London. A. Math. Phys. Sci.* **1971**, *324*, 301–313.

[47] B. . Derjaguin, V. . Muller, Y. . Toporov, *J. Colloid Interface Sci.* **1975**, *53*, 314–326.

[48] N. Burnham, A. Kulik, *Handb. micro/nanotribology* **1999**, 1–31.

[49] G. Luengo, J. Pan, M. Heuberger, J. N. Israelachvili, *Langmuir* **1998**, *14*, 3873–3881.

[50] L. Limozin, K. Sengupta, *Chemphyschem* **2009**, *10*, 2752–68.

[51] A. S. G. Curtis, *J. Cell Biol.* **1964**, *20*, 199–215.

[52] J. S. Ploem, *Reflection Contrast Microscopy as a Tool for Investigation of the Attachment of Living Cells to a Glass Surface*, Blackwell, Oxford, **1975**.

[53] J. Raedler, E. Sackmann, *Langmuir* **1992**, *8*, 848–853.

[54] M. Kühner, E. Sackmann, *Langmuir* **1996**, *12*, 4866–4876.

[55] J. Raedler, E. Sackmann, *J. Phys. II* **1993**, *3*, 727–748.

[56] S. Attili, R. P. Richter, *Langmuir* **2012**, *28*, 3206–16.

[57] D. J. Muller, J. Helenius, D. Alsteens, Y. F. Dufrene, D. J. Müller, Y. F. Dufrêne, *Nat. Chem. Biol.* **2009**, *5*, 383–390.

[58] J. N. Israelachvili, *Intermolecular and Surface Forces*, Academic Press, **2011**.

[59] L. L. Kiessling, J. C. Grim, *Chem. Soc. Rev.* **2013**, *42*, 4476–91.

[60] J. Huskens, *Curr. Opin. Chem. Biol.* **2006**, *10*, 537–43.

[61] J. Huskens, A. Mulder, T. Auletta, C. a Nijhuis, M. J. W. Ludden, D. N. Reinhoudt, *J. Am. Chem. Soc.* **2004**, *126*, 6784–97.

[62] H. Krobath, B. Różycki, R. Lipowsky, T. R. Weikl, *Soft Matter* **2009**, *5*, 3354.

[63] G. Wiegand, K. R. Neumaier, E. Sackmann, *Appl. Opt.* **1998**, *37*, 6892–905.

[64] J. Erath, S. Schmidt, A. Fery, *Soft Matter* **2010**, *6*, 1432.

[65] L. Hartmann, K. Watanabe, L. L. Zheng, C.-Y. Kim, S. E. Beck, P. Huie, J. Noolandi, J. R. Cochran, C. N. Ta, C. W. Frank, *J. Biomed. Mater. Res. B. Appl. Biomater.* **2011**, *98*, 8–17.

[66] D. L. Elbert, J. a Hubbell, *Biomacromolecules* **2001**, *2*, 430–41.

[67] M. B. Browning, E. Cosgriff-Hernandez, *Biomacromolecules* **2012**, *13*, 779–86.

[68] P. Edman, B. Ekman, I. Sjöholm, *J. Pharm. Sci.* **1980**, *69*, 838–842.

[69] M. J. Hey, D. P. Jackson, H. Yan, *Polymer* **2005**, *46*, 2567–2572.

[70] Y. Zhang, P. S. Cremer, *Annu. Rev. Phys. Chem.* **2010**, *61*, 63–83.

[71] Y. Zhang, P. S. Cremer, *Curr. Opin. Chem. Biol.* **2006**, *10*, 658–63.

[72] J. M. Broering, A. S. Bommarius, *J. Phys. Chem. B* **2005**, 20612–20619.

[73] F. Tjerneld, *Adv. Mol. Cell Biol.* **1996**, *15*, 539–546.

[74] C. Ren, W. Tian, I. Szleifer, Y. Ma, *Macromolecules* **2011**, *44*, 1719–1727.

[75] B. A. Deyerle, Y. Zhang, *Langmuir* **2011**, *27*, 9203–10.

[76] D. Pussak, Synthesis and Functionalization of Poly(ethylene Glycol) Microparticles for Biosensing, Freie Universität Berlin, **2010**.

[77] N. A. Peppas, P. Bures, W. Leobandung, H. Ichikawa, *Eur. J. Pharm. Biopharm.* **2000**, *50*, 27–46.

[78] Y. Sugawara, R. Ando, H. Kamioka, Y. Ishihara, S. A. Murshid, K. Hashimoto, N. Kataoka, K. Tsujioka, F. Kajiya, T. Yamashiro, et al., *Bone* **2008**, *43*, 19–24.

[79] T. G. Kuznetsova, M. N. Starodubtseva, N. I. Yegorenkov, S. A. Chizhik, R. I. Zhdanov, *Micron* **2007**, *38*, 824–33.

[80] A. B. Mathur, A. M. Collinsworth, W. M. Reichert, W. E. Kraus, G. A. Truskey, *J. Biomech.* **2001**, *34*, 1545–1553.

[81] M. Lekka, D. Sainz-Serp, A. J. Kulik, C. Wandrey, *Langmuir* **2004**, *20*, 9968–77.

[82] T. Neumann, *JPK Instruments Appl. Rep.* **2008**, 1–9.

[83] M. M. Flake, P. K. Nguyen, R. A. Scott, L. R. Vandiver, R. K. Willits, D. L. Elbert, *Biomacromolecules* **2011**, *12*, 844–50.

[84] C. M. Nolan, C. D. Reyes, J. D. Debord, A. J. García, L. A. Lyon, *Biomacromolecules* **2005**, *6*, 2032–2039.

[85] D. Pussak, M. Behra, S. Schmidt, L. Hartmann, *Soft Matter* **2012**, *8*, 1664–1672.

[86] M. H. Schneider, Y. Tran, P. Tabeling, *Langmuir* **2011**, *27*, 1232–40.

[87] W. T. Yang, B. Rånby, *J. Appl. Polym. Sci.* **1997**, *63*, 1723–1732.

[88] W. J. Lee, D. K. Choi, Y. Lee, D.-N. N. Kim, J. W. Park, W.-G. G. Koh, *Sensors and Actuators B-Chemical* **2008**, *129*, 841–849.

[89] W. Yang, B. Rånby, *Macromolecules* **1996**, *29*, 3308–3310.

[90] Z. Ma, M. Kotaki, S. Ramakrishna, *J. Memb. Sci.* **2006**, *272*, 179–187.

[91] E. T. Kang, K. L. Tan, K. Kato, Y. Uyama, Y. Ikada, *Macromolecules* **1996**, *29*, 6872–6879.

[92] G. Li, G. He, Y. Zheng, *J. Appl. Polym. Sci.* **2012**, 1951–1959.

[93] Y. Osada, *J. Polym. Sci. Polym. Chem.* **1979**, *17*, 3485–3498.

[94] Y. Nho, J. Jin, *J. Appl. Polym. Sci.* **1997**, *63*, 1101–1106.

[95] M. L. Miller, J. Skogman, *J. Polym. Sci. Part A Gen. Pap.* **1964**, *2*, 4551–4558.

[96] L. Hartmann, M. Bedard, H. G. Borner, H. Mohwald, G. B. Sukhorukov, M. Antonietti, *Soft Matter* **2008**, *4*, 534–539.

[97] D. Pussak, D. Ponader, S. Mosca, S. V. Ruiz, L. Hartmann, S. Schmidt, *Angew. Chem. Int. Ed.* **2013**, *52*, 6084–6087.

[98] Z. Grabarek, J. Gergely, *Anal. Biochem.* **1990**, *185*, 131–135.

[99] P. M. Claesson, T. Ederth, V. Bergeron, M. W. Rutland, *Adv. Colloid Interface Sci.* **1996**, *67*, 119–183.

[100] A. Oláh, G. J. Vancso, *Eur. Polym. J.* **2005**, *41*, 2803–2823.

[101] J. N. Israelachvili, G. E. Adams, *J. Chem. Soc. Trans. I* **1978**, *74*, 975–1001.

[102] A. Razatos, Y.-L. Ong, F. Boulay, D. L. Elbert, J. A. Hubbell, M. M. Sharma, G. Georgiou, *Langmuir* **2000**, *16*, 9155–9158.

[103] R. Buzio, A. Bosca, S. Krol, D. Marchetto, S. Valeri, U. Valbusa, *Langmuir* **2007**, *23*, 9293–9302.

[104] M. K. Chaudhury, G. M. Whitesides, *Langmuir* **1991**, *7*, 1013–1025.

[105] V. T. Moy, Y. Jiao, T. Hillmann, H. Lehmann, T. Sano, *Biophys. J.* **1999**, *76*, 1632–1638.

[106] P. Jonkheijm, D. Weinrich, H. Schröder, C. M. Niemeyer, H. Waldmann, *Angew. Chem. Int. Ed.* **2008**, *47*, 9618–47.

[107] D. Gingell, I. Todd, *Biophys. J.* **1979**, *26*, 507–526.

[108] M. Giesbers, J. M. Kleijn, M. A. Cohen Stuart, *J. Colloid Interface Sci.* **2002**, *252*, 138–148.

[109] M. Meng, L. Stievano, J.-F. Lambert, *Langmuir* **2004**, *20*, 914–923.

[110] D. Choi, W. Lee, J. Park, W. Koh, *Biomed. Mater. Eng.* **2008**, *18*, 345–356.

[111] J. R. Tauro, B.-S. Lee, S. S. Lateef, R. A. Gemeinhart, *Peptides* **2008**, *29*, 1965–1973.

[112] X. Arys, a. Laschewsky, a. M. Jonas, *Macromolecules* **2001**, *34*, 3318–3330.

[113] C. R. Bertozzi, *Science (80-.).* **2001**, *291*, 2357–2364.

[114] H. Ghazarian, B. Idoni, S. B. Oppenheimer, *Acta Histochem.* **2011**, *113*, 236–247.

[115] M. Mammen, S.-K. Choi, G. M. Whitesides, *Angew. Chemie Int. Ed.* **1998**, *37*, 2754–2794.

[116] J. S. Daniels, N. Pourmand, *Electroanalysis* **2007**, *19*, 1239–1257.

[117] G. N. M. Ferreira, A.-C. da-Silva, B. Tome, *Trends Biotechnol.* **2009**, *27*, 689–697.

[118] X. Zeng, C. A. S. Andrade, M. D. L. Oliveira, X.-L. Sun, *Anal. Bioanal. Chem.* **2012**, *402*, 3161–3176.

[119] D. J. Muller, Y. F. Dufrene, *Nat. Nanotechnol.* **2008**, *3*, 261–269.

[120] N. Weil, O. Farago, *Phys. Rev. E* **2011**, *84*, 051907.

[121] E. Reister-Gottfried, K. Sengupta, B. Lorz, E. Sackmann, U. Seifert, A.-S. Smith, *Phys. Rev. Lett.* **2008**, *101*, 208103.

[122] A. Albersdörfer, T. Feder, E. Sackmann, *Biophys. J.* **1997**, *73*, 245–57.

[123] K. Tomizaki, K. Usui, H. Mihara, *Chembiochem* **2005**, *6*, 782–99.

[124] K. Kendall, M. Kendall, F. Rehfeldt, *Adhesion of Cells, Viruses and Nanoparticles*, Springer Netherlands, Dordrecht, **2011**.

[125] M. E. Nimni, D. Cheung, B. Strates, M. Kodama, K. Sheikh, *J. Biomed. Mater. Res.* **1987**, *21*, 741–71.

[126] I. Migneault, C. Dartiguenave, M. J. Bertrand, K. C. Waldron, *Biotechniques* **2004**, *37*, 790–6, 798–802.

[127] H. H. Weetall, *Anal. Chem.* **1974**, *46*, 602A–615A.

[128] A. J. Engler, S. Sen, H. L. Sweeney, D. E. Discher, *Cell* **2006**, *126*, 677–689.

[129] B. M. Friedrich, S. a. Safran, *Soft Matter* **2012**, *8*, 3223.

[130] A.-S. Smith, E. Sackmann, *Chemphyschem* **2009**, *10*, 66–78.

[131] R. Simson, E. Wallraff, J. Faix, J. Niewöhner, G. Gerisch, E. Sackmann, *Biophys. J.* **1998**, *74*, 514–22.

[132] C. Forrey, J. F. Douglas, M. K. Gilson, F. Douglas, *Soft Matter* **2012**, *8*, 6385–6392.

[133] M. A. Hjorsto, J. W. Roos, Eds., *Cell Adhesion in Bioprocessing and Biotechnology*, CRC Press, **1994**.

[134] A. G. Moreira, C. M. Marques, *J. Chem. Phys.* **2004**, *120*, 6229–37.

[135] N. W. Moore, T. L. Kuhl, *Biophys. J.* **2006**, *91*, 1675–87.

[136] G. Entlicher, J. V. Koštíř, J. Kocourek, *Biochim. Biophys. Acta - Protein Struct.* **1971**, *236*, 795–797.

[137] I. J. Goldstein, C. E. Hollerman, E. E. Smith, *Biochemistry* **1965**, *4*, 876–883.

[138] C. Fasting, C. a Schalley, M. Weber, O. Seitz, S. Hecht, B. Koksch, J. Dernedde, C. Graf, E.-W. Knapp, R. Haag, *Angew. Chemie Int. Ed.* **2012**, *51*, 10472–10498.

[139] D. Ponader, F. Wojcik, F. Beceren-Braun, J. Dernedde, L. Hartmann, *Biomacromolecules* **2012**, *13*, 1845–1852.

[140] D. Ponader, P. Maffre, J. Aretz, D. Pussak, N. M. Ninnemann, S. Schmidt, P. H. Seeberger, C. Rademacher, G. U. Nienhaus, L. Hartmann, *J. Am. Chem. Soc.* **2014**, *136*, 2008–2016.

[141] A. Kussrow, E. Kaltgrad, M. L. Wolfenden, M. J. Cloninger, M. G. Finn, D. J. Bornhop, *Anal. Chem.* **2009**, *81*, 4889–97.

[142] D. K. Mandal, C. F. Brewer, *Biochemistry* **1993**, *32*, 5116–5120.

[143] X. Qian, R. E. Holmlin, G. M. Whitesides, C. Y. Chen, M. Schiavoni, S. P. Smith, F. Assi, M. G. Prentiss, *J. Phys. Chem. B* **2002**, *106*, 9159–9164.

[144] J. Buensow, J. Erath, P. M. Biesheuvel, A. Fery, W. T. S. Huck, J. Bünsow, *Angew. Chemie Int. Ed.* **2011**, *50*, 9629–9632.

[145] T. V Ratto, K. C. Langry, R. E. Rudd, R. L. Balhorn, M. J. Allen, M. W. McElfresh, *Biophys. J.* **2004**, *86*, 2430–7.

[146] D. Pussak, D. Ponader, S. Mosca, T. Pompe, L. Hartmann, S. Schmidt, *Langmuir* **2014**, *30*, 6142–6150.

[147] G. I. Bell, *Science* **1978**, *200*, 618–27.

[148] L.-C. Xu, C. a Siedlecki, *Langmuir* **2009**, *25*, 3675–81.

[149] R. Merkel, P. Nassoy, a Leung, K. Ritchie, E. Evans, *Nature* **1999**, *397*, 50–3.

[150] I. U. Vakarelski, A. Toritani, M. Nakayama, K. Higashitani, *Langmuir* **2001**, *17*, 4739–4745.

[151] W. I. Weis, K. Drickamer, *Annu. Rev. Biochem.* **1996**, *65*, 441–73.

[152] C. Weber, C. Coester, J. Kreuter, K. Langer, *Int. J. Pharm.* **2000**, *194*, 91–102.

[153] G. Zemplén, A. Kunz, *Berichte der Dtsch. Chem. Gesellschaft (A B Ser.* **1923**, *56*, 1705–1710.

[154] C. a Tarling, S. G. Withers, *Carbohydr. Res.* **2004**, *339*, 2487–97.

[155] N. M. Anande, S. K. Jain, N. K. Jain, *Int. J. Pharm.* **2008**, *359*, 182–9.

[156] M. Bezanilla, S. Manne, D. E. Laney, Y. L. Lyubchenko, H. G. Hansma, *Langmuir* **1995**, *11*, 655–659.

[157] M. Lekka, P. Laidler, J. Dulińska, M. Łabedź, G. Pyka, *Eur. Biophys. J.* **2004**, *33*, 644–50.